MICROSEGREGATION IN TERNARY IRON-CARBON-CHROMIUM ALLOYS

by

DAVID ROBERT POIRIER

B.S. Northeastern University (1961)

S.M. Massachusetts Institute of Technology (1963)

Submitted in partial fulfillment of the

requirements for the degree of

DOCTOR OF SCIENCE

at the

Massachusetts Institute of Technology

(1966)

Signature of Author
Department of Metallurgy

Signature of Professor
in Charge of Research

Signature of Chairman of
Departmental Committee
on Graduate Students

MICROSEGREGATION IN TERNARY IRON-CARBON-CHROMIUM ALLOYS

by

DAVID ROBERT POIRIER

Submitted to the Department of Metallurgy on April 14, 1966

in Partial Fulfillment of the Requirements for the

Degree of DOCTOR OF SCIENCE

ABSTRACT

An analytical and experimental study has been made of microsegregation in dendritic solidification of ternary iron-carbon-chromium alloys. The most realistic model considered assumes uniform concentrations of carbon and chromium in the interdendritic liquid, equilibrium at the solid liquid interface, no diffusion of chromium in the solid, and a uniform concentration of carbon in the solid.

Alloys studied experimentally were all of 1.5 per cent chromium, with carbon contents ranging from .96 to 3.00 per cent carbon. Estimates of the extent of diffusion for carbon and chromium as well as microprobe analyses showed that carbon diffuses extensively in the solid during solidification and chromium diffuses only a limited amount.

Segregation ratios of common alloying elements in medium carbon, low alloy steel were compiled from the literature. Some of these data were combined with measurements from this investigation to illustrate the overall effect of carbon on the segregation ratio of chromium in iron-low chromium alloys.

An alternative measure of microsegregation to the "Segregation Ratio", S, was introduced. This measure, σ^m, was termed "Microsegregation Deviation". Comparison of theory and experiment was made for the segregation ratio and the segregation deviation parameter for iron-1.5 per cent chromium alloys with carbon. Experimental results for σ^m were determined for carbon contents between .96 and 1.75 per cent carbon and compared to theoretical calculations for carbon contents from .96 to 3.00 per cent. Theoretical values (based on no diffusion of chromium in the solid) of σ^m increased from .22 at .96 per cent carbon to .35 at 1.75 per cent carbon and

then decreased to .16 at 3.00 per cent carbon. The experimental values were somewhat lower (15 to 30 per cent lower) due, it is believed, to limited diffusion of chromium in the solid.

Segregation ratios were experimentally and theoretically determined for alloys between .96 to 3.00 per cent carbon, and measurements of other investigators at lower carbon contents were used. The segregation ratio increased from unity at zero per cent carbon to about 4.5 - 5.0 at 1.5 per cent carbon and then decreased to 3 at three per cent carbon. Theoretically derived segregation ratios between .96 and 3.00 per cent carbon showed the same general dependence; however, the theoretical values were lower except at one per cent.

Fundamental to the study of solute redistribution during solidification is detailed knowledge of the solid-liquid equilibria. For this reason the determination of the austenite-liquidus of the iron-carbon-chromium system was made which included evaluating the activity of iron, carbon, and chromium in liquid iron and austenite as functions of temperature and composition.

Thesis Supervisor: Merton C. Flemings

Title: Associate Professor of Metallurgy

TABLE OF CONTENTS

LIST OF ILLUSTRATIONS

LIST OF TABLES

ACKNOWLEDGEMENTS

The author wishes, in particular, to express his gratitude to two individuals who made possible and supported his endeavor to carry out the investigation. His wife, Nancy, has made many sacrifices in order to make the past six years very rewarding despite the problems of utilizing a student's earnings to maintain a home. Professor Merton C. Flemings has not only provided the necessary guidance to complete this investigation but, as a fine educator, encouraged the author's independent (sometimes floundering) thinking.

The author also wishes to express his appreciation to all those individuals who shared their talents so that this investigation could be completed.

Dr. Harold D. Brody for programming many of the calculations for this investigation and Mr. Richard V. Barone for his introduction to computer time sharing operations.

Mr. Richard W. Strachan for sharing his "know-how" and time in the design and operation of temperature control equipment for some of the experimental work.

Mr. Richard A. Berry and Mr. Richard F. Polich for their aid in experimentation.

Miss Frances Gedzium for typing the manuscript and Mrs. Patricia Sollitto for assisting in some of the calculations.

Professor John Chipman and Mr. Edwin Brush for indicating some of the thermodynamic data available in the literature.

The many graduate students and staff members of the Casting and Solidification Section who were always available for discussion.

The work was done in part at the Computation Center, M.I.T., Cambridge, Massachusetts.

The research program was sponsored in part by the Army Materials Research Agency under Contract DA-19-020-AMC-5443(X).

I. INTRODUCTION

The quantitative aspects of solute redistribution during solidification has received considerable attention in recent years. In most metal alloy systems the composition of the solid that precipitates from the melt continually changes and diffusion in the solid state is sufficiently slow so that the final structure is "cored". Scheil[1] demonstrated the use of a simple materials' balance to describe solute partitioning during solidification. The same material balance became more reknown to metallurgists in 1958 when Pfann[2] applied the material balance to the problem of single crystals grown with plane-front solidification (normal freezing). For the most part, however, the quantitative aspects of microsegregation for dendritic solidification have been dormant until Flemings[3] emphasized the importance of such considerations in 1964.

The importance of this topic comes forth when one realizes the multitude of manifestations in which solute partitioning plays a role. Hot tearing, a common casting defect, has been related to the stresses (mechanical and thermal) which arise during solidification[4,5]; the reaction of the casting to these stresses depends on the partitioning behavior of the particular alloy. The casting fluidity of alloys depends on solute partitioning in addition to heat flow[6,7]. Banding in wrought materials has been recognized as being caused by the dendritic segregation of alloying elements during solidification of ingots[8-14]. Most recently the problem of macrosegregation has been

analyzed using the fundamentals of heat and momentum transport along with solute partitioning, and numerous types of macrosegregation can now be explained and understood[15].

The simplest quantitative approach to determining microsegregation in dendritically freezing alloys is the "non-equilibrium lever rule" derived by Scheil[1]:

$$C_S^* = kC_o(1 - f_S)^{k-1} \qquad (1)$$

where: C_S^* = interface composition of solid, weight per cent

C_o = initial alloy composition, weight per cent

k = equilibrium partition ratio

f_S = weight fraction solidified

From the same analysis, the fraction solid within a unit volume of the two-phase zone of a freezing alloy can be described as a function of temperature.

$$(1 - f_S) = \left(\frac{m_L C_o}{T_m - T} \right)^{\frac{1}{1-k}} \qquad (2)$$

m_L = slope of liquidus line

T_m = melting point of pure solvent

The assumptions involved in the development of equations (1) and (2) have been discussed by Flemings[3] and Brody et al[16]. The equations are valid for the following assumptions:

1. Negligible supercooling for the formation of initial solid.
2. Negligible interface supercooling from kinetic of curvature effects.
3. Negligible constitutional supercooling.
4. The equilibrium partition ratio applies at the interface.
5. No diffusion in the solid.
6. The liquidus and the solidus are straight lines, so that k and m_L are constant.
7. And solute is conserved within the dendrite unit volume.

Assumptions (1) through (4) have been justified[3,16] and are valid for all usual casting processes where dendritic growth is the mode of transformation. Assumptions (5) and (6) are mathematical conveniences, and assumption (7) implies no macrosegregation.

Equation (2) has been applied by Flemings and Taylor[17] to Al-4.5 per cent copper and was found to agree reasonably well with the experimental results of Stonebrook and Sicha[18]. Recently Brody[19] used a numerical analysis procedure to examine in detail the effect of diffusion in the solid during and after solidification. Also, the restriction of a constant partition ratio was voided and a number of binary aluminum alloys were considered. Utilizing the concepts for calculating solute redistribution, Koump and Tien[20] were able to determine the growth of the mushy zone for solidification of various binary alloys using numerical analysis. Earlier Adams[21] analytically solved the solidification problem for an Al-4 per cent copper alloy.

Presently microsegregation is being analyzed by Barone[22,23] for iron-base binary alloys. Some of the systems being considered, notably iron-nickel, solidify not in an equilibrium manner but the amount of solid diffusion is so great that Brody's analysis[19] does not apply and, his model has been improved. In addition because so much diffusion does occur in some of these alloys, various geometric models for the diffusion path are being studied.

The relationship between the solidification and the deoxidation practice of steel has been demonstrated by Turkdogan[24]. For a low carbon steel the enrichment of solutes (carbon, oxygen, manganese, and silicon) in the interdendritic liquid during solidification was calculated using partition ratios of the respective iron binary systems. With these expressions and the equilibrium constants for the various deoxidation reactions in liquid iron, the occurrence of the carbon monoxide evolution reaction was predicted and proper silicon and manganese levels could be established as a function of carbon and oxygen contents.

The foregoing examples illustrate the importance of microsegregation to the production of castings and ingots. In addition microsegregation affects the characteristics of metals. The property changes may be a result of concentration variations within solid solution or influence the amount, form, and distribution of second phases including undersirable second phases such as inclusions and undissolved eutectic components. Corrosion, stress

corrosion, wear characteristics and surface finish of bearings, and mechanical properties can all be affected by microsegregation[3], further demonstrating that microsegregation is an important phenomena to be understood by metallurgists.

With present day availability of high speed digital computers, it seems only natural to demonstrate the application of the quantitative theory to ternary alloys making the theory all the more applicable to operating metallurgy. Thus a major purpose of the following argument is not only to further substantiate the quantitative theory of microsegregation but also perhaps be another step in the development of the theory to systems with an unlimited number of components. Fundamental to the study of microsegregation is the knowledge of the appropriate component equilibria between the solid and liquid phases so that the equilibrium distribution coefficients are known. For multicomponent alloys this requires phase diagram determinations unless the important solutes are present in dilute amounts; because multicomponent phase diagram tie-lines are not available in the literature, quantitative analysis of solute redistribution for most alloys will require solid-liquid equilibria determinations.

II. EXPERIMENTAL PROCEDURES

A. Liquidus Determinations

In order to supplement and check the data available in the literature[25-27] on the gamma liquidus surface for iron-carbon-chromium alloys, five heats were made in which the liquidus temperature for eleven alloys were determined by a cooling curve technique. Each of the heats, 1 through 4, consisted only of one alloy. Heat 5 was made with a constant chromium content, and carbon was added periodically to yield a series of seven different carbon contents.

A commerically available iron was used in the preparation of the alloys; it consisted of 1/4 inch and 1/8 inch diameter bars manufactured from vacuum melted electrolytic iron. A high purity graphite of low ash residue was used to attain the carbon contents and the chromium was added as 99.35 per cent chromium. The compositions of these charge materials are listed in Table I.

The iron, chromium, and graphite were charged (80 - 100 grams total) into an alumina crucible and melted under a vacuum in a Balzer's induction furnace. A schematic diagram of the experimental set-up is shown in Figure 1. After meltdown helium was introduced to a pressure of 30 cm. mercury. Much unlike melting untreated electrolytic iron under vacuum, all melts lacked boiling thus "hang-up" problems were absent. Also, the surface of each melt was "mirror-like"; only one melt, that with the highest chromium content

(No. 4), had an oxide on its surface. A preliminary cooling curve was then made to approximately indicate the liquidus temperature. Subsequently, 20 - 30°C superheat was added, and then the cooling curve was made at a rate where thermocouple lag was negligible. Temperatures were charted continuously with a recorder suppressed so that an interval of 10 mv covered full scale (ten inch chart paper). In the neighborhood of the liquidus arrest, temperatures were simultaneously measured with a potentiometer capable of reading to .001 mv.

The thermocouple assembly is shown in Figure 2; the essential feature of the assembly is that a relatively small alumina thermocouple protection tube is used to minimize thermal lag. In the process of standardizing the thermocouple with a pure nickel standard, it was found that a cooling rate of 78°C per minute only caused an error of 2°C when compared to a cooling rate of 6°C per minute. Cooling rates of 20 to 30°C per minute were found to be within a 1°C error, and thus this cooling rate was used to determine the liquidus temperatures of the alloys.

In heat 5 the graphite was added after each liquidus determination by attaching it to the end of a rod with analytical grade iron wire. The rod was designed to pass through a ball and socket vacuum feed through valve. Samples for the melt analysis in heat 5 were taken by dipping a copper tube, coated with alumina wash, into the melt at 5 to 10°C superheat. In this manner samples of 3

to 5 grams were extracted. In heats 1 - 4 samples were removed from the solidified and cooled ingots by drilling. The chemical analyses of these heats and the respective liquidus temperatures are given in Table II.

B. Production of Small Ingots with Various Carbon Contents in Iron-1.5 Per Cent Chromium Alloys

The effect of carbon on the microsegregation of chromium in iron during dendritic solidification was studied by preparing six melts (90 - 100 grams) each with approximately 1.5 per cent chromium. The melts were made in the Balzer's induction furnace in the same manner as the melts for the liquidus determinations, the only exception being the thermocouple assembly. A .016 inch diameter thermocouple was employed and it was protected with a 6 mm O.D. fused silica tube.

After meltdown the melts were adjusted to about 50°C superheat and then allowed to solidify with a cooling rate of about 60°C per minute in the solidification interval.

After cooling drillings were removed for chemical analyses, and the ingots were sectioned for subsequent metallographic preparation. The overall chemical analyses, cooling rates, and dendrite element spacings are given in Table III.

C. Production of AISI 52100 Steel Ingot

To obtain data on a commercial alloy based on iron-carbon-chromium, a mold capable of producing unidirectional solidification was made with

platinum/platinum-10 per cent rhodium thermocouples placed at fixed distances from the chill, Figure 3. A charge consisting of electrolytic iron, chromium, and high purity cast iron was induction melted in a magnesia crucible under a blanket of argon gas. Deoxidation was carried out with 0.1 per cent aluminum, and the ingot, was then cast at 1600°C. Chemical analysis of the ingot corresponding to AISI 52100, is given in Table IV. After cooling, the ingot was sectioned to assure attainment of a columnar structure. The cooling curves for the ingot, obtained by a sixteen-point recorder for the thermocouples 4.0 to 11.4 cm from the chill and by a continuous strip chart recorder for the thermocouple 1.7 cm from the chill, are shown in Figure 4.

To obtain data on the effect of cooling rates on the microsegregation of chromium, specimens were removed for subsequent metallographic determination of dendrite element spacings and microprobe analysis. In order to delineate the dendritic structure, the specimens were heated for fifteen minutes at 825 - 850°C in an argon atmosphere and quenched in water. At the upper temperature carbides coexist with austenite, and quenching results in a martensitic matrix with a higher distribution of carbides in chromium-rich areas that represent interdendritic spaces. Typical microstructures can be seen in Figure 5, and the dendritic element spacings are given in Figure 6.

D. Austenite-Liquid Equilibria of Chromium in Iron-Carbon-Chromium Alloys

Two different techniques were employed for the determination of the solid chromium concentration in equilibrium with liquid iron-carbon-chromium alloys. Both methods involved the use of the apparatus depicted in Figures 7 and 8.

The first method involved the insertion of a pure iron-bar into the alloy melt held at a constant temperature above its liquidus. After sufficient time an interface with the equilibrium partition of chromium is established that moves very slowly with time. The interface could be established at any position without the collapse of the liquid column. This collapse was prevented by containing the iron rod within an alumina tube and applying a vacuum to its free end, as depicted in Figure 7. At the end of a run the alumina tube with its contents was withdrawn from the melt; the liquid remaining in the bottom of the tube solidified dendritically relatively fast. Subsequent sectioning and metallographic preparation showed the interfaces, and the samples were microanalyzed to determine the concentration of chromium in the solid in equilibrium with the liquid alloys. The liquid concentration was determined by chemically analyzing the remaining solidified ingot.

The second method employed the same apparatus with the exception that no iron rod was immersed. Instead, the alloy was cooled to some temperature between its liquidus and solidus. The

temperature of the solid-liquid ingot was held constant for a period of time and then cooled by shutting off the power and immersing an iron rod, 1/4 inch diameter. The ingots cooled at a rate of approximately 1/2°C per second, while completing solidification, and then 3°C per second down to 800°C.

All alloys were made by charging the materials listed in Table I and were melted in alumina crucibles under a helium atmosphere. Before entering the system, the helium was passed through anhydrous calcium sulfate and then titanium chips heated to 700°C. The temperature control was maintained by means of a tungsten-3 rhenium/tungsten-25 rhenium thermocouple connected to a control system utilizing a null detector. Four heats were run for each of the two methods described, and the temperature of all the heats were held at $\pm$ 1/2°C of the set point.

Macrostructures obtained from both methods are shown in Figures 9a and 9b. In Figure 9b, a "solid-liquid" ingot, the solid was not distributed uniformly but rather was concentrated all in one area. This was due to radiation heat loss from the top of the ingot, thus the entire ingot was not isothermal. The solid of interest which was in equilibrium with the liquid is therefore that right next to the liquid. Also, material could easily be removed from the ingots for chemical analyses representing just the liquid, itself.

A brief summary of these heats is presented in Table V along with compositions of chromium in the solid in equilibrium determined by microprobe analysis.

E. Microprobe Analyses

1. Unidirectional Ingot.

Four specimens were removed from the unidirectional ingot at various distances from the chill (1/2, 2, 3, and 4 inches). The samples were metallographically prepared and viewed from the plane perpendicular to heat flow during solidification, i.e., as shown in Figure 5a. Diamond hardness indentations were made around two areas where minima in chromium concentrations could be found and six areas where maxima were suspected.

In these structures, the concentration gradients of chromium are shallow in the areas that solidified first; however, the gradients can be quite steep in the interdendritic regions. Thus the chromium minima could be found easily, and it was only necessary to direct the scan across the dendrite cores. To determine maxima the samples were manually scanned in the interdendritic areas, and the instaneous intensity was observed. When a maximum intensity was detected, point counts (30 second integration times) were made at close intervals, 1 - 3μ, across the maximum.

For these samples, the normalized, intensities were converted to compositions by the use of a calibration curve based on homogenized standards all with approximately 1 per cent carbon. Analyses were carried out using an A.R.L. microprobe with a "take-off" angle of 52.5°. The results of these microprobe analyses are given in Table VI.

2. Solid-Liquid Equilibria Specimens.

Because these specimens were expected to have significant differences in carbon concentrations from point-to-point within one sample and different carbon concentrations from one sample to another, the relative intensities of chromium were converted to weight per cent by utilizing empirical relations developed by Ogilvie and Ziebold[28] for ternary systems. To utilize the empirical relations, the normalized intensities of both chromium and iron were recorded.

Since carbon atoms do not flouresce either iron or chromium atoms, nor absorb chromium or iron characteristic radiation, the empirical equations reduce to:

$$\frac{C_2}{K_2} = C_3(a_{23} - 1) + 1 \qquad (3)$$

and

$$\frac{C_3}{K_3} = C_2(a_{32} - 1) + 1 \qquad (4)$$

where: C_2 = composition of chromium, weight fraction

C_3 = composition of iron, weight fraction

K_2 = normalized intensity of chromium

K_3 = normalized intensity of iron

a_{23}, $^2{}_{32}$ = constants determined by the use of standards

The standards used were derived from average normalized intensities of the liquid portions (dendritic areas) of the eight

specimens, in Table V. The average normalized intensities were made by continuous scans within the dendritic areas at a speed of 96μ per minute. While scanning, 30 second integrations were recorded. The number of readings taken in this manner varied from 30 to 110, thus total distances scanned varied from 1440 to 5280μ, several times greater than dendritic spacings. By plotting C_2/K_2 versus C_3 and C_3/K_3 versus C_2, a_{23} and a_{32} were determined, respectively for equations (3) and (4). With these values and by solving equations (3) and (4) simultaneously the following expression for chromium was obtained:

$$C_2 = \frac{(1.325\ K_3 + 1)\ K_2}{1 - .9185\ K_3\ K_2} \qquad (5)$$

It should be indicated here that equation (5) would not be valid for analyses of chromium in iron-carbon-chromium alloys for all microprobe analyzers because the values of a_{23} and a_{32} depend on the detectors' characteristics as well as electron and X-ray phenomena (absorption, flourescence, etc.). A microstructure showing a probe path and the analysis across the interface is shown in Figure 10. These analyses were also carried out using an A.R.L. microprobe with a "take-off" angle of 52.5°.

3. Small Ingots with Various Carbon Contents.

The metallographic specimens for all of these ingots were analyzed for microsegregation. To convert the X-ray intensities

to weight per cent chromium equation (1) was used. Iron intensities were not measured but C_3 in equation (1) could be easily estimated. To determine the parameter a_{23}, the average intensity ratios for the specimens from heats 9, 10, and 11 were determined by scanning each sample in a random manner for approximately 400 seconds while collecting detector counts. All three specimens yielded the same parameter within 2 per cent of each other.

These same specimens (from heats 9, 10 and 11) were scanned 5000 microns at speeds of 40, 80, and 80 microns per minute, respectively, and rate meter intensities were recorded continuously on a strip chart. These analyses were performed in order to determine the fraction of material associated with various chromium concentrations. This type of analysis is the same as the metallographic determination of volume fraction second phase. This is schematically represented in Figure 11 where the fraction of material, L_f, with a composition of C_i and greater is given by:

$$L_f = \frac{\ell_1 + \ell_2 + \ell_3}{L} \tag{6}$$

As with metallographic determinations the accuracy of the result depends upon the amount of material scanned. The statistics for lineal analysis as given by Cahn and Hilliard[29] apply and their equation is utilized. If the fraction second phase is small (less than .2):

$$\left(\frac{\sigma_f}{\bar{L}_f}\right)^2 = \frac{1}{L}\left[\left(\frac{\sigma_\ell}{\bar{\ell}}\right)^2 + 1\right] \tag{7}$$

where: $\bar{L}_f = \frac{1}{L}\sum_{n=1}^{N} \ln$ = volume fraction above C_i

N = number of path segments above C_i

$\bar{\ell}$ = average segment length

σ_f = standard deviation of $\bar{L}_f$

σ_ℓ = standard deviation of ℓ_n

The probable error, E, assuming normal density function is:

$$E \cong \frac{2}{3}\,\sigma_f \tag{8}$$

In addition to determining the concentration profiles of the specimens from heats 9, 10, and 11, maxima and minima for the six samples were determined. The analyses of these six specimens were carried out with a Phillips microprobe with a "take-off" angle of 15.5°.

III. LIQUID-AUSTENITE EQUILIBRIA FOR THE IRON-CARBON-CHROMIUM SYSTEM

A. Liquidus Surface

The carbon-chromium-iron liquidus surface was studied by Griffing et al[27]. Saturation experiments, thermal analyses during freezing, and metallographic and X-ray diffraction studies were employed to obtain information which, with other published data, made possible their construction of a comprehensive carbon-chromium-iron liquid surface. This discussion concentrates solely on the gamma liquidus surface, and the isotherms are drawn rather differently than those presented by Griffing et al.

The vertical sections through the iron-carbon-chromium system, showing the freezing temperatures, are presented in Figures 12 - 16. The liquidus for null chromium is that presented by Benz and Elliott[30]. The other vertical sections are composed of data from Adcock[31], Austin[25], Tofaute et al as reported by Kinzel and Craft[26], and Table II. From these vertical sections the gamma liquidus surface is constructed, Figure 17. The positions of the eutectic valleys and the locus where gamma precipitates rather than delta iron were not determined precisely; the eutectic valleys and the demarcation between the gamma liquidus and delta liquidus are from Figures 12 - 16 and approximately correspond to Griffing et al[27]. The dip in some of the isotherms at approximately 16 per cent chromium is real although not indicated by Griffing et al[27]. The data at chromium:iron atom ratio equal to 0.25 which causes the curves to

rise back up towards higher carbon levels is solely from Austin[25] whose other data agrees with this investigation and that of Tofaute et al[26]. This may be a manifestation of the binary iron-chromium phase diagram in which the liquidus and solidus meet at a minimum point (22 per cent chromium) and the partition ratio passes from less than one to greater than one. More careful consideration of this behavior is in order; however since the solidification of iron-carbon-chromium alloys with only 1.5 per cent chromium will be considered, nothing more will be said except that these "dips" do exist.

B. Solidus Surface

The solidus surface presented in Figure 18 was developed on the basis of knowing the activity of carbon, chromium, and iron for both the liquid phase and austenite at all temperatures and compositions involved for the iron-carbon-chromium system covered in Figure 17. The development of suitable equations to describe the activities is involved, and is not treated in detail in this section; the complete thermodynamic analysis is treated in the Appendix. The treatment in the Appendix relies upon activity data of carbon in iron-carbon austenite, iron-carbon liquid, and the effect of chromium on the activity of carbon in both austenite and liquid iron, as well as the thermodynamics of the iron-chromium binary system in both the liquid and solid states. Using all this data, the results of the chromium austenite-liquid equilibria

(Table I), and applying Gibbs-Duhem relation for ternary systems, the activities of all three components is analytically described.

In principal if the activities of all three components in a ternary system are known, then both the liquidus and solidus surfaces can be constructed with tie lines. In the case at hand, the liquidus is known, and it is only necessary to consider the activity of two components. For reasons explained in the Appendix, it was most convenient to calculate the liquid-austenite equilibria based on the activities of carbon and chromium.

The solidus derived in this manner shown in Figure 18 is not presented in the customary manner, i.e., a series of isotherms with tie-lines in the two phase region; instead the entire equilibria is represented by showing the locii of compositions in austenite that are in equilibrium with the liquidus. For this particular alloy system, the one representation of the liquidus and the one representation of the solidus replace fourteen isothermal sections if the equilibria were presented in the customary manner.

IV. SOLIDIFICATION MICROSEGREGATION

A. Measurements of Microsegregation

The degree of microsegregation can be detected principally by four methods: (1) metallography, (2) microradiography, (3) autoradiography, and (4) electron beam microprobe analysis. With all four methods, quantitative measurements can be made. Specifically metallography is suitable for the determination of amounts of second phase that result entirely or in part from non-equilibrium solidification. Microradiography and autoradiography can be used to gain quantitative results but both methods are tedious and rather indirect. The most direct, expedient, and accurate method is microprobe analysis.

The microprobe analyzer has been used by several investigators to measure microsegregation in ferrous and non-ferrous alloys both in cast and wrought materials. Such investigations have included analysis of second phase particles, inclusions, and "coring" or "banding" associated with microsegregation. Analysis of second phase particles or inclusions have yielded compositions; "coring" or "banding" phenomena have been reported as "degree of microsegregation", "segregation index", or "segregation ratio"; all terminologies are defined as the ratio of the maximum concentration to the minimum concentration of a particular solute in an alloy. In alloys where eutectic second phase particles are present this ratio is still sometimes applied along with the fraction of second

phase present which depends upon solute redistribution during solidification.

A number of investigations[13,32-39] have been made of segregation in ferrous-alloys, notably medium carbon, low alloy steels; results for these steels are presented in Table VII. Results reported are for the common alloying elements (manganese, nickel, chromium, molybdenum, silicon, tungsten, and copper); impurity elements (sulfur, phosphorus, and arsenic) are excluded as well as less frequently encountered elements (tin, niobium). Average values of the segregation ratios are given in Figure 19 (along with the number of alloys in which the segregation ratio was determined and the range of composition for the applicable ratio). Figure 19 indicates that segregation ratios for manganese and nickel lie between 1 and 2 for all alloys examined. Segregation ratios for chromium and molybdenum are higher and show more scatter. The casting conditions of the various alloys investigated vary widely. Ingots ranged from 100 tons to laboratory size; structures included columnar and equiaxed zones; some material was solidified very rapidly; others slowly. In all ingots carbon was from 0.21 - 0.62 per cent and limits on composition of other elements are given in Figure 19.

The effect of carbon on various elements has not been examined thoroughly but Philibert et al[40] have indicated the importance of carbon on microsegregation of various elements in iron alloys. Carbon was found to affect the segregation of these elements, and

it was stated that the extent of this effect depended on the absolute value of thermodynamic interaction parameter of the third element with carbon in liquid iron. For example, carbon affects the segregation of arsenic more strongly than chromium and does not alter the segregation of nickel. This observation by Philibert et al[40], although perhaps valid, is not fundamental for understanding solute redistribution during solidification of iron-carbon-X alloys, as will be shown in later sections.

B. Analysis of Microsegregation

To describe the solute redistribution during solidification of multicomponent alloys material balances for each solute must be simultaneously obeyed. In the case at hand, the behavior of the two solutes, carbon and chromium, differ vastly during solidification. Carbon diffuses interstitially while chromium migrates as substitutional atoms; thus carbon could be expected to approach equilibrium in the solid much more closely than chromium.

Ingots and castings of alloys contain three zones during solidification, the extent of these zones depending on alloy analysis and thermal conditions. The zones are (1) completely solid, (2) partially solid and partially liquid, and (3) completely liquid. The redistribution of solute which is considered herein occurs within a unit volume situated in the liquid-solid zone as it passes from being completely liquid to completely solid. Also, the possibility

exists for diffusion in the solid after solidification while the casting cools to ambient temperature.

The assumptions used for developing expressions of solute redistribution during the dendritic solidification of alloys have been discussed in detail by Flemings[3], and Brody et al[16]. These assumptions are briefly outlined below:

1. Negligible undercooling before formation of solid.
2. Negligible interface supercooling from kinetic or curvature effects.
3. Equilibrium partition ratio applies at the interface.
4. Negligible constitutional supercooling.
5. No thermal gradient in the liquid.
6. No macroscopic mass flow.
7. Solidification proceeds, at a given point in a casting or ingot, by continuous advance of a liquid-solid interface (e.g., continuous thickening of dendrite arms).

Before the material balances are presented to describe solidification under various conditions, it is convenient to summarize what the afore-mentioned assumptions mathematically imply. For dendritic solidification as the solid forms within a unit volume, the liquid it encounters is uniform in composition and the equilibrium partition ratio applies at the interface. The equilibrium partition ratio may vary as solidification proceeds and the composition of the solid may or may not be uniform.

1. Equilibrium Solidification.

This case refers to complete diffusion of both solutes within the solid. For both solutes the material balance takes the form:

$$C_o = f_S C_S + f_L C_L \tag{9}$$

where: C_o = overall weight percentage of component

C_S, C_L = weight percentage of component in solid and liquid, respectively

f_S, f_L = weight fraction of solid and liquid, respectively

Differentiating (9), utilizing the partition ratio, and separating variables for subsequent integration from f_S' to f_S''.

$$-\int_{C_S'}^{C_S''} \frac{1}{1-k} \frac{dC_S}{C_S} = \int_{f_S'}^{f_S''} \frac{df_S}{1 + (k-1)f_S} \tag{10}$$

where: k = partition ratio = $\frac{C_S}{C_L}$

Integration for a small interval, so that k can be considered constant, yields

$$\frac{C_S''}{C_S'} = \frac{1 - (1-k)f_S'}{1 - (1-k)f_S''} \tag{11}$$

2. Normal Non-Equilibrium Solidification.

This material balance is written for no solid diffusion of either solute. For both components the increase of solute in the liquid equals the amount of solute partitioned at the interface.

$$f_L dC_L = (C_L - C_S^*)\, df_S \tag{12}$$

where: C_S^* = interface composition of solid, weight percentage

Integration from f_S' to f_S'', yields

$$\frac{C_S''}{C_S'} = \left[\frac{1 - f_S'}{1 - f_S''} \right]^{1-k} \tag{13}$$

3. Non-Equilibrium Solidification with Solid Diffusion.

This material balance has been derived by Brody[19] and is valid for limited diffusion of solute within the solid during solidification; this analysis is referred to in the following argument.

An additional term is added to equation (12) to account for the increase of solute in the solid due to diffusion. When this solute increase is taken into account, the material balance becomes:

$$(C_L - C_S^*)df_S = f_S d\bar{C}_S + f_L dC_L \tag{14}$$

where: $\bar{C}_S$ = average concentration of solid

The solute increase due to diffusion is equated to the flux at the interface:

$$f_S d\bar{C}_S = [\, D_S \nabla C_i \,]\, d\theta \tag{15}$$

where: ∇C_i = gradient at the interface in the solid

$d\theta$ = differential time element during which the solid composition increases by $d\bar{C}_S$

To simplify the analysis, diffusion is assumed one-dimensional (this assumption has some validity despite the complexity of dendritic geometry[3,16,19]), and the concentration gradient in the solid does not change significantly after the interface passes, i.e.,

$$\nabla C_i = \frac{dC_S^*}{dX_i} \tag{16}$$

where: X_i = position of the interface

For the assumed one-dimensional model,

$$f_S = \frac{2X_i}{d} \tag{17}$$

where, "d" is the dendrite arm spacing of two arms progressively solidifying towards each other.

Brody[19] has considered the interface to be a continuous function of time.

Parabolic $X_i = \lambda\sqrt{\theta}$ (18)

or

Linear $X_i = u\theta$ (19)

a. Parabolic Growth

Equation (14) becomes:

$$(C_L - C_S^*)df_S = \alpha f_S dC_S^* + (1 - f_S)dC_L \quad (20)$$

where, $$\alpha = \frac{2D_S}{\lambda^2} \quad (21)$$

Integrating (20) over a small interval of solidification so that D_S and the partition ratio are constant, we obtain:

$$\frac{C_S''}{C_S'} = \left[\frac{1 - (1 - \alpha k)f_S'}{1 - (1 - \alpha k)f_S''}\right]^{\left(\frac{1 - k}{1 - \alpha k}\right)} \quad (22)$$

b. Linear Growth

Equation (14) becomes:

$$(C_L - C_S^*)df_S = \alpha_L dC_S^* + (1 - f_S)dC_L \quad (23)$$

where $$\alpha_L = \frac{2D_S}{ud} \quad (24)$$

Again integrating over a small interval of solidification:

$$\frac{C_S''}{C_S'} = \left[\frac{1 + \alpha_L k - f_S'}{1 + \alpha_L k - f_S''} \right]^{1 - k} \tag{25}$$

Equations (22) and (25) show the effect of solid diffusion during solidification; both reduce to equation (13), normal non-equilibrium solidification, when $D_S = 0$. Thus the extent of diffusion in the solid depends upon α or α_L. By referring to their definitions (18) and (19), these parameters can be written as:

$$\alpha = \frac{8 D_S \theta_f}{d^2} \tag{26}$$

$$\alpha_L = \frac{4 D_S f}{d^2} \tag{27}$$

The effect of cooling rate on microsegregation can be seen if we combine (26) and/or (27) with the empirical relation that the dendrite arm spacing is proportional to a fractional power of the solidification time:

$$d = \gamma \theta_f^{\,n} \tag{28}$$

where: n, γ = constants

θ_f = solidification time

If $n = 1/2$,

$$\alpha = \frac{8D_S}{\gamma^2} \tag{29}$$

or

$$\alpha_L = \frac{4D_S}{\gamma^2} \tag{30}$$

And so in this case the extent of solid diffusion, in a given alloy, is independent of cooling rate.

The exponent, n, has been determined for aluminum and magnesium alloys to be 0.39 - 0.40[16,41]; for AISI 52100 steel n equals 0.62[42] and for iron-26 per cent nickel alloy n = 0.42[22]. Thus, because the exponent n approximately equals 1/2, the extent of microsegregation should not be very sensitive to cooling rate.

4. Diffusion in the Solid After Solidificaton.

A useful parameter for discussion of homogenization of microsegregation is δ_i, where:

$$\delta_i = \frac{C_M - C_m}{C_M^\circ - C_m^\circ} \tag{31}$$

where: δ_i = residual microsegregation index of component i

C_M = maximum solute concentration of component i at time θ

C_m = minimum solute concentration of component i at time θ

C_M° = maximum initial concentration of component i

C_m° = minimum initial concentration of component i

Before any homogenization has taken place, $\delta_i = 1$; after complete homogenization, $\delta_i = 0$. Regardless of the complexity of the model or initial solute distribution (but assuming dendrites of different arm spacings are geometrically similar, δ_i is a function only of the dimensionless group of variables, $D_S\theta_h/L^2$, where:

D_S = diffusion coefficient for solute

θ_h = homogenization time

L = segregate spacing

To describe the diffusion kinetics of homogenization, Fick's second law is used

$$\frac{\partial C}{\partial \theta} = D_S \nabla^2 C \qquad (32)$$

For a single phase alloy with "coring" no net gain or loss of solute occurs within a dendritic unit volume. Various geometric models have been considered to describe the solute concentration as a function of position in space. Poirier et al[14] developed expressions for parallel plate and spherical geometry, and Kattamis and Flemings[43] considered a two dimensional geometry. By comparing experimental results with diffusion models Poirier et al[14] concluded that for homogenizing AISI 52100 steel the one dimensional model was sufficient to describe the kinetics providing the segregate spacing, L was chosen as one-half the primary arm spacing.

For the one dimensional parallel plate model, the diffusion equation to be solved is:

$$\frac{\partial C}{\partial \theta} = D_S \frac{\partial^2 C}{\partial X^2} \tag{33}$$

with the boundary conditions,

$$\frac{\partial C}{\partial X} (0, \theta) = 0 \qquad \theta > 0 \tag{34}$$

$$\frac{\partial C}{\partial X} (L, \theta) = 0 \qquad \theta > 0 \tag{35}$$

and the initial condition,

$$C(X, 0) = f(X) \qquad 0 \leq X \leq L \tag{36}$$

The solution to this problem is presented by Crank[44] and is

$$C = A_o + \sum_{n=1}^{\infty} A_n \exp[-n^2\pi^2 \frac{D_S \theta}{L^2}] \cos \frac{n\pi X}{L} \tag{37}$$

where,

$$A_o = \frac{1}{L} \int_0^L f(X')dX' = \bar{C} \tag{38}$$

$$A_n = \frac{2}{L} \int_0^L f(X') \cos \frac{n\pi X'}{L} dX' \tag{39}$$

Recognizing that $C(0, \theta)$ is C_m in equation (31) and $C(L, \theta)$ is C_M, the following expression is developed for δ_i.

$$\delta_i = \frac{2 \sum_{n=1,3...odd}^{\infty} A_n \exp\left[-n^2\pi^2 \frac{D_S\theta_h}{L^2}\right] \cos\frac{n\pi X}{L}}{C_M^\circ - C_m^\circ} \tag{40}$$

The foregoing of course is applicable for a constant diffusion coefficient but the same expression can be used for non-isothermal conditions such as the diffusion that occurs in the solid during cooling after solidification. This can be seen if diffusion is allowed to occur in repeated steps rather than at one temperature for time, θ_h, i.e., to use equation (40), the dimensionless group $D_S\theta_h/L^2$ is replaced by $(D_S\theta/L^2)_{eff}$, the effective group for diffusion.

$$\left(\frac{D_S\theta}{L^2}\right)_{eff} = \sum_{n=1}^{N} \left(\frac{D_S\theta}{L^2}\right)_n \tag{41}$$

If the repeated diffusion intervals become infinitely small and a different diffusion coefficient applies for each step, then

$$\left(\frac{D_S\theta}{L^2}\right)_{eff} = \int_0^\theta \frac{D_S(\theta)}{L^2}\, d\theta \tag{42}$$

For castings equations (42) can be used for evaluating (40) because temperature is known as a function of time; hence $D_S(\theta)$ is known. To apply (42), $\theta = 0$, at the instant solidification is complete and the integral is evaluated until D_S becomes negligible.

The case of describing diffusion kinetics for two phase alloys has been treated by Brody and Flemings[45] using finite-difference

method. An analytic solution applicable to this problem could be developed for small amounts of second phase but is not considered here.

C. Solute Redistribution for Iron-1 Per Cent Carbon-1.5 Per Cent Chromium Alloys

In this section the solidification of the ternary alloy, iron-1 per cent carbon-1.5 per cent chromium is considered. This composition corresponds to the nominal composition of AISI 52100 steel which also contains some manganese and silicon. Calculations were performed for three cases of solidification based on the phase diagram presented in Figures 17 and 18.

1. Equilibrium Solidification of Both Carbon and Chromium, Case 1.

In this case the solid diffusion of both carbon and chromium is assumed complete. Therefore, equation (11) was applied to both solutes. Using computer techniques, the partition ratios of both carbon and chromium were allowed to vary according to the respective liquid compositions encountered during solidification.

2. Non-Equilibrium Solidification of Both Carbon and Chromium, Case 2.

In this case no diffusion of carbon and chromium is permitted in the solid; hence, equation (13) was applied to both solutes and as before the partition ratios were allowed to vary throughout solidification.

3. Equilibrium Solidification of Carbon and Non-Equilibrium Solidification of Chromium, Case 3.

In this case carbon is allowed to diffuse completely, whereas chromium does not diffuse at all in the solid. For carbon equation (11) was applied, and for chromium equation (13) was applied. Actually by using equation (11), carbon has a uniform concentration in the solid at any time during solidification. By stating that carbon diffuses completely, this is not actually true because the solid has a non-uniform distribution of chromium. A refinement of this model should account for the fact that an equilibrium profile for carbon in the solid would be such that the activity of carbon is uniform and not necessarily its composition.

The results of these calculations are presented in Figures 20 - 22, and in Figure 23 the fraction solidified as a function of temperature for all three cases is presented. Equilibrium solidification, Figure 20, of course results in no microsegregation and the solidification is completed at a higher temperature than in both non-equilibrium situations. The other extreme for solidification is when both carbon and chromium do not diffuse in the solid, Figure 21. In this case the liquid becomes so enriched in both solutes that it reaches a three phase equilibrium valley in the phase diagram ($L \rightarrow \gamma + [Fe,Cr]_3C$), see Figure 17. At this point equation (13) is no longer valid, and it is assumed that the eutectic solidifies with no undercooling. The final case, which seems the most reasonable for this particular alloy is

presented in Figure 22. It appears that this situation causes the chromium to segregate the most severely in the sense that the highest concentration of chromium is reached. This is not true in the sense that the only reason chromium did not go to higher concentrations in Figure 21 is that the eutectic valley was encountered. In Figure 22, the requirement of carbon equilibrium is such that the alloy solidifies before the cementite eutectic valley is reached by the interdendritic liquid. The chromium rises extremely rapidly in the last fractions of solidification; the interdendritic liquid may actually become so enriched that the peritectic reaction $L + \delta \rightarrow \gamma$ is encountered. However, the fraction solid involved with this reaction is extremely small, less than .003, and can be ignored, especially if limited diffusion of chromium in the solid is admitted.

4. Estimate of Diffusion in Solid

Equations (22) and (25) that take into account the effect of limited solid diffusion are quite useful in that they bring forth the dimensionless parameter, α (or α_L). The equations are not useful in the sense that they do not quantitatively indicate how the composition of the solid behind the interface changes. Depending upon which growth law, parabolic or linear, is chosen, the α factor is written:

$$\alpha = \frac{aD_S\theta_f}{d^2} \tag{43}$$

where, a = constant, 4 or 8

If $\alpha << 1$, diffusion in the solid is negligible

$\alpha >> 1$, diffusion in the solid is complete

By referring to Figure 23 the effect of solid diffusion for carbon and chromium can be indicated. The alloy starts to solidify at 1460°C and when fifty per cent of the alloy has solidified, the temperature must lie between those of the two extremes representations of solidification, i.e., 1420°C. From Figures 4 and 6, θ_f and d are evaluated for the material at 6.5 cm from the chill. As previously indicated, the amount of solid diffusion in a given alloy is almost insensitive to the cooling rate, so that any position from the chill may be considered.

From Figure 6, $d = 160 \times 10^{-4}$ cm and from Figure 4, $\theta_f = 650$, 860, or 1560 seconds depending on which solidus temperature is taken from Figure 23.

The diffusion coefficients of carbon[46] and chromium[47] in austenite are:

$$D_C = 0.12 \exp \left[- \frac{16,100}{T} \right] \tag{44}$$

$$D_{Cr} = 2.35 \times 10^{-5} \exp \left[- \frac{17,300}{T} \right] \tag{45}$$

With these relations and the above dendrite arm spacings and solidification times, at 1460°C

$$.010 < \alpha_{Cr} < .053$$

$$120 < \alpha_{C} < 610$$

and at 1420°C

$$.0081 < \alpha_{Cr} < .042$$

$$93 < \alpha_{C} < 490$$

Thus, diffusion of chromium is slight, and on the other hand, carbon can be considered to solidify in an equilibrium manner up to this point.

Again, referring to Figure 23 and projecting the idea that carbon diffuses completely, when 90 per cent of the alloy has solidified the temperature is now located between case 1 and case 3, i.e., 1360°C. At this temperature,

$$.0056 < \alpha_{Cr} < .038$$

$$65 < \sigma_{C} < 188$$

and again chromium still diffuses slightly, whereas carbon diffuses completely.

5. Comparison of Theory with Experiment.

The results of these calculations indicate that the solidification of iron-1 per cent carbon-1.5 per cent chromium alloy

occurs with complete diffusion of carbon and some diffusion of chromium in the solid. The amount of the alloy solidified as a function of temperature (Figure 23) is sensitive to the solid diffusion of chromium. However, the microsegregation of chromium is, of course, sensitive to the diffusion in the solid because the factor α indicates that the diffusion of chromium to be neither negligible nor complete. However, the microsegregation of chromium is almost independent of cooling rate.

The amount of diffusion that occurs after solidification depends on $[D_S\theta/L^2]_{eff}$ by equations (41) or (42) along with the cooling curves for the AISI 52100 unidirectional ingot (Figure 4). Referring to Figure 23, the non-equilibrium solidus is somewhere between 1283°C (case 3) and 1333°C (case 1). By converting the time-temperature data of Figure 4 into D_S versus θ for times between 1300°C and 700°C, the integral for equation (42) was determined at 1.7, 4.0, 6.5, 9.1, and 11.4 cm from the chill. For all positions from the chill, $[D_S\theta/L^2]_{eff} \cong .001$ and thus the amount of diffusion in the solid during cooling after solidification is independent of cooling rate. Also, when $[D_S\theta/L^2]_{eff}$ is compared to α_{Cr} which is the dimensionless parameter that applies during solidification, the amount of diffusion in the solid after solidification can be ignored. This may not be the case for steels with higher solidus temperature or with solutes with higher diffusion coefficients.

These results are confirmed experimentally in Table VI (Apparatus Chapter) where samples removed from the unidirectional ingot of AISI 52100 steel were analyzed with the microprobe analyzer. The minimum and maximum values of chromium compositions and the corresponding segregation ratios do not change appreciably with cooling rate. Minimum values all conform closely to that predicted by Figure 22 and the maximums are all below that of Figure 22. It is reasonable to see that limited diffusion of chromium in the solid would affect the microsegregation especially near the end of solidification where the diffusion of chromium up to this point has lessened the liquid concentration relative to that predicted by assuming no diffusion of chromium; also the partitioning effect of chromium tends to form a steep concentration gradient in the latter stages of solidification.

D. Effect of Carbon on the Microsegregation of Chromium

As previously mentioned, Philibert et al[40] reported that carbon influences the microsegregation of other solutes in iron alloys. The effect of carbon was found to be stronger, the greater the absolute value of the solute's interaction parameter for carbon. Such an effect, even if valid, only vaguely suggests carbon's role of influencing microsegregation of other elements. Understanding how one element may affect the other element requires knowledge of the phase equilibria between liquid and solid and an estimation of the diffusion that occurs in the solid. To do this an appropriate phase diagram must be considered. The phase diagram equilibria

yields partition ratios and temperatures which enter the suitable material balance as presented herein. Thus merely by knowing the interaction parameter, only the thermodynamics of the liquid phase is recognized as important. The thermodynamics of the solid phase and the ability of a solute to diffuse in the solid must also be considered to understand microsegregation.

1. Segregation Ratio of Chromium in the Presence of Carbon.

To demonstrate the role of carbon on the microsegregation of chromium, the six laboratory ingots of iron-1.5 per cent chromium alloys with carbon contents ranging from .96 to 3.00 per cent carbon were studied. The compositions, cooling rates during solidification, and dendrite spacings of these ingots are given in Table III. Microprobe analysis was performed for all six ingots; maximum and minimum concentrations of chromium were determined for specimens from all six ingots. In addition concentration profiles (weight per cent chromium versus volume fraction of material) were obtained for three of the alloys, namely, .96, 1.54, and 1.75 per cent carbon.

All alloys with the exception of the alloy leanest in carbon (.96 per cent) solidified with eutectic formation. This was evidenced metallographically as ledeburite; small amounts were observed in 1.54 per cent carbon alloy and the amounts increased as the carbon increased to 3.00 per cent. Cooling curves also

indicated the eutectic arrests during solidification except for .96 per cent carbon and the arrests increased with increasing carbon levels.

The segregation ratios for these alloys are presented in Figure 24 along with the chromium data of the low alloy steels in Table VII and the AISI 52100 unidirectional ingot of Table VI. For the data presented, the alloys solidify without formation of ledeburite up to approximately 1.5 per cent chromium. For these ledeburite-containing alloys, the segregation ratio is plotted for two different definitions: the upper curve defines the maximum concentration based on the chromium concentration in the carbide phase of the ledeburite; the lower is based on the average concentration of the ledeburite which represents the concentration of the last liquid to solidify.

The alloys of Figure 24 may be classified into three groups:

1. Up to approximately 0.5 per cent carbon, initially ferrite solidifies,
2. From 0.5 per cent to approximately 1.5 per cent carbon, only austenite forms during the solidification, and
3. When more than 1.5 per cent carbon is present, the alloys solidify as austenite with ledeburite forming as the liquid becomes enriched enough in carbon that the ledeburite-liquid eutectic valley is reached.

Thus, the segregation ratio increases as carbon increases until ledeburite forming alloys are reached where the segregation index decreases as carbon increases still more.

2. Concentration Profiles of Chromium in Iron-1.5 Per Cent Chromium Alloys Containing Carbon.

Calculations were made for the six alloys based on Case 3 solidification as previously defined. Based on these calculations, Figure 25 is constructed. In order to demonstrate the choice of this solidification model Figure 26 is presented where the extent of diffusion of carbon and chromium in the solid is estimated by the α factors. Choosing "a" equal to 6 in equation (43), and referring to Table III, the α factors are calculated for each alloy at the temperature corresponding to fifty per cent solid in Figure 25. For these alloys (.96 to 3 per cent carbon),

$$50 < \alpha_C < 150$$

$$.0045 < \alpha_{Cr} < .013$$

Thus diffusion of chromium is slight and carbon diffuses extensively for all six alloys.

Calculated concentration profiles for the three leanest alloys (.96, 1.54, and 1.75 per cent carbon) are compared with experimental profiles in Figures 27 - 29. Figure 27 (.96 per cent carbon, 1.48 per cent chromium) shows that the experimental measurements of

chromium contents are somewhat higher than the calculated curve for no diffusion of chromium up to a volume fraction of 0.8; above this coincident point, the calculated curve is somewhat higher. This is in complete accord with the fact that some solid diffusion of chromium does occur during solidification as discussed previously or may reflect inaccuracies in the phase diagram. The measured maximum was found to be 3.34 per cent chromium as apposed to approximately 4.5 per cent for the unidirectional ingot of AISI 52100. This could be attributed to the silicon and manganese in AISI 52100 as well as the somewhat higher chromium content (1.63 per cent chromium).

Figure 28 (1.54 per cent carbon, 1.45 per cent chromium) indicates very close agreement between the experimental curve and the theoretical curve up to approximately 0.7 volume fraction; the experimental curve is somewhat higher for remaining volume fractions except for the last .001 fraction. The area under the experimental curve yields an average composition somewhat greater than the overall composition of the alloy. This could be attributed to a statistically inadequate microprobe scan length; the statistical probable error limits almost put the two curves within experimental error.

Figure 29 (1.75 per cent carbon, 1.48 per cent chromium) again indicates good agreement between experiment and theory with some differences for the high volume fractions. Some diffusion of chromium during solidification appears evident. For all three alloys the exact value of the maximum chromium concentration at the end of

solidification is difficult to theoretically evaluate because the chromium concentrations asymptotically approach the volume fraction of unity. Experimentally the maximum is also difficult to determine in such situations where concentration gradients are steep in interdendritic areas. In such cases the segregation ratio loses some of its significance. The use of a segregation ratio is also lacking when the segregation tendency of an alloy that solidifies as a single phase is compared to an alloy that forms eutectic at the end of solidification. Thus, segregation ratios are really non-informative unless qualifications are presened with their use. A better parameter is one which depends upon the entire concentration profile, not merely the maximum and the minimum concentrations, and also indicates the alloys' deviation from the equilibrium state.

3. Segregation Deviation Parameter.

Consider the parameter defined as the average concentration deviation from the mean alloy concentration normalized by the mean concentration:

$$\sigma^m = \frac{1}{C_o} \int_0^1 |C - C_o| \, dV_f \qquad (46)$$

where: σ^m = segregation deviation parameter

V_f = volume fraction

C_o = mean concentration

C = concentration at a volume fraction, V_f

This parameter has the following properties. If there is no segregation, $\sigma^m = 0$; for maximum segregation the partition ratio equals zero and the alloy must solidify so that

$$C = 0 \qquad 0 \leq V_f < \left(1 - \frac{C_o}{C_M}\right)$$

$$C = C_M \qquad \left(1 - \frac{C_o}{C_M}\right) < V_f \leq 1$$

where: C_M = maximum concentration, and

$$\sigma^m = 1 - \frac{C_o}{C_M} \tag{47}$$

For alloys that are homogenized at a temperature such that the equilibrium state is a single phase, σ^m approaches zero with time. For alloys whose equilibrium state is two phases,

$$\sigma^m \longrightarrow \frac{2(C_o - C_\alpha)(C_o - C_\beta)}{C_o(C_\alpha - C_\beta)} \tag{48}$$

where: C_α, C_β = concentrations of the two equilibrium phases

To eliminate experimental difficulties in determining the exact concentration profile for the latter stages of solidification, equation (46) is written:

$$\sigma^m = \frac{2}{C_o} \int_0^{V_f^*} |C - C_o| \, dV_f \tag{49}$$

where: V_f^* = volume fraction at C equal to C_o

Thus the segregation deviation parameter and microprobe analyses of statistically long scans are more meaningful than the present use of segregation ratios because:

1. Concentration profiles can be experimentally determined and compared with theory,
2. Random microprobe scans eliminate the need for seeking maxima if σ^m is used as a measure of segregation,
3. σ^m is more meaningful than a segregation ratio because it depends on the entire concentration profile and not merely the concentration in the center of dendrites and in the interdendritic areas,
4. σ^m allows comparison of single phased and eutectic forming alloys, and
5. σ^m is a parameter that can be introduced into solutions of Fick's second law used to describe homogenization kinetics.

The segregation deviation index, σ^m, was calculated for all six alloys from the theoretical concentration profiles and plotted in Figure 30 with the experimental values derived from Figures 27-29. The theoretical curve shows carbon's effect on the segregation of chromium solely due to the phase diagram partition ratios. The experimental curve which lies somewhat lower reflects the same effect of carbon's role in partition ratios and in addition the reduction in segregation due to diffusion in the solid. Figure 26 indicates that as the carbon concentration is increased, the amount

of diffusion in the solid decreases. In the range considered the effect is not great because α decreases less than an order of magnitude.

4. Comparison of Experimental Segregation Ratios with Theoretical Segregation Ratios.

Segregation ratios for iron-1.5 per cent chromium alloys are shown in Figure 31 and compared with theoretical values calculated for Case 3 solidification. Those alloys for which theory predicts no formation of ledeburite have theoretical segregation ratios calculated using the chromium concentration corresponding to .99 volume fraction. It is necessary to select such a volume fraction because of the asymptotical behavior of chromium concentrations as previously discussed. For those alloys which theoretically reach the eutectic valley, the segregation ratio is defined as the composition of the eutectic liquid to the minimum chromium concentration. This eutectic liquid is the same as an average value of the ledeburite composition.

The theoretical segregation ratios are limited to the alloys studied within, i.e., alloys on the gamma-liquidus. For these alloys, the theoretical curve has the same general shape as the experimental curve but is lower, except at about one per cent carbon where the two are approximately the same.

The experimental curve is extended to zero per cent carbon with data from other investigators for alloys on the delta liquidus. With no carbon, iron-1.5 per cent chromium alloy does not segregate[48,40], and the segregation ratio is unity. Although these alloys were not studied herein, the lack of segregation is thought to be due to the high diffusivity of chromium in bcc iron. As the carbon content increases, the segregation ratio increases up to about 5 at 1.5 per cent chromium; with additional amounts of carbon, both the experimental and theoretical segregation ratios decrease.

As mentioned previously, alloys containing 1.54 per cent carbon and greater form ledeburite at the end of solidification. However, Figure 25 as well as Figure 31 indicate that if perfect diffusion of carbon in the solid exists, then no ledeburite should form until the carbon level is greater than 2 per cent. This discrepancy between theory and experiment may be largely due to the fact that carbon seeks a uniform activity rather than composition in the solid. Due to the chromium gradients that exist in the austenite carbon must not be uniform in composition because the activity of carbon depends upon the chromium concentration.

Equation C1 gives the activity of carbon:

$$\ln a_1 = \frac{A_0}{RT} + \frac{A_1}{RT}\left(\frac{X_1}{1 - X_1}\right) + \frac{A_2}{RT}\left(\frac{X_2}{1 - X_1}\right) + \ln\left(\frac{X_1}{1 - 2X_1}\right) \quad \ldots\ldots\ldots\ldots\ldots (50)$$

For small values of X_1, and approximating weight per cent-mole fraction conversions, the carbon differential that accomodates a given chromium difference in order to maintain a constant activity is approximately:

$$\frac{d\ \%\ C_1}{d\ \%\ C_2} = \frac{-.01\ A_2\ \%\ C_1}{.05\%\ C_1\ A_1 + RT} \qquad (51)$$

The effect is examined for the alloys that theoretically do not form ledeburite at a temperature corresponding to .90 per cent solid in Figure 25.

For .96 per cent carbon, $d\%C_1/d\%C_2 = 0$; 1.54 per cent carbon, .026; 1.75 per cent carbon, .037. This effect is negligible for the leanest alloy but is appreciable for the alloys of 1.54 per cent and greater. With a carbon gradient existing in the solid, the composition of the liquid is richer in carbon and a eutectic may form for a leaner carbon content than predicted by Case 3 solidification.

V. SUMMARY AND CONCLUSIONS

1. An analytical and experimental study has been made of solute redistribution in dendritic solidification of ternary iron-carbon-chromium alloys. Three possible cases of solidification were considered; all assumed uniform concentrations of carbon and chromium in the interdendritic liquid, and equilibrium at the solid-liquid interface. Case 1 solidification assumed further complete diffusion of both carbon and chromium in the solid; Case 2 solidification assumed no diffusion of either carbon or chromium in the solid; Case 3 solidification assumed no diffusion of chromium and complete diffusion of carbon in the solid.

2. Estimates of the extent of diffusion for carbon and chromium as well as microprobe analysis showed Case 3 to be the best of the three models for iron-1.5 per cent chromium with carbon contents between 0.96 per cent and 3.00 per cent.

3. Microprobe analyses were carried out to determine "Segregation Ratios", S, of chromium, and data from the literature were compiled which include segregation ratios of common alloying elements in medium carbon, low alloy steel.

4. An alternative measure of microsegregation to the "Segregation Ratio" was introduced. By the use of statistically long microprobe scans and a new parameter, σ^m, termed "Microsegregation Deviation",

more meaningful information could be gained. Advantages of describing microsegregation by σ_m rather than S include:

(a) σ_m is readily measured experimentally, and for many alloys (e.g., solid solutions) it is expected that measurements of σ_m will be more reliable than those of S.

(b) σ^m depends on all values of the concentration and not merely the minimum and maximum.

(c) For certain alloys (e.g., complete solid solutions) small amounts of diffusion in the solid may change S markedly, with relatively little effect on σ_m.

(d) σ^m allows comparison of single phased and eutectic forming alloys, and

(e) σ^m is a parameter that can be introduced into formulations of homogenization kinetics.

5. The solidification curves (fraction solid as a function of temperature) for iron-1.5 per cent chromium alloys containing carbon between 0.96 and 3.00 per cent have been calculated. Calculations for these alloys indicate that for carbon contents greater than about 2.1 per cent carbon, ledeburite will form at the end of solidification. Experimental results show that ledeburite forms in those alloys containing about 1.5 per cent carbon and greater.

6. The concentration profiles (chromium composition versus volume fraction of material) were calculated for three alloys of 1.5 per cent chromium and .96, 1.54, and 1.75 per cent carbon and compared directly with concentration profiles determined by the use of statistically long microprobe scans. Estimates of the extent of diffusion in the solid as well as comparison of the theoretical

and measured concentration profiles indicate that limited diffusion of chromium in the solid occurs during solidification.

7. Segregation ratios of chromium in iron-1.5 per cent chromium alloys were measured for six alloys containing 0.96 per cent to 3.00 per cent carbon. Measurements of other investigators at lower carbon contents were also used. The segregation ratio for chromium was found to increase from unity (i.e., no microsegregation) at zero per cent carbon to about 4.5 to 5 at 1.5 per cent carbon; with higher concentrations of carbon the segregation ratio decreased to about 3 for three per cent carbon. Theoretically derived segregation ratios between 0.96 and 3.00 per cent carbon showed the same general dependence of carbon on the segregation ratio; however, the theoretical values were lower except at one per cent carbon.

8. The segregation deviation parameter, σ^m, was calculated for six iron-1.5 per cent chromium alloys containing 0.96 per cent to 3.00 per cent carbon based on the respective theoretical concentration profiles. The segregation deviation parameter was also calculated for the three experimental concentration profiles with carbon contents of 0.96, 1.54 and 1.75 per cent carbon, respectively. Theoretical values of σ^m increased from 0.22 at 0.96 per cent carbon to .35 at 1.75 per cent carbon and then decreased to .16 at 3.00 per cent carbon. The three experimental values were somewhat lower (15 to 30 per cent lower) because of limited diffusion of chromium in the solid.

9. To explain the occurrence of ledeburite in alloys containing as little as 1.5 per cent chromium when theory predicts that ledeburite should not be detected until about 2.1 per cent carbon is present, the assumption that carbon maintains a uniform concentration in the solid was examined. Due to the chromium gradients that exist in the austenite during solidification, carbon could not be uniform in composition. The high diffusivity of carbon must lead, instead, to a uniform activity of carbon resulting in average carbon compositions in solid being lower than its solid interface composition. Hence the liquid phase is richer in carbon than predicted by the theory, and this effect was thought to be largely responsible for this discrepancy between theory and experiment.

10. Fundamental to the study of microsegregation is the knowledge of the equilibria between liquid and solid. For this reason the study of solidification was preceded by the determination of the austenite-liquidus equilibria for the iron-carbon-chromium system. Results of this study include:

(a) The gamma-liquidus surface was determined for iron-carbon-chromium alloys containing up to twenty per cent chromium.

(b) An experimental method was devised to measure the solid-liquid equilibria partition ratios in a ternary system. The method should be applicable to measure the equilibria of any element in multicomponent systems that can be measured with a microprobe analyzer. Specifically, the partition ratio was measured for chromium in iron-carbon-chromium alloys between austenite and liquid iron.

(c) Using data from the literature concerning the thermodynamics of the iron-carbon-chromium system, and the chromium equilibrium measurements between austenite and liquid, the activities of carbon, chromium, and iron were determined as functions of composition and temperature for both liquid and austenite.

(d) The austenite solidus surface was determined based on the thermodynamic study. A presentation for ternary systems was devised to represent two-phase equilibria other than the customary manner of presenting a series of isotherms with tie lines.

VI. SUGGESTIONS FOR FURTHER WORK

1. The solidification model should be extended to include a finite difference solution to diffusion in the solid during solidification. A mass balance must be incorporated into such a solution; this mass balance should account for the fact that carbon seeks a uniform activity in the solid rather than a uniform concentration.

2. In the literature data exist for the thermodynamics of other iron-carbon ternary solutions of austenite and liquid iron. Comprehensive reviews of such data should be made in order to develop the equilibria between solid and liquid phases. In this way, analysis of the solidification of other ternary systems can be made.

3. Analyses of problems associated with solute redistribution during solidification should be made. These would include heat flow, formation of inclusions, and macrosegregation during solidification; also, casting phenomena such as hot tearing and fluidity characteristics of alloys may be better evaluated. All these factors should be taken into account in order to design processes for metals and develop new alloys.

4. Microsegregation measurements should include concentration profiles and segregation deviation parameters in addition to segregation ratios. Such measurements could be of immediate

practical importance, explaining ingot and casting properties and predicting heat treatment requirements. The technique for measuring concentration profiles could be readily standardized and data could be reduced easily by computer techniques.

5. Solidification studies should be made for the large class of steels that solidify as ferrite.

REFERENCES

1. Scheil, E. "Bermurkingen zur Schichtkristalbildung", Z. für Metal., 34, 1942, p. 70.

2. Pfann, W. G., Zone Melting, John Wiley, New York, 1958, p. 10.

3. Flemings, M. C., "Microsegregation in Castings and Ingots", Hoyt Memorial Lecture, Trans. AFS, 72, 1964, p. 353.

4. Beckius, K., Flemings, M. C., and Taylor, H. F., "A Study of Hot Tearing in Steel Castings", SFSA, J. of Steel Castings Research, October, 1960, p. 1.

5. Rosenberg, R. A., Flemings, M. C., and Taylor, H. F., "Hot Tearing in Non-Ferrous Binary Alloys", Trans. AFS, 68, 1960, p. 518.

6. Niesse, J. E., Flemings, M. C., and Taylor, H. F., "Application of Theory to Understanding Fluidity of Metals", Trans. AFS, 67, 1959, p. 685.

7. Flemings, M. C., "Fluidity of Metals", Transactions 30th International Foundry Congress, Prague, 1963, p. 61.

8. Lavender, J., and Jones, F., "An Investigation of Banding", JISI, 163, 1949, p. 14.

9. Jatczak, C. F., Giradi, D. J., and Rowland, E. S., "On Banding in Steel", Trans. ASM, 48, 1956, p. 279.

10. Bastein, P. G., "Formation of Banded Structures", JISI, 187, 1957, p. 281.

11. Ward, R. G., "The Dendritic Segregation of Manganese in Steel Ingots", JISI, 188, 1958, p. 337.

12. Nield, B. J., "Investigation of Abnormal Structure in a 1.5% Mn Mild Steel", JISI, 199, 1961, p. 22.

13. Smith, T. B., Thomas, J. S., and Goodall, R., "Banding in a 1-1/2% Nickel-Chromium-Molybdenum Steel", JISI, 209, 1963, p. 602.

14. Poirier, D. R., Polich, R. F., and Flemings, M. C., "Development of Superior Steels for Precision Gyro Spin Bearings", MIT, Contract No. AF33(615)-1030, Wright-Patterson Air Force Base, Ohio, 1964.

15. Flemings, M. C., and Nereo, G. E., "Macrosegregation", 95th AIME Annual Meeting, New York, 1966.

16. Brody, H. D., Bower, T. F., and Flemings, M. C., "Measurements of Solute Redistribution in Dendritic Solidification", Trans. AIME, to be published.

17. Flemings, M. C., and Taylor, H. F., "Adapting Theory to Practice in the Manufacture of Light Alloy Castings", Transactions 25th International Foundry Congress, Brussels, 1958, p. 149.

18. Stonebrook, E. E., and Sicha, W. E., "Correlation of Cooling Curve Data with Casting Characteristics of Aluminum Alloys", Trans. AFS, 57, 1949, p. 489.

19. Brody, H. D., "Solute Redistribution in Dendritic Solidification", Doctor of Science Thesis, Department of Metallurgy, MIT, 1965.

20. Koump, V., and Tien, R. H., "Growth of the Mushy Zone During One-Dimensional Solidification of Alloys", 95th AIME Annual Meeting, New York, 1966.

21. Adams, C. M., "Thermal Considerations in Freezing", Liquid Metals and Solidification, American Society of Metals, Cleveland, 1958, p. 187.

22. Barone, R. V., Brody, H. D., and Flemings, M. C., "Investigation of Solidification of High-Strength Steel Castings", MIT, Contract No. DA-19-020-AMC-5443(X), U.S. Army Materials Research Agency, Watertown, Massachusetts, 1964.

23. Barone, R. V., "Redistribution of Solute in Iron Based Alloys", Doctor of Science Thesis, Department of Metallurgy, MIT, 1966.

24. Turkdogan, E. T., "Causes and Effects of Deoxidation Occurring During Cooling and Solidification of Steel", Trans. AIME, 233, 1966, p. 2100.

25. Austin, C., "Alloys in the Ternary System Fe-Cr-C", JISI, 108, 1923, p. 235.

26. Kinzel, A. B., and Crafts, W., The Alloys of Iron and Chromium, McGraw-Hill, New York, 1937, p. 65.

27. Griffing, N. R., Forgeng, W. D., and Healy, G. W., "C-Cr-Fe Liquidus Surface", Trans. AIME, 224, 1962, p. 148.

28. Ziebold, T. O., and Ogilvie, R. E., "An Empirical Method for Electron Microanalysis", Anal. Chem., 36, 1964, p. 322.

29. Hilliard, J. E., and Cahn, J. W., "An Evaluation of Procedures in Quantitative Metallography for Volume-Fraction Analysis", Trans. AIME, 221, 1961, p. 344.

30. Benz, M. G., and Elliott, J. F., "The Austenite Solidus and Revised Iron-Carbon Diagram", Trans. AIME, 221, p. 323.

31. Adcock, F., "The Chromium-Iron Constitutional Phase Diagram", JISI, 124, 1931, p. 99.

32. Philibert, J., and Bizouard, H., "Quelques Nouvelles Applications de la Microsonde Électronique de Castaing et leur Importance Practique", Mémoires Scientifiques de la Revue de Metallurgie, 56, 1959, p. 187.

33. Crussard, C., Kohn, A., de Beaulieu, C., and Philibert, J., "Etude de la Ségrégation de l'As et du Cu Parla Technique Autoradiographique et Examen Quantitatif à la Microsconde de Castaing", Rev. Met., 56, 1959, p. 395.

34. Steven, W., and Thorneycroft, D. R., "Variations of Transformation Characteristics within Samples of an Alloy Steel", JISI, 187, 1957, p. 15.

35. "Investigation of Solidification of High Strength Steel Castings", Casting and Solidification Section, MIT, Contract No. DA-19-020-ORD-5443(X), U.S. Army Materials Research Agency, Watertown, Mass., 1963.

36. Zhurenkov, P. M., and Golikov, I. N., "Dendritic Liquation of Alloyed Elements in Structural Steels", Metal Sci. Heat Treat Metals, No. 5-6, 1964, p. 293.

37. Ahearn, P. J., and Quigley, F. C., "Mass Effect and Microsegregation in a High Strength Steel Casting", Modern Castings, 47, 1964, p. 435.

38. de Beaulieu, C., and Philibert, J., "Etude Quantitative de l'hétérogéneité Dendritique dans les Alliages de Fer", Comptes Rendus, 246, 1958, p. 3615.

39. Colling, D. A., Ahearn, P. J., and Flemings, M. C., "Effect of Solidification Variables on Mechanical Properties of Cast Steel", Trans. AFS, 70, 1962, p. 1083.

40. Philibert, J. Weinryb, E., and Ancey, M., "A Quantitative Study of Dendritic Segregation in Iron-Base Alloys with the Electron Probe Microanalyser", Metallurgia, November 1965, p. 203.

41. Holmberg, U. T., "The Effect of Grain Size on Cast Structure", Master of Science Thesis, Department of Metallurgy, MIT, 1966.

42. Polich, R. F., "The Effect of Cooling Rate on the Structure of AISI 52100 Steel", Master of Science Thesis, Department of Metallurgy, MIT, 1965.

43. Kattamis, T. Z., and Flemings, M. C., "Dendrite Morphology, Microsegregation, and Homogenization of Low Alloy Steel", Trans. AIME, 233, 1965, p. 992.

44. Crank, J., The Mathematics of Diffusion, Oxford University Press, London, 1957, p. 58.

45. Brody, H. D., and Flemings, M. C., "Solute Redistribution in Dendritic Solidification", to be published, Trans. AIME.

46. Wells, C., and Mehl, R. F., "Rate of Diffusion of Carbon in Austenite in Plain Carbon, in Nickel and in Manganese Steels", Trans. AIME, 140, 1940, p. 279.

47. Peterson, N. L., "Diffusion in Refractory Metals", WADD Technical Report 60-793 (AMR-1107), 1960, p. 117.

48. Barone, R. V., Department of Metallurgy, MIT, private communication.

49. Smith, R. P., "Equilibrium of Iron-Carbon Alloys with Mixtures of $CO-CO_2$ and CH_4-H_2", JACS, 68, 1946, p. 1163.

50. Schenck, H., and Kaiser, H., "Untersuchungen über die Aktivität des Kohlenstoffs in kristallisierten binären und ternären Eisen-Kohlenstoff-Legierungen", Archiv für das Eisenhüttenwesen, 31, 1960, p. 227.

51. Scheil, E., Schmidt, T., and Wünning, J., "Ermittlung der Gleichgewichte von Kohlenoxyd-Kohlensäure-Gemischen mit dem γ-Mischkristall, mit Zementit und mit Graphit", Archiv für das Eisenhüttenwesen, 32, 1961, p. 1.

52. Bundgardt, K., Preisendanz, H., and Lehnert, G., "Einfluss von Chrom auf den Aktivitätsverlauf von Kohlenstoff im System Eisen-Chrom-Kohlenstoff bei 1000°C", Archiv für das Eisenhüttenwesen, 35, 1964, p. 1.

53. Rist, A., and Chipman, J., "Activity of Carbon in Liquid Iron-Carbon Solutions," The Physical Chemistry of Steelmaking, Technology Press and John Wiley, New York, 1958, p. 3.

54. Richardson, F. D., and Dennis, W. E., "Thermodynamic Study of Dilute Solutions of Carbon in Molten Iron", Trans. Faraday Soc., 49, 1953, p. 171.

55. Kirkaldy, J. S., and Purdy, G. R., "The Thermodynamics of Dilute Ternary Austenite Solutions", Canadian J. of Physics, 40, 1962, p. 202.

56. Elliott, J. F., Gleiser, M., and Ramakrishna, V., Thermochemistry for Steelmaking. (II), Addison-Wesley, Reading, Mass., 1963, p. 788.

57. Ibid., p. 503.

58. Ohtani, M., "On the Activities of Cr and C in Molten Fe-Cr-C Alloys", Tetsu to Hagane, 42, 1956, p. 1095.

59. Fuwa, T., and Chipman, J., "Activity of Carbon in Liquid-Iron Alloys", Trans. AIME, 215, 1959, p. 708.

60. Richardson, F. D., and Dennis, W. E., "Effect of Chromium on the Thermodynamic Activity of Carbon in Liquid Iron", JISI, 175, 1953, p. 257.

61. Goto, K., Ban-ya, S., Matoba, S., "Activity of Carbon and Oxygen in Molten Iron-Nickel and Iron-Chromium Alloys", Tetsu to Hagane, 49, 1963, p. 138.

62. Chipman, J., private communication.

63. Ban-ya, S., and Matoba, S., "The Effect of Si, Cr and Mn on the Equilibrium of Carbon and Oxygen in Molten Iron Saturated with Carbon (II)", Technology Reports, Tohoku Univ., 22, 1957, p. 97.

64. Sanbongi, K., Ohtani, M., and Toita, K., "On The Effect of Alloying Elements on the Solubility of Carbon in Molten Iron", Sci. Repts. Research Inst. Tohoku Univ., 9, 1957, p. 147.

65. Neumann, F., Schenck, H., and Patterson, W., "Eisen-Kohlenstoff-Legierungen in thermodynamischer Betrachtung", Giesserei, 23, 1959, p. 21.

66. Kirkaldy, J. S., and Brigham, R. J., "The Interaction Parameter for Solutions of Carbon and Chromium in Austenite at 1000°C", Trans. AIME, 227, 1963, p. 538.

67. Brown, L. C., and Kirkaldy, J. S., "Carbon Diffusion in Dilute Ternary Austenites", Trans. AIME, 230, 1964, p. 223.

68. Wagner, C., Thermodynamics of Alloys, Addison-Wesley, Reading, Mass., 1952, p. 18.

69. Jeannin, Y., Mannerskantz, C., and Richardson, F. D., "Activities in Iron-Chromium Alloys", Trans. AIME, 227, 1963, p. 300.

70. Kubaschewski, O., and Heymer, G., Acta Met., 8, 1960, p. 416.

BIOGRAPHICAL NOTE

David Robert Poirier was born May 15, 1938 in Somerville, Massachusetts and recieved his secondary school education at Medford High School in Medford, Massachusetts. He attended Northeastern University and recieved a Bachelor of Science degree in Chemical Engineering in June 1961. As an undergraduate, the author maintained a cooperative job for the Casting and Solidification Section, Department of Metallurgy at the Massachusetts Institute of Technology. In September 1961, he started graduate study at M.I.T. and recieved a Master of Science degree in Metallurgy in June 1963. While working for this degree the author recieved the Foundry Educational Foundation-Wheelabrator Fellowship. The author began to work on the Doctor of Science Degree in Metallurgy in September 1963. During this period, he recieved a Howard F. Taylor Scholarship. The author has recieved an appointment as an Assistant Professor in Metallurgy for the Department of Minerals and Metallurgical Engineering, University of Wisconsin.

The author is a member of the Metallurgical Society of A.I.M.E., American Society for Metals, American Foundrymen's Society, and the American Institute of Chemical Engineers. He has co-authored reports for the Air Force Systems Command: "Effect of Processing Hisotry on Fracture of Materials at High Strength Levels", September, 1963. "Development of Superior Steels for Precision Gyro Spin Bearings", August, 1964. "Effects of Processing History on Fracture at High Strength Levels", November, 1964.

TABLE I

ANALYSES OF CHARGE MATERIALS

	% C	% Mn	% W	% P	% S	% Si	% Ni	% Cr	% Mo	% V	% Co	% u
Iron, Ferrovac E Crucible Steel	.005	.001	.02	.003	.006	.006	.021	.010	.001	.004	.01	.006
Chromium, Elchrome VG Union Carbide	.05	.02	-	.001	.01	.04	.001	99.35	-	-	.001	.003
Graphite, Grade AUC National	<0.08 % ash residue											

TABLE II

ANALYSES OF HEATS FOR LIQUIDUS TEMPERATURES

Heat	% C	% Cr	% Cr/% Fe	Liquidus Temperature, °C
1	3.26	4.23	.0457	1270
2	3.08	4.01	.0432	1280
3	2.82	3.15	.0335	1318
4	3.13	8.16	.0920	1270
5a	.75	5.09	.0541	1468
b	1.62	5.02	.0538	1396
c	2.02	5.08	.0547	1366
d	2.45	4.87	.0525	1331
e	3.05	5.01	.0545	1279
f	3.61	4.96	.0542	1230
g	4.03	4.91	.0539	1174
			.0542 Avg.	

TABLE III

EXPERIMENTAL CONDITIONS FOR DETERMINING THE EFFECT OF CARBON ON THE MICROSEGREGATION OF CHROMIUM

Heat Number	Melt Analyses % C	% Cr	Solidification Interval Cooling Rate, °C/second	Dendrite Element Spacing, μ
6	3.00	1.44	.91	55
7	2.32	1.48	1.03	72
8	2.01	1.49	.94	84
9	1.75	1.48	.89	70
10	1.54	1.45	.92	72
11	0.96	1.48	.87	87

TABLE IV

ANALYSIS OF AISI 52100 UNIDIRECTIONAL INGOT

Heat Number	% C	% Cr	% Mn	% Si	% S	% P
12	1.02	1.63	0.47	0.60	.008*	.004*

* Typical values, using electrolytic iron, obtained in the M.I.T. Solidification Laboratory.

TABLE V

AUSTENITE-LIQUID EQUILIBRIA OF CHROMIUM IN Fe-C-Cr ALLOYS

Heat Number	Time of Run, hrs.	Set-Point Temperature, °C	Liquid Composition % C	Liquid Composition % Cr	Solid Composition % Cr
Interface Heats					
13	3	1430	1.64	1.85	1.37
14	2	1412	2.08	2.52	1.68
15	2-3/4	1340	2.46	3.02	2.19
16	3	1300	2.86	4.25	3.50
Solid-Liquid Heats					
17	2-3/4	1270	3.26	4.23	2.54
18	3/4	1450	1.25	1.60	.99
19	2-1/2	1270	3.13	8.16	5.74
20	3	1320	2.62	4.32	3.08

TABLE VI

MICROSEGREGATION OF CHROMIUM IN AISI 52100
UNIDIRECTIONAL INGOT

Distance from Chill, Inches	Minimum % Cr, $C°_m$	Maximum % Cr, $C°_M$	Segregation Ratio $S = C°_m/C°_M$
1/2	1.2	4.6	4.0
2	1.2	4.8	4.1
3-1/2	1.0	4.3	4.3
5	1.0	4.2	4.0

TABLE VII

SUMMARY OF MICROSEGREGATION MEASUREMENTS IN MULTICOMPONENT CARBON STEELS

	Ingot Composition, Weight Per Cent							Segregation Ratio*, S°					
Reference	C	Mn	Si	Ni	Cr	Mo	Others	Mn	Ni	Cr	Mo	Others	Remarks
32	.24	.53	.30	2.5	.65	.27	-	-	1.2-1.3	2	7	-	Columnar and equiaxed zones
33	.44	.65	.35	-	-	-	.57(Cu)	1.6	-	-	-	1.4(Cu)	Columnar, bottom of ingot
32	.35	.50	-	2.5	.66	.29	-	-	1.3	1.9	7.3	-	100 ton ingot
34	.38	.60	.20	1.35	.99	.24	-	1.1	1.2-1.4	1.4-1.5	-	-	Columnar and equiaxed zones
13	.30	.37	.13	1.51	.97	.27	-	-	1.1-1.3	1.2-1.5	-	-	Edge and center of ingot, columnar and equiaxed
13	.35	.09	.08	1.48	1.02	.33	-	-	1.1-1.3	1.2-1.4	-	-	Edge and center of ingot, columnar
13	.36	.58	.48	1.49	1.05	.28	-	-	1.4	1.7	-	-	Edge and center of ingot, equiaxed
35	.40	.70	.30	1.80	.80	0.25	-	1.4-1.8	1.1-1.3	1.5-2.4	-	-	Columnar, 1.7 to 5.7 inches from chill
36	.21	-	-	4.03	1.45	-	.75(W)	-	1.2	1.4	-	1.6(W)	2.9 ton ingot
36	.21	.93	-	-	1.22	-	-	1.4	-	1.4	-	-	3.6 ton ingot
36	.23	-	.40	-	3.13	-	-	-	-	1.4	-	-	2.6 ton ingot
36	.42	-	-	-	1.55	-	-	-	-	1.9	-	-	2.9 ton ingot
36	.42	.68	-	-	1.0	-	-	1.6	-	1.9	-	-	3.6 ton ingot
36	.45	1.50	-	-	-	-	-	1.5	-	-	-	-	4.6 ton ingot
37	.31	.84	.35	2.79	0.79	.53	-	1.4-1.5	1.2-1.3	1.3-1.5	3.7-4.0	-	Columnar, 0 - 3-1/2 inches from chill
38	.36	1.30	-	-	-	.5	-	1.6	-	-	6.8	-	
38	.47	-	-	-	.50	-	-	-	-	4	-	-	2.2 pound ingot cooling rate 4°C/minute
38	.62	.51	-	-	-	-	-	1.6	-	-	-	-	
39	.40	1.85	1.29	1.75	.83	.28	-	1.4-1.6	1.4-1.6	1.4-1.5	-	1.5-1.7(Si)	8 inch diameter ingot
32	.46	-	-	1.48	-	-	-	-	1	-	-	-	

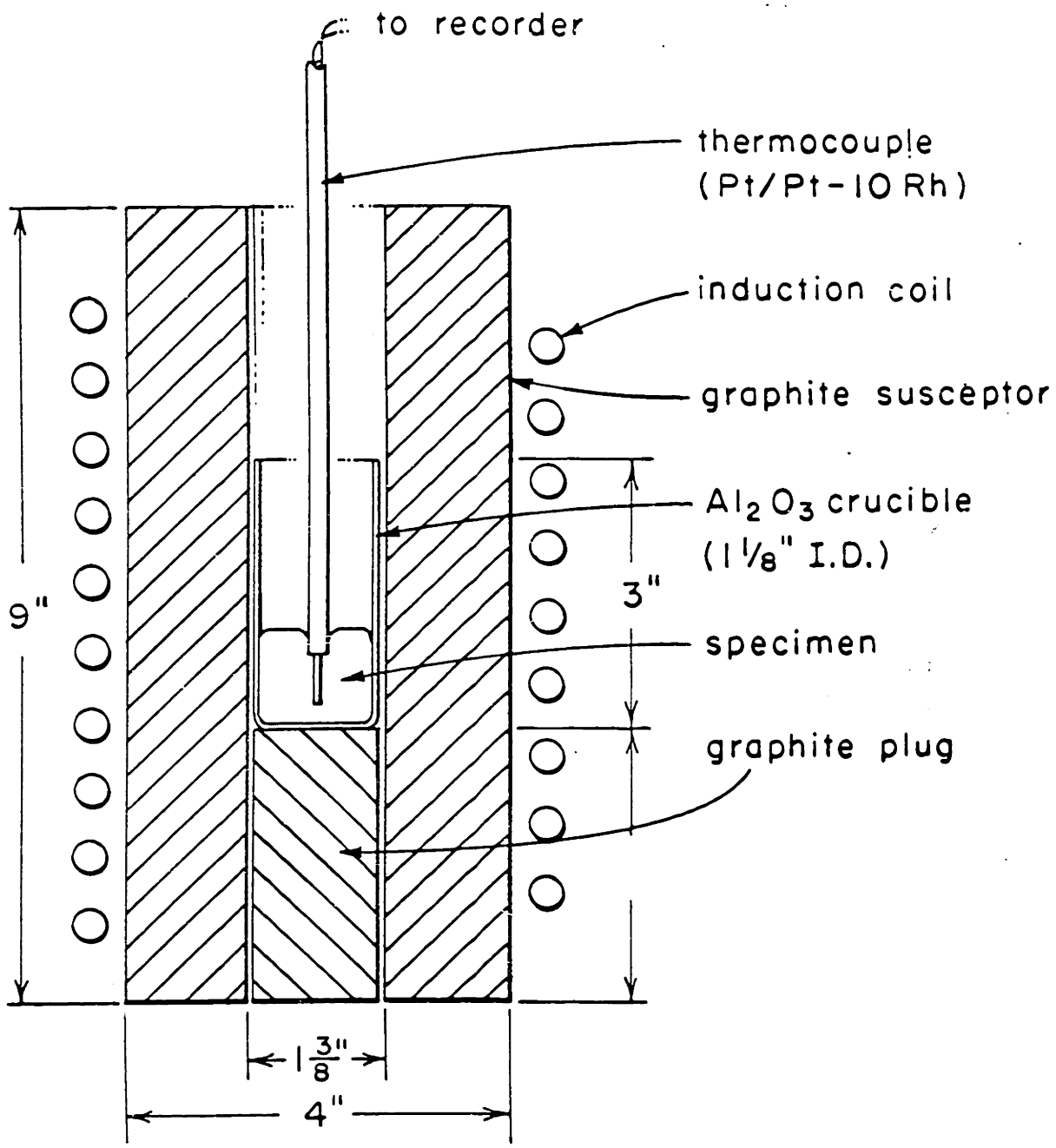

Figure 1: Assembly used for cooling curves of small melts.

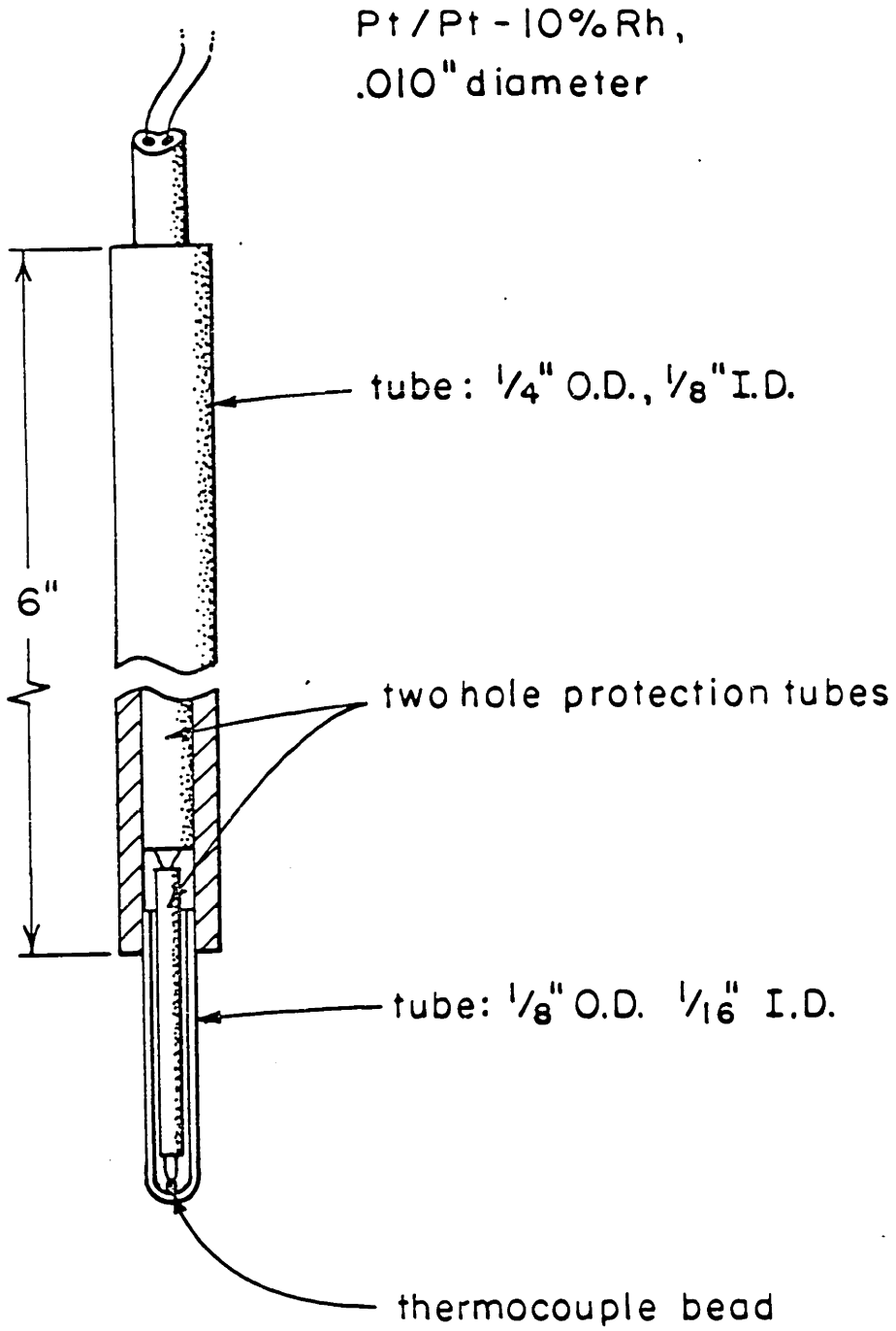

Figure 2: Thermocouple assembly for liquidus temperature measurements.

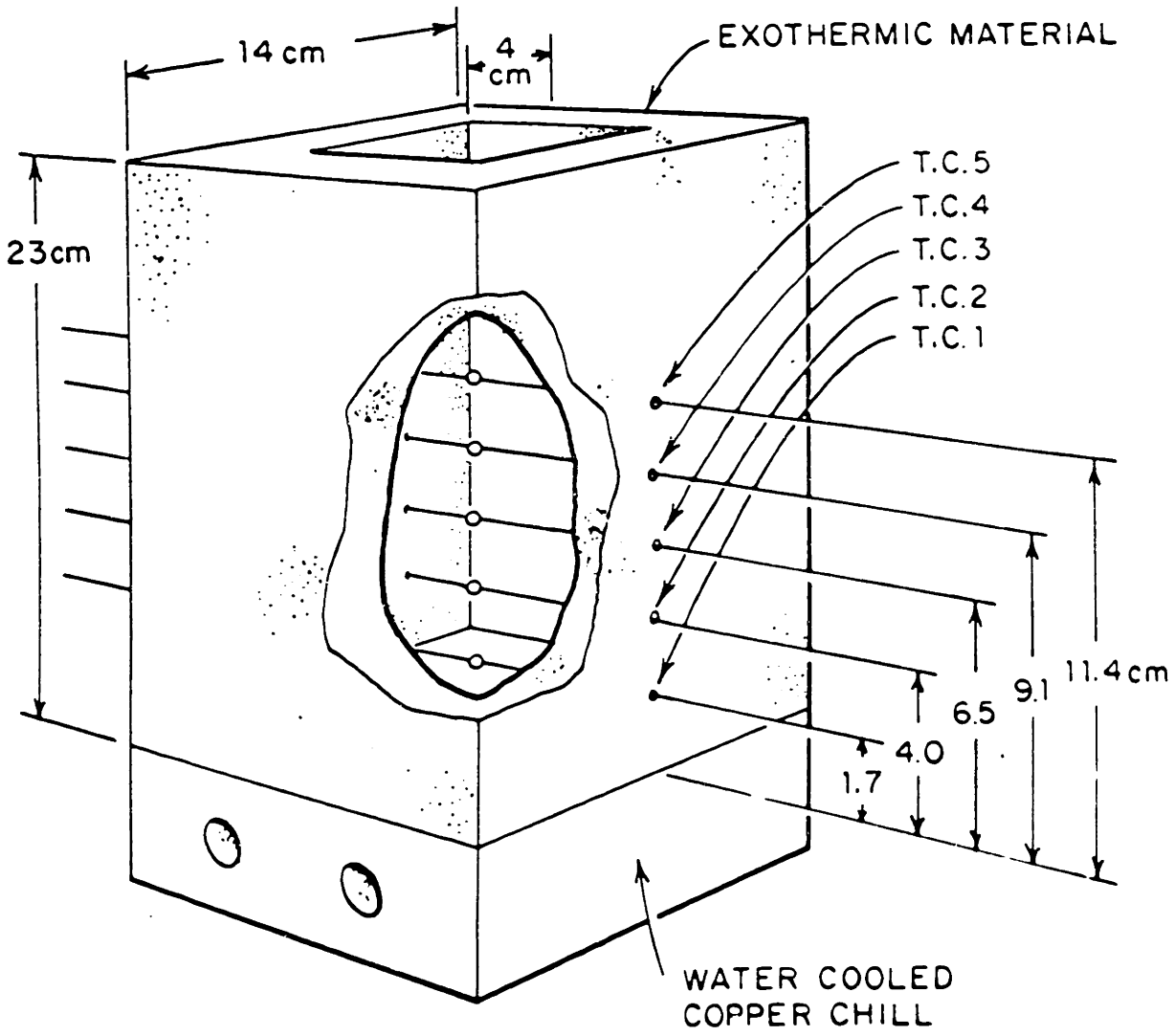

Figure 3: Mold for producing unidirectional ingot. Shown are locations of thermocouples used to obtain cooling curves.

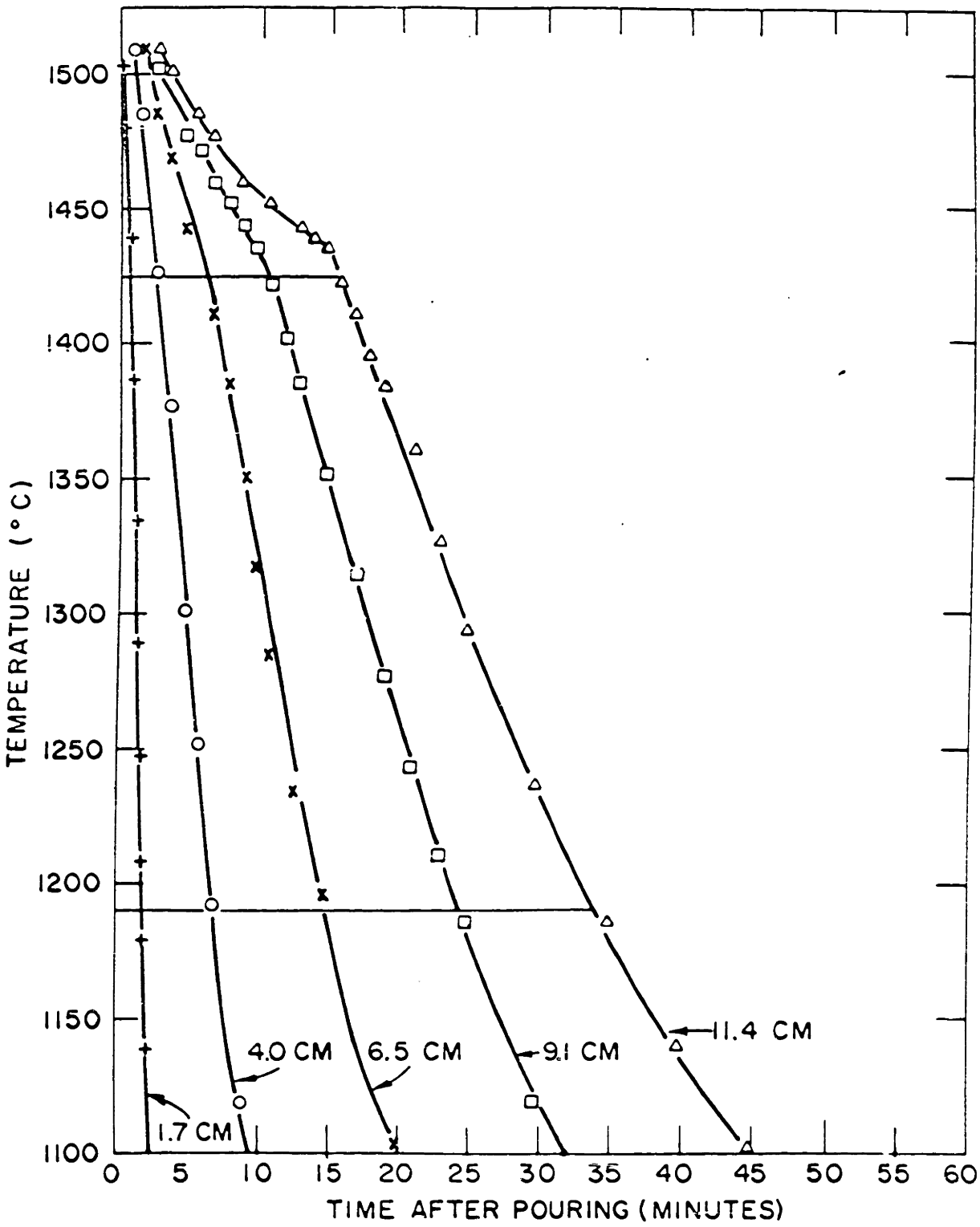

Figure 4: Cooling curves for the unidirectionally solidified 52100 ingot.

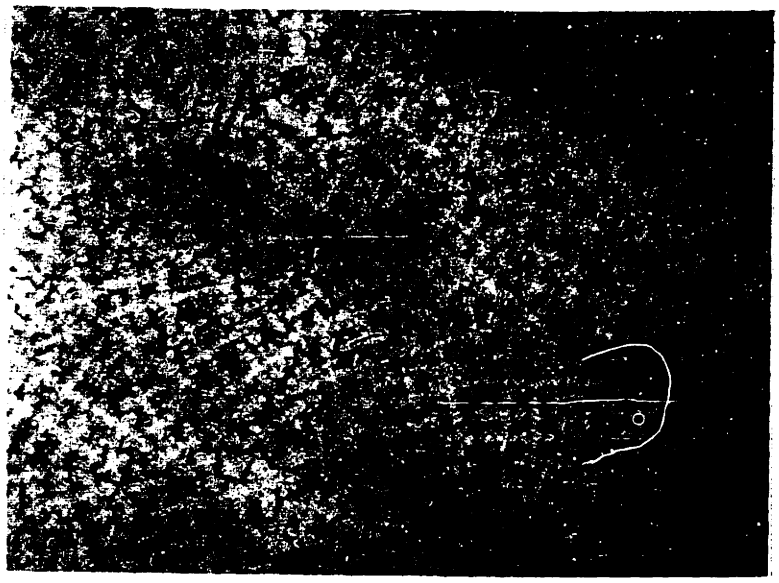

(a)

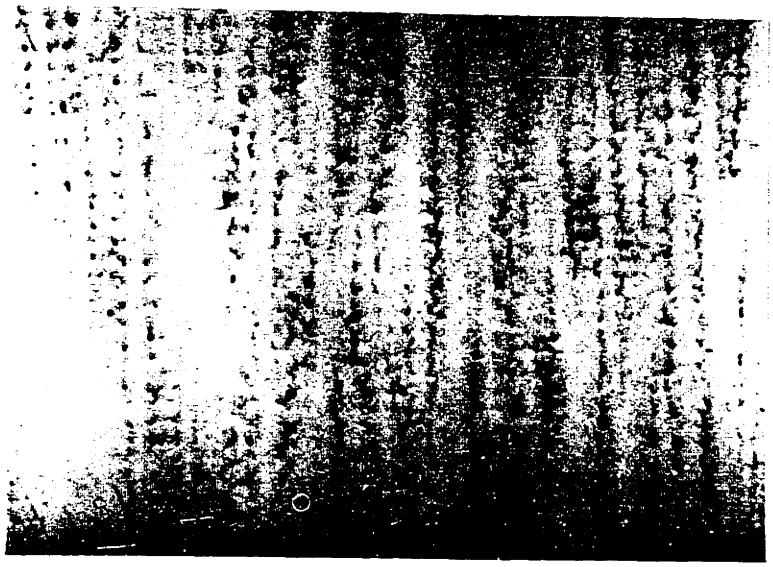

(b)

Figure 5: Dendritic structure of 52100 unidirectional ingot two inches from the chill.

(a) perpendicular to heat flow, 12X
(b) parallel to heat flow, 12X

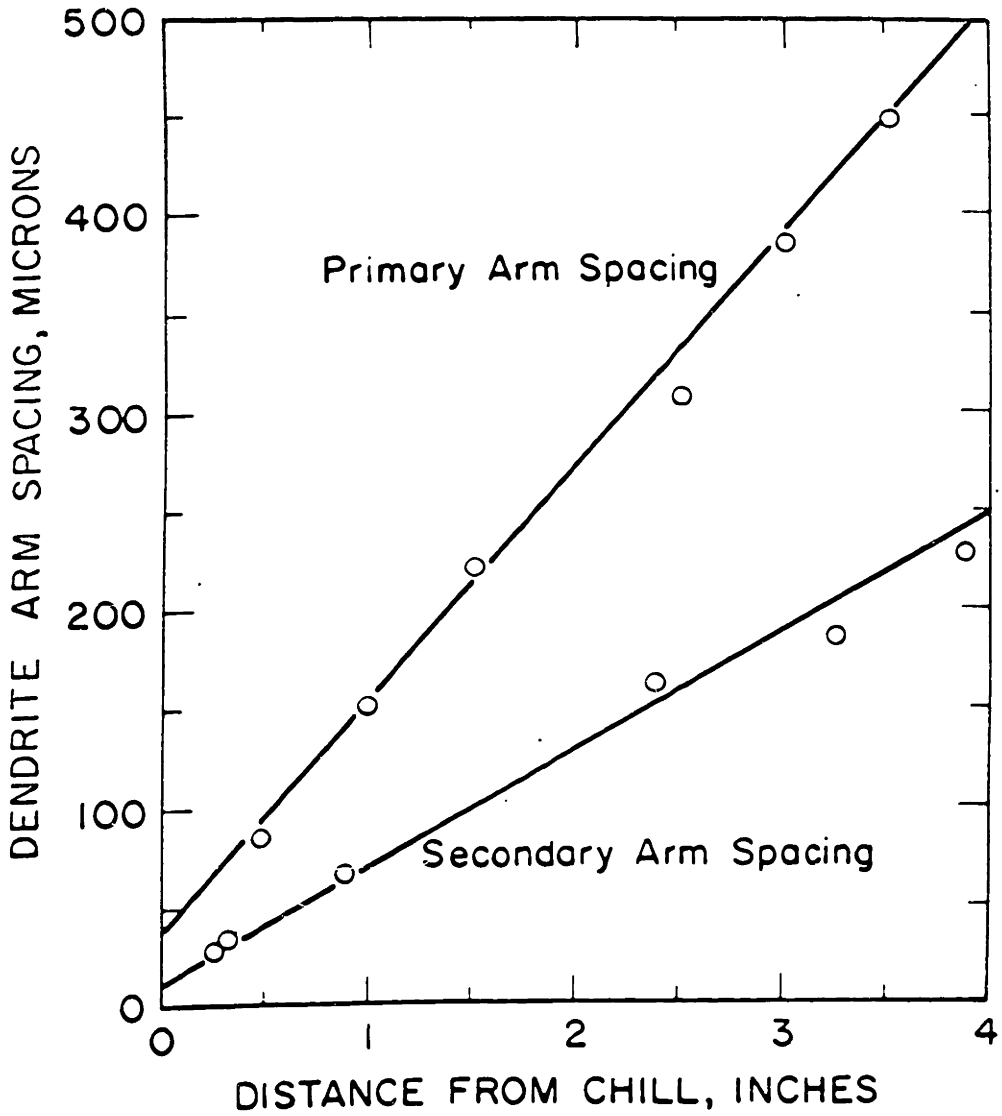

Figure 6: Dendrite arm spacing in 52100 unidirectional ingot.

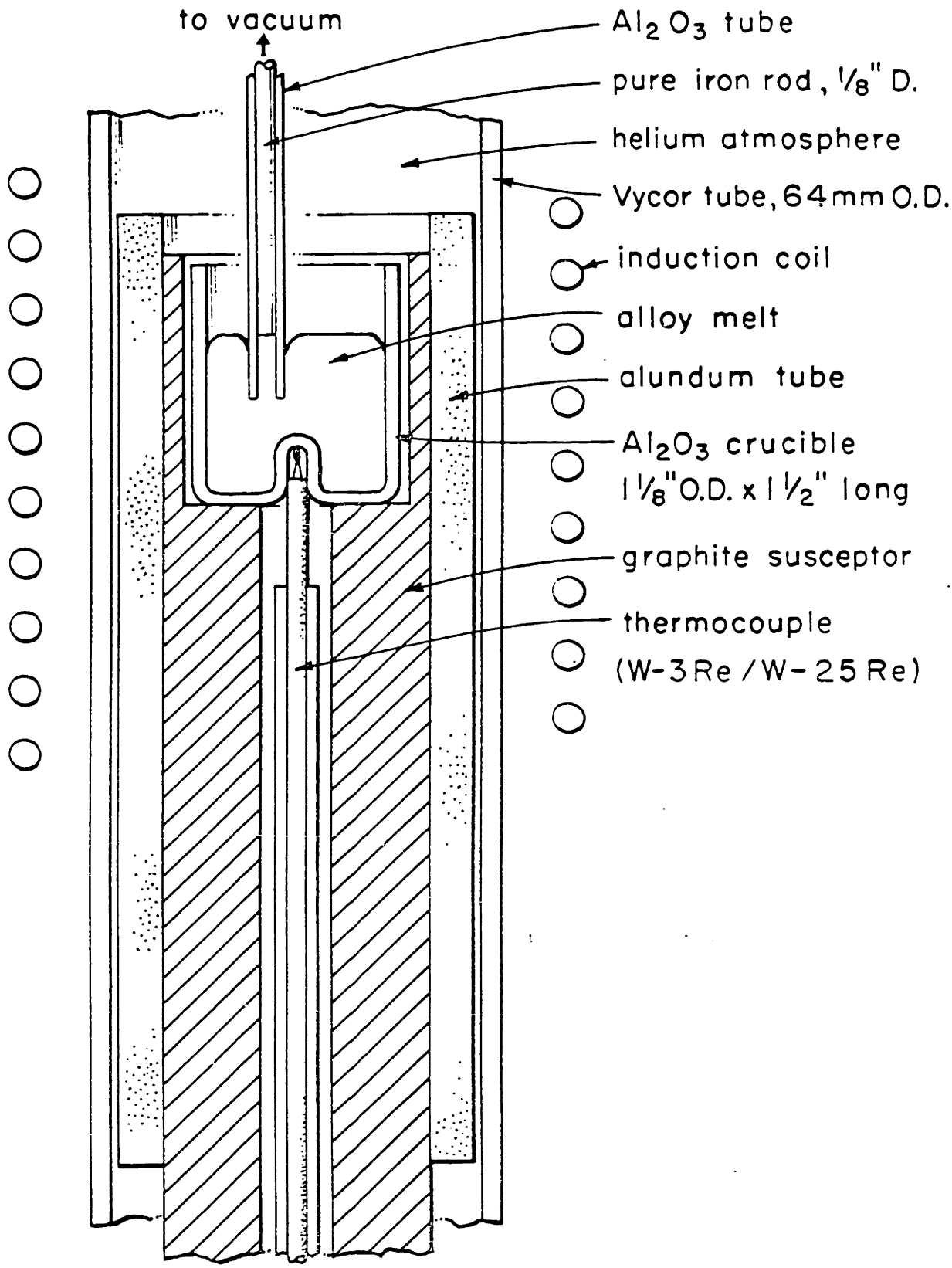

Figure 7: Schematic diagram of apparatus used for austenite-liquid equilibria of chromium.

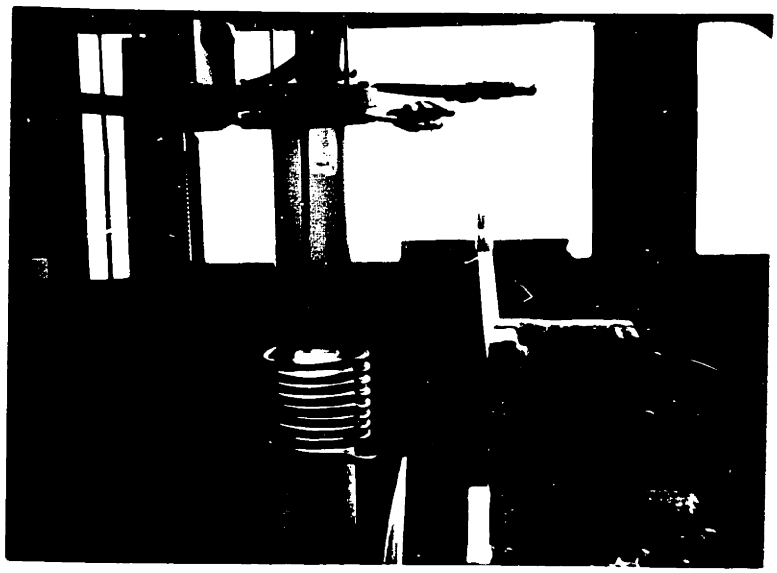

Figure 8: Apparatus for austenite-liquid equilibria of chromium.

(a)

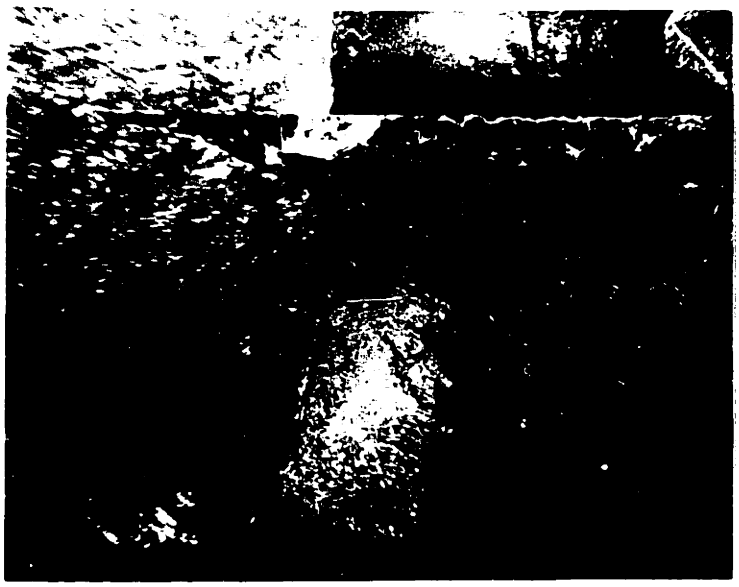

(b)

Figure 9: Macrophotographs of austenite-liquid chromium equilibria specimens.

(a) heat number 15, 4X
(b) heat number 19, 4X

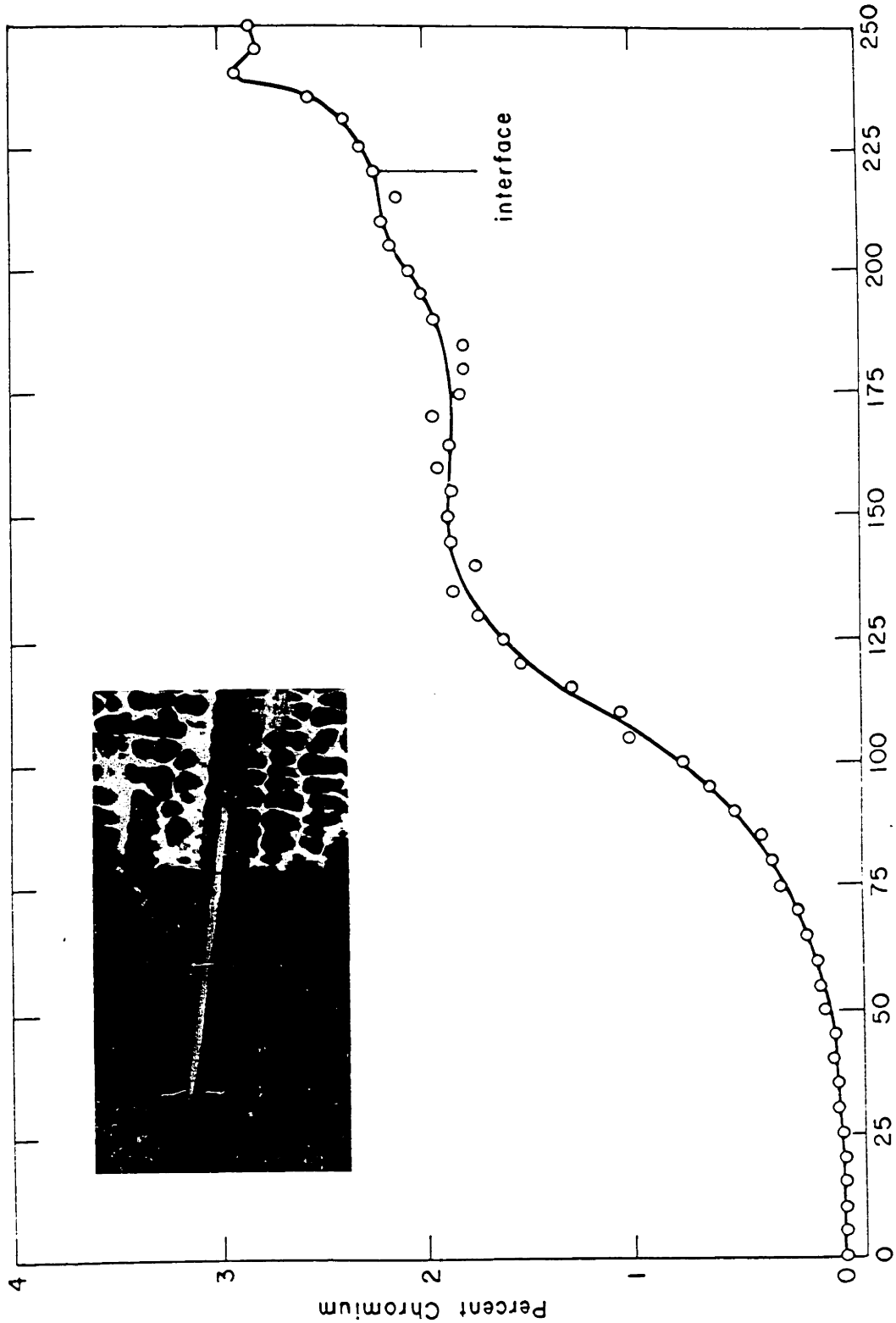

Figure 10: Microprobe path and analysis across the interface.
Heat number 15, photomicrograph at 150X.

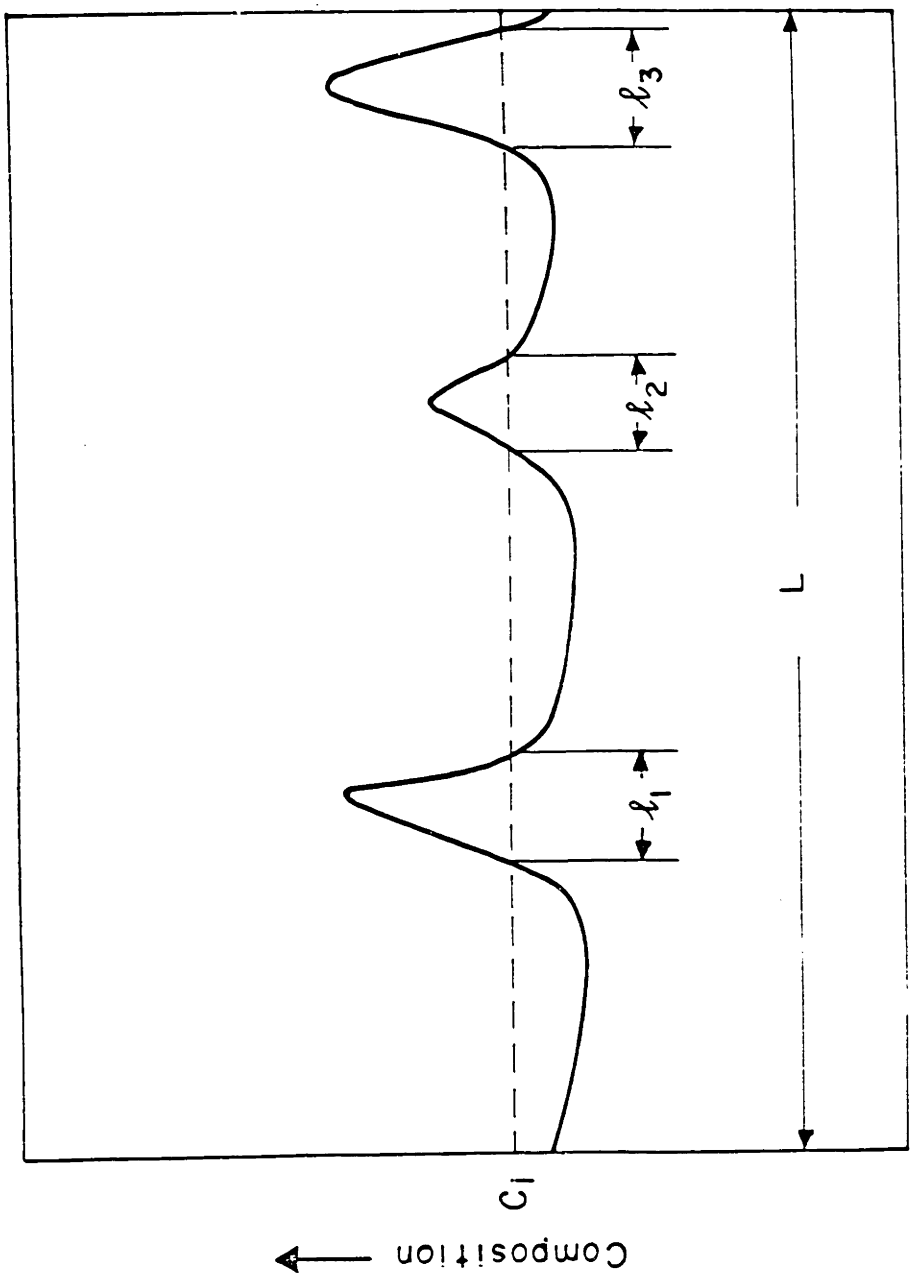

Figure 11: Schematic microprobe analysis to determine volume fraction of material with a composition of C_i and greater.

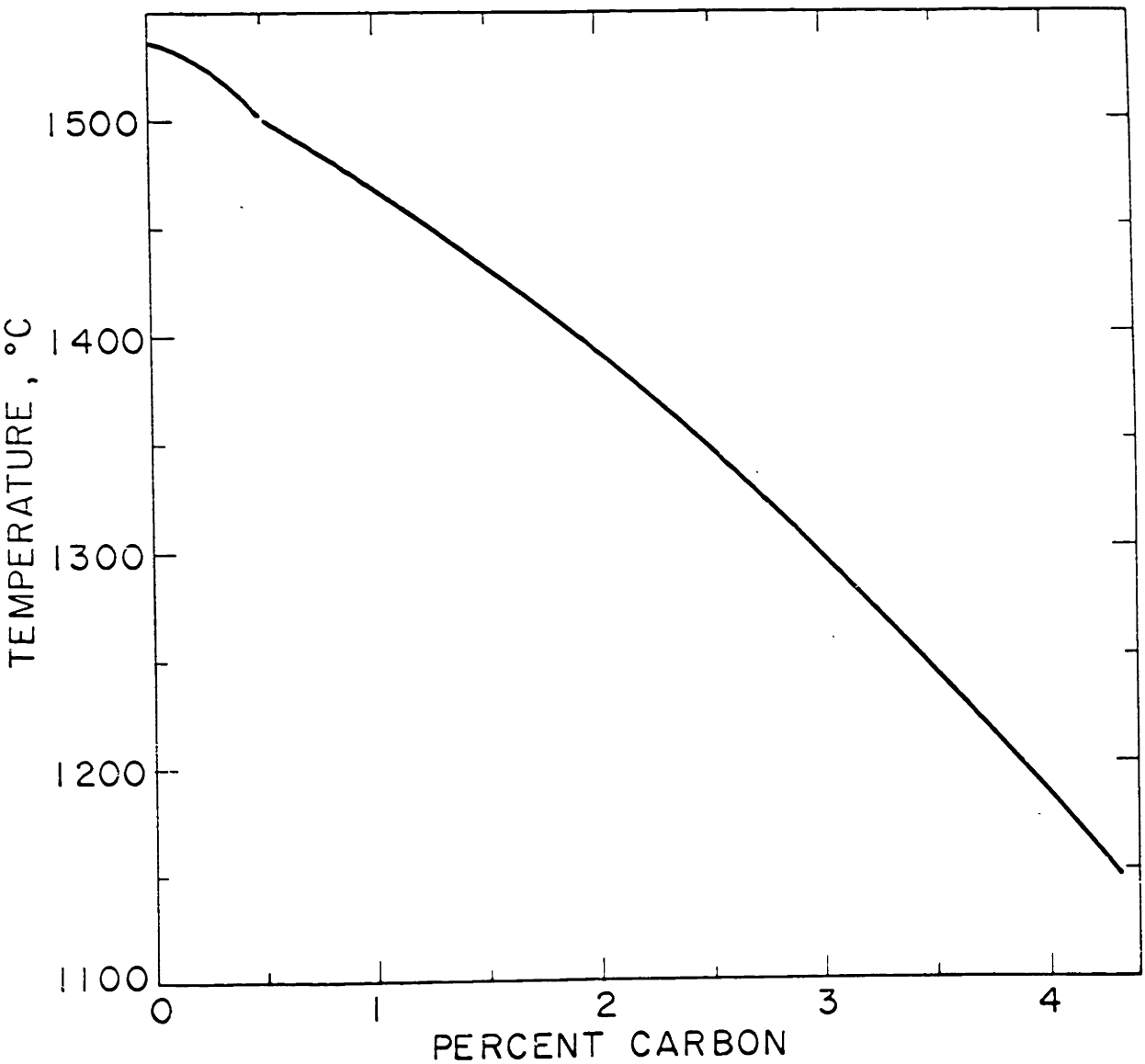

Figure 12: The liquidus at zero per cent chromium [30].

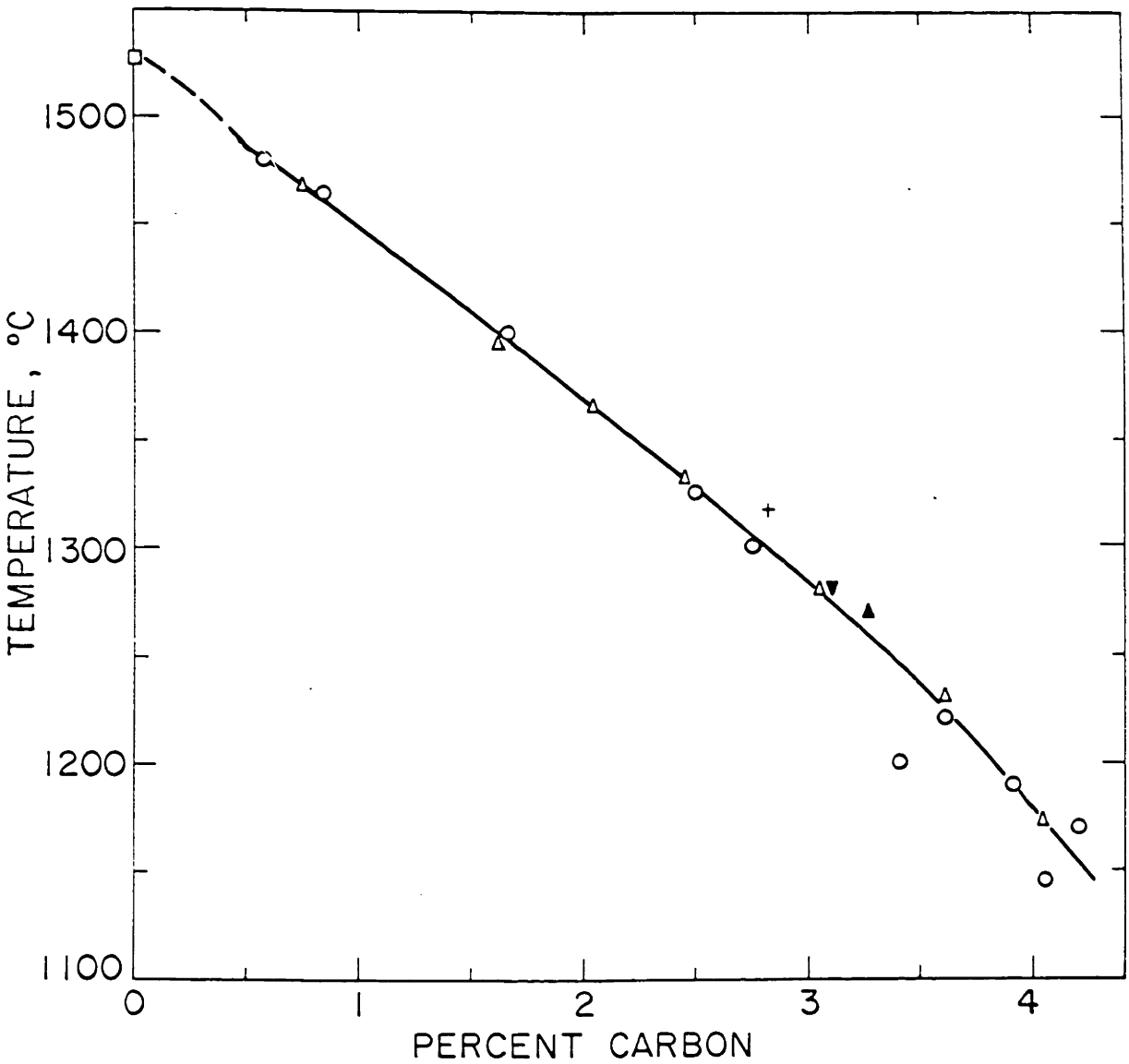

Figure 13: The liquidus at a chromium-iron ratio of .053.

□ Adcock[31]
o Austin[25], %Cr/%Fe=.0526
Δ %Cr/%Fe=.0542
▲ %Cr/%Fe=.0457
▼ %Cr/%Fe=.0432
\+ %Cr/%Fe=.0335

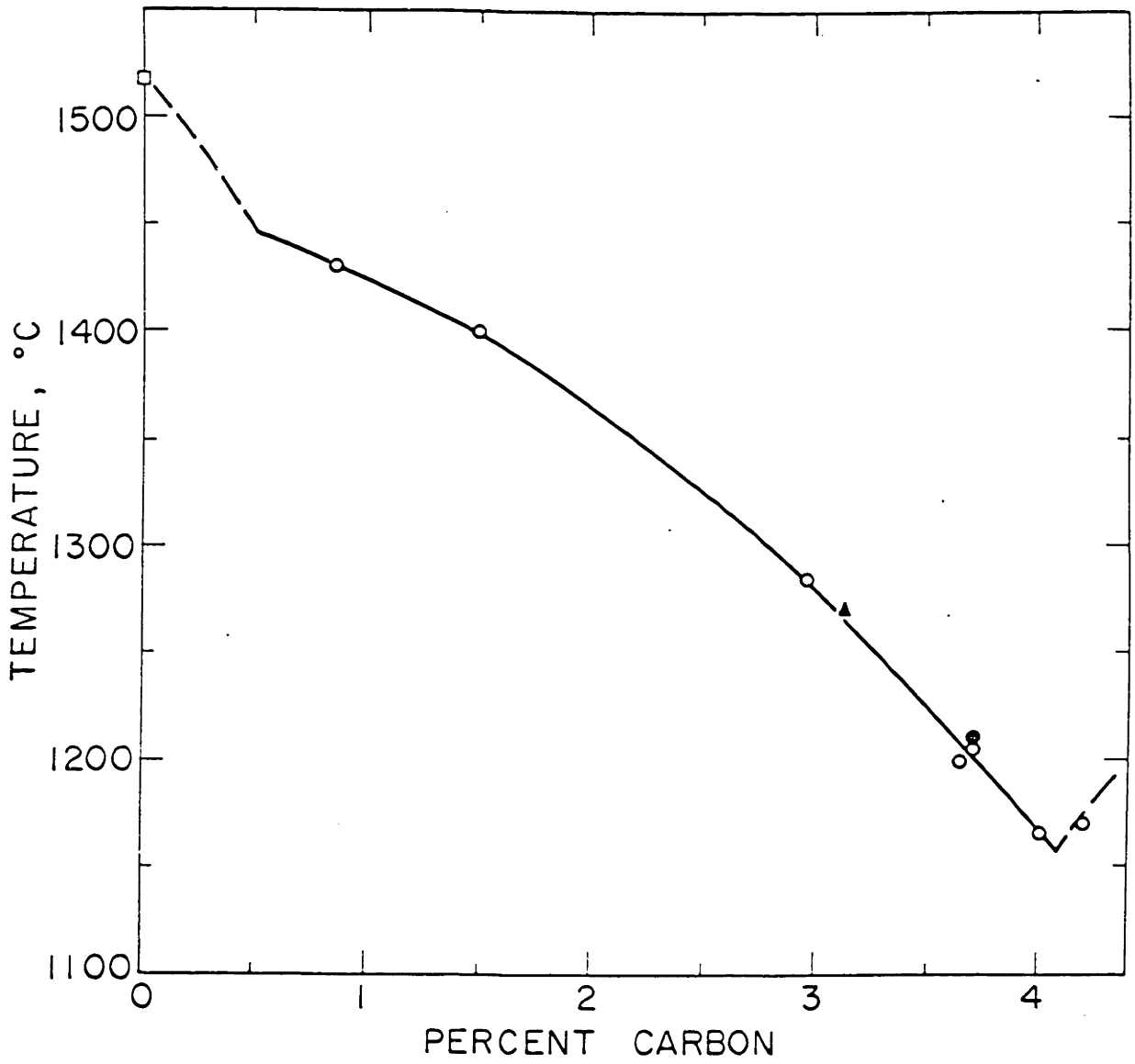

Figure 14: The liquidus at a chromium-iron ratio of .111.

□ Adcock[31]
○ Austin[25], %Cr/%Fe = .111
● Austin[25], %Cr/%Fe = .099
▲ %Cr/%Fe = .092

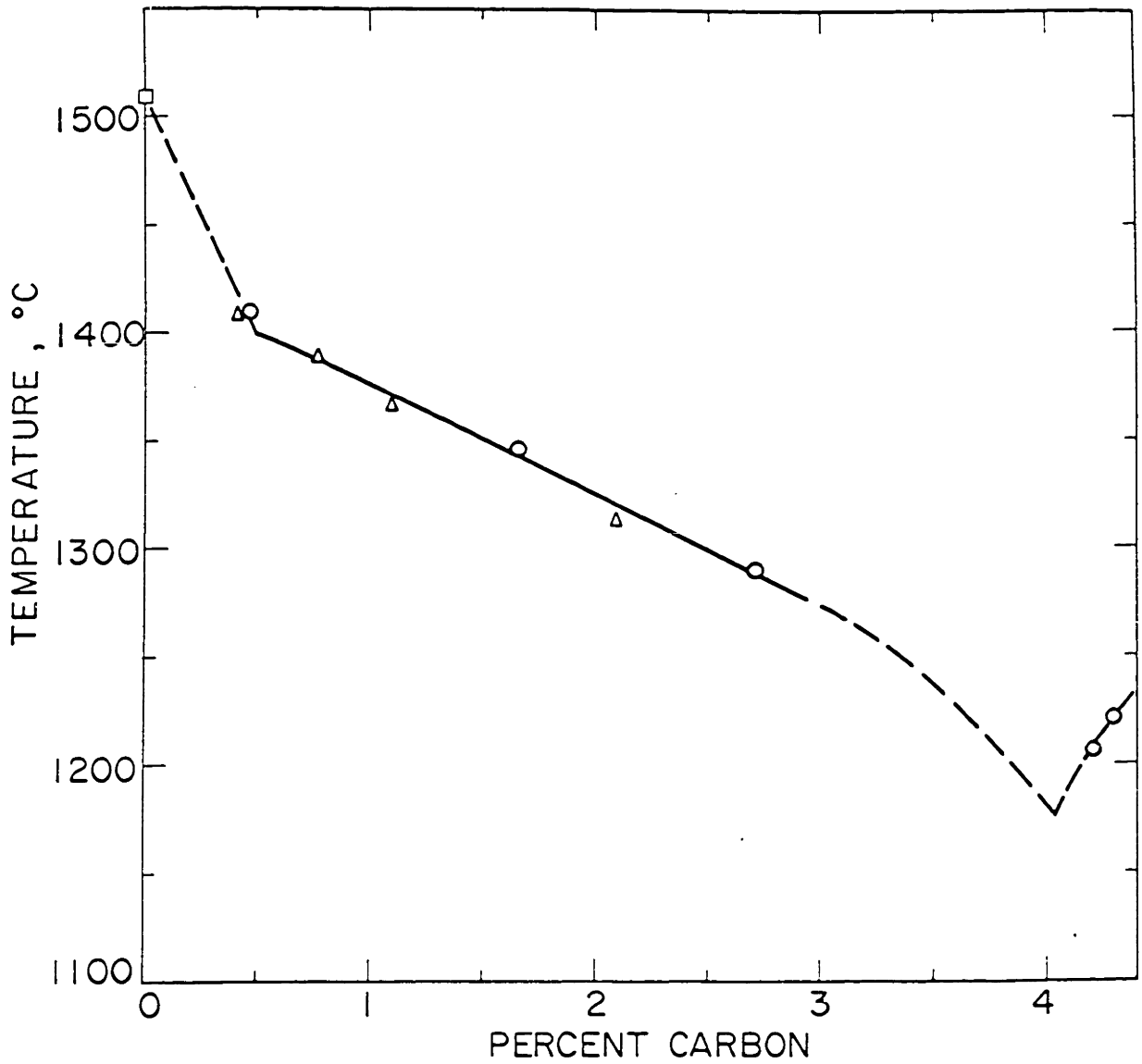

Figure 15: The liquidus at a chromium-iron ratio of .176.

- □ Adcock[31]
- o Austin[25], %Cr/%Fe = .176
- Δ Tofaute et al (reported by Kinzel and Crafts[26]), %Cr/%Fe = .176

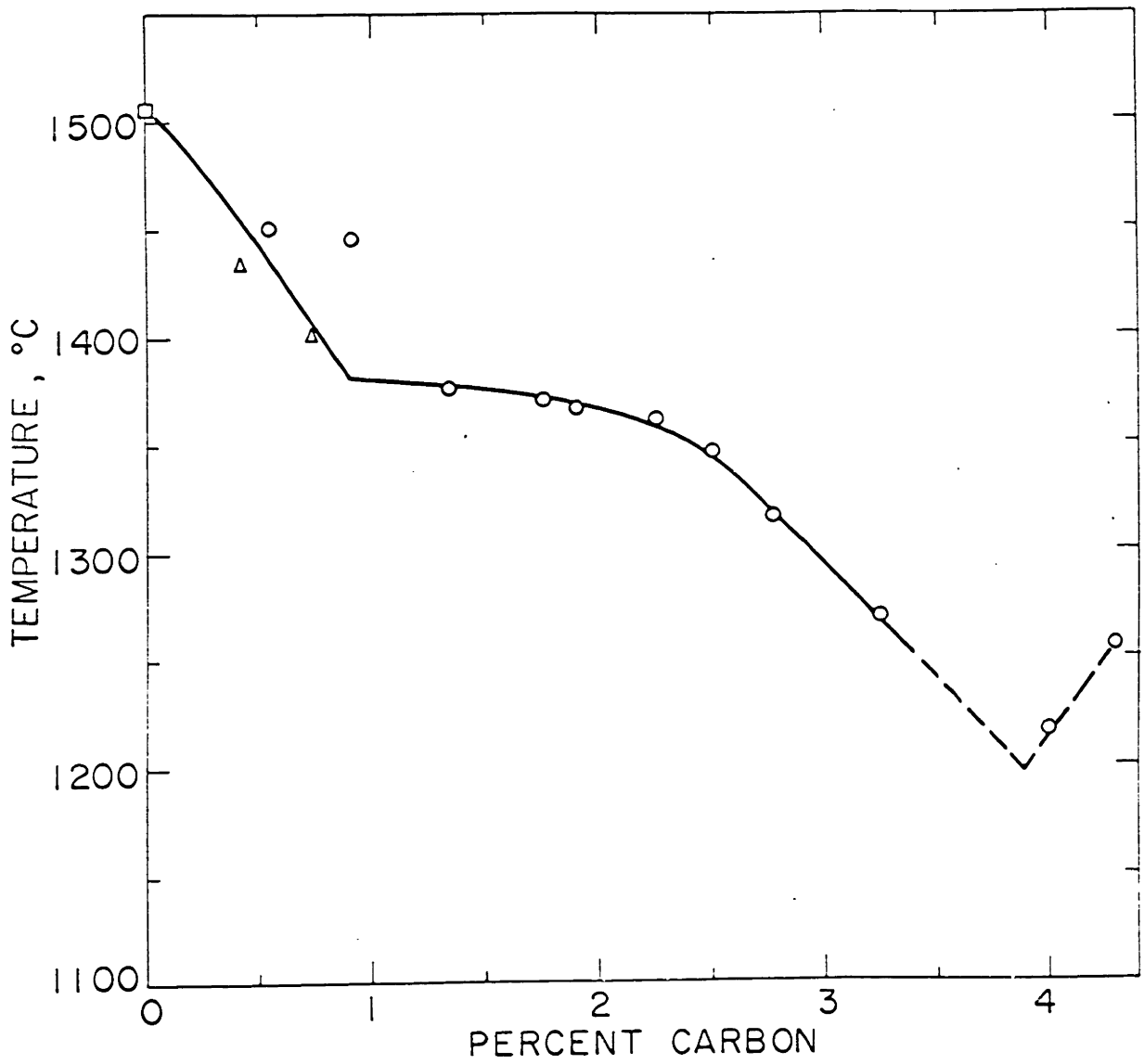

Figure 16: The liquidus at a chromium-iron ratio of .250.

- □ Adcock[31]
- o Austin[25]
- Δ Tofaute et al (reported by Kinzel and Crafts[26])

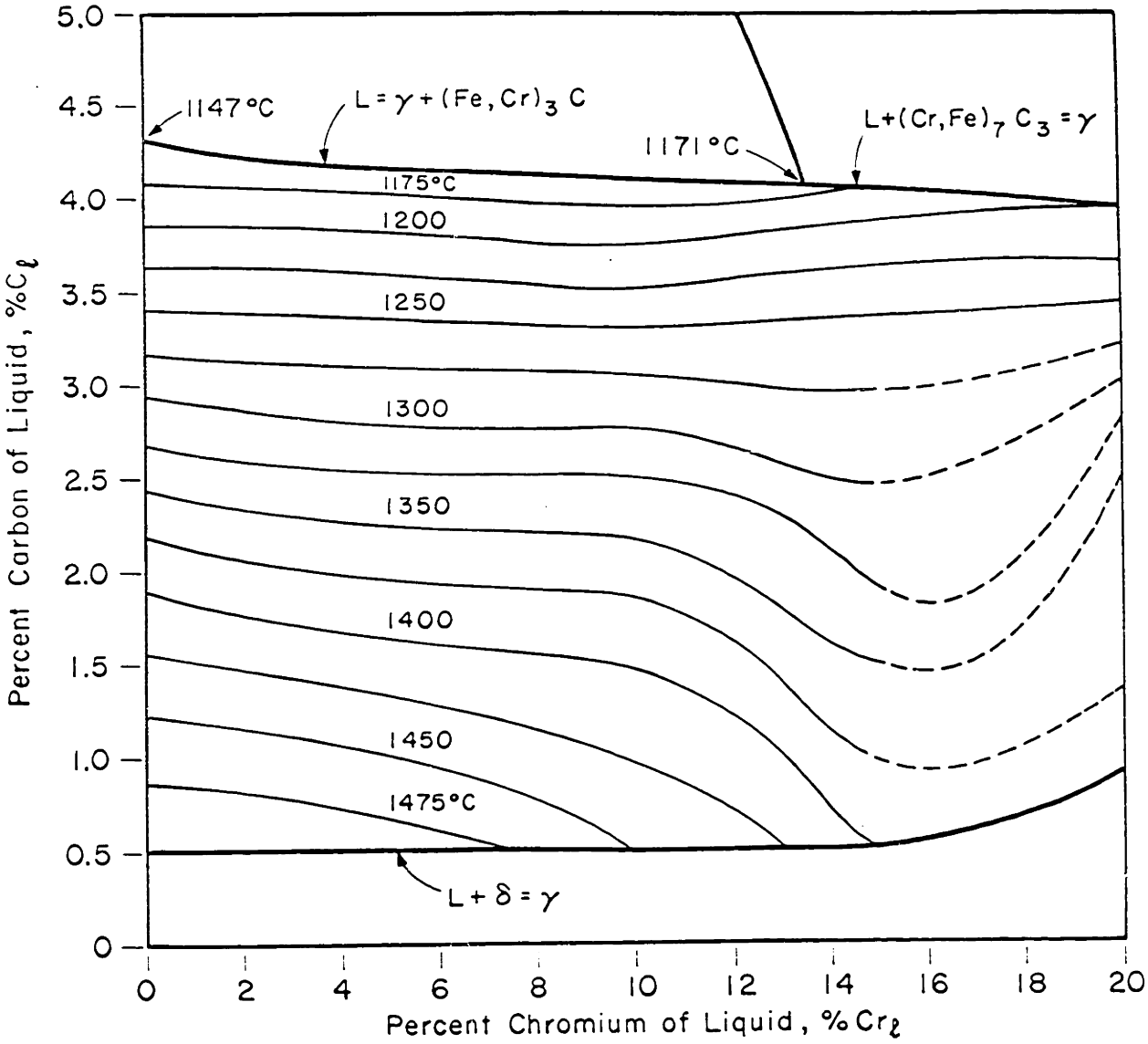

Figure 17: The iron-carbon-chromium gamma liquidus surface.

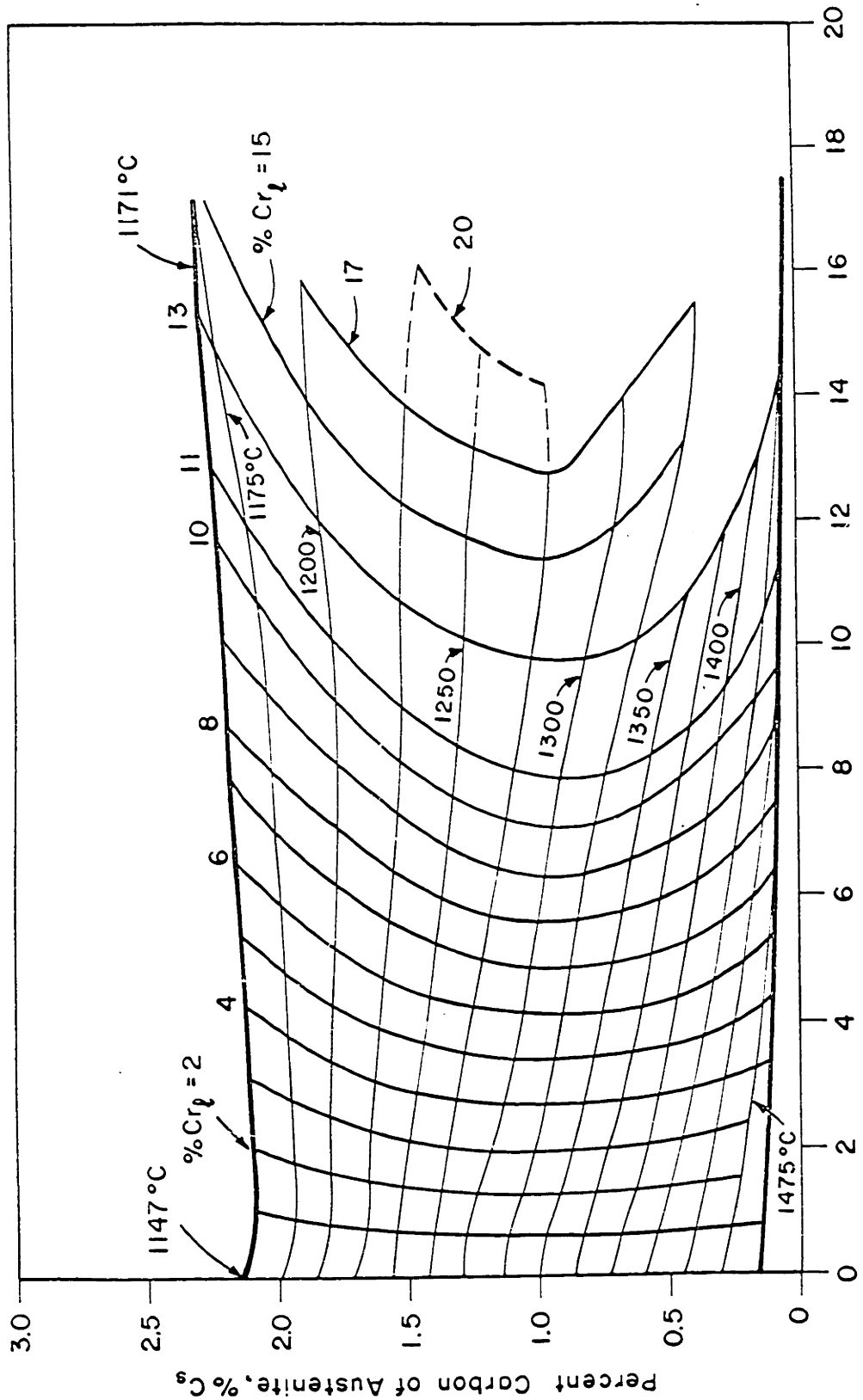

Figure 18: The iron-carbon-chromium gamma solidus surface.

The austenite in equilibrium with a particular liquid composition is found by the intersection of the liquid chromium concentration with the appropriate isotherm.

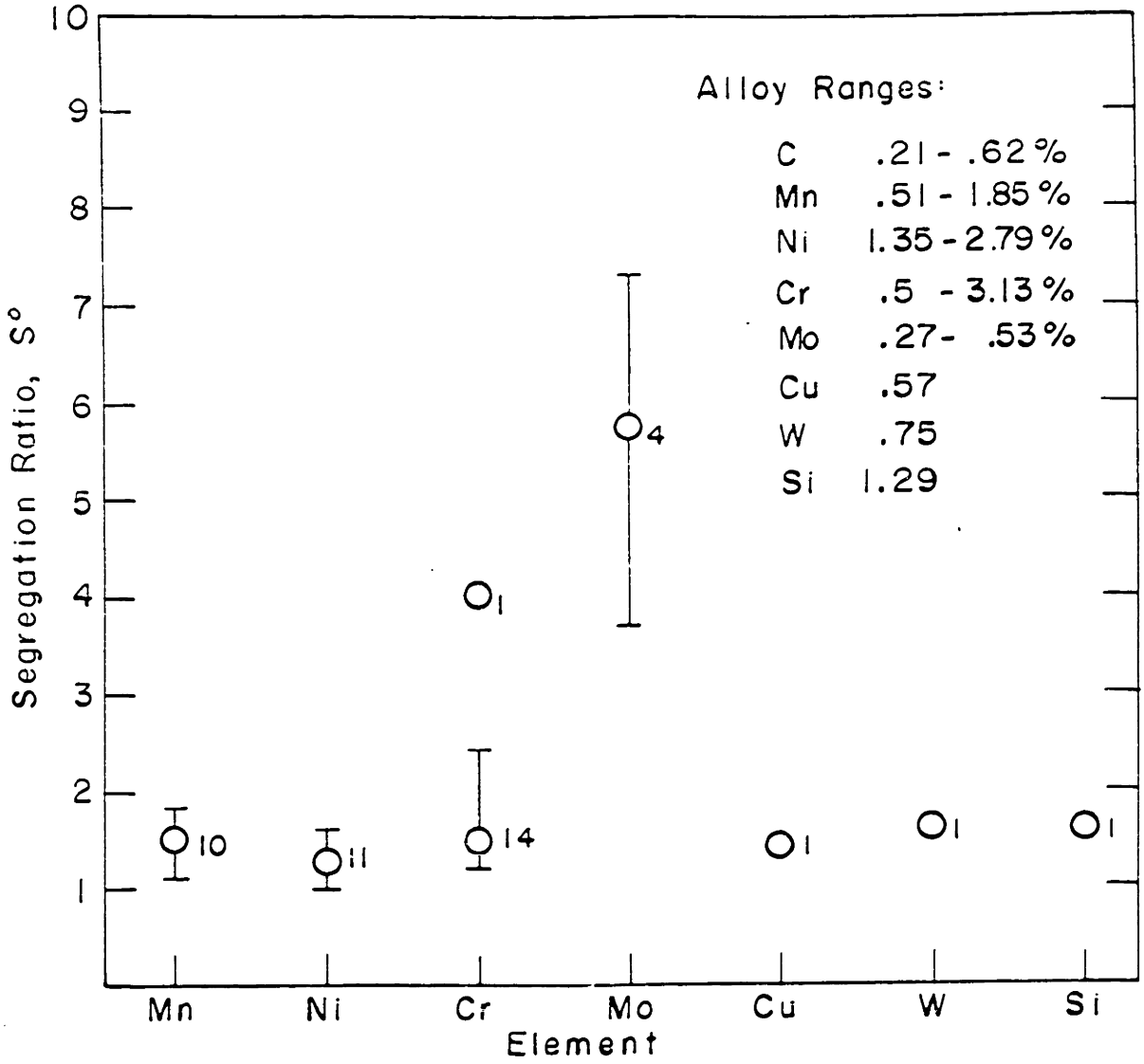

Figure 19: Segregation ratios for common alloying elements in medium carbon, low alloy steels. Numbers beside the points represent the number of alloys involved for the respective elements.

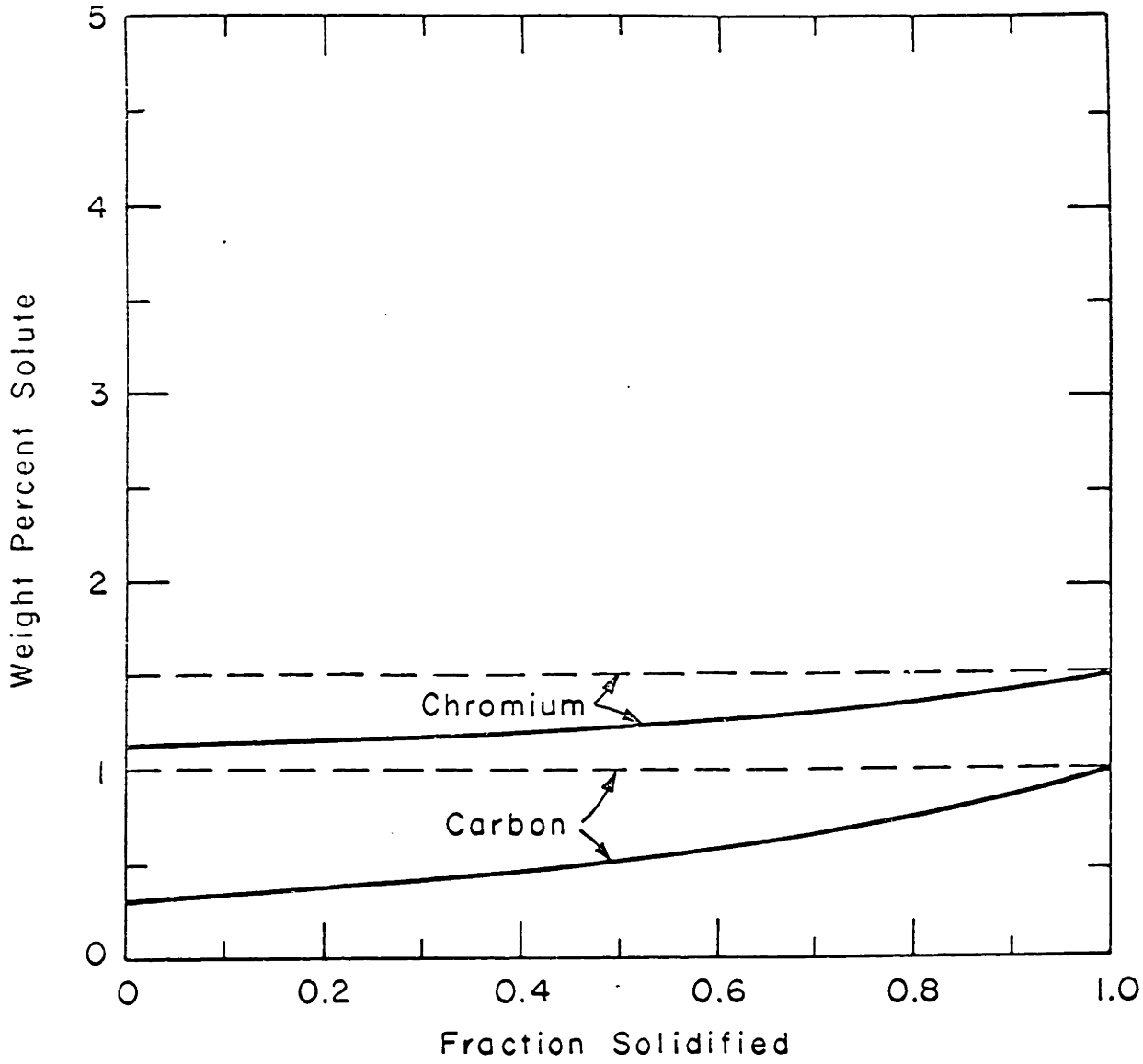

Figure 20: Composition of the solid for the solidification of Fe-1%C-1.5%Cr alloy assuming equilibrium solidification of both solutes, Case 1.

Solid lines represent compositions during solidification and the dotted lines represent the final solidified alloy.

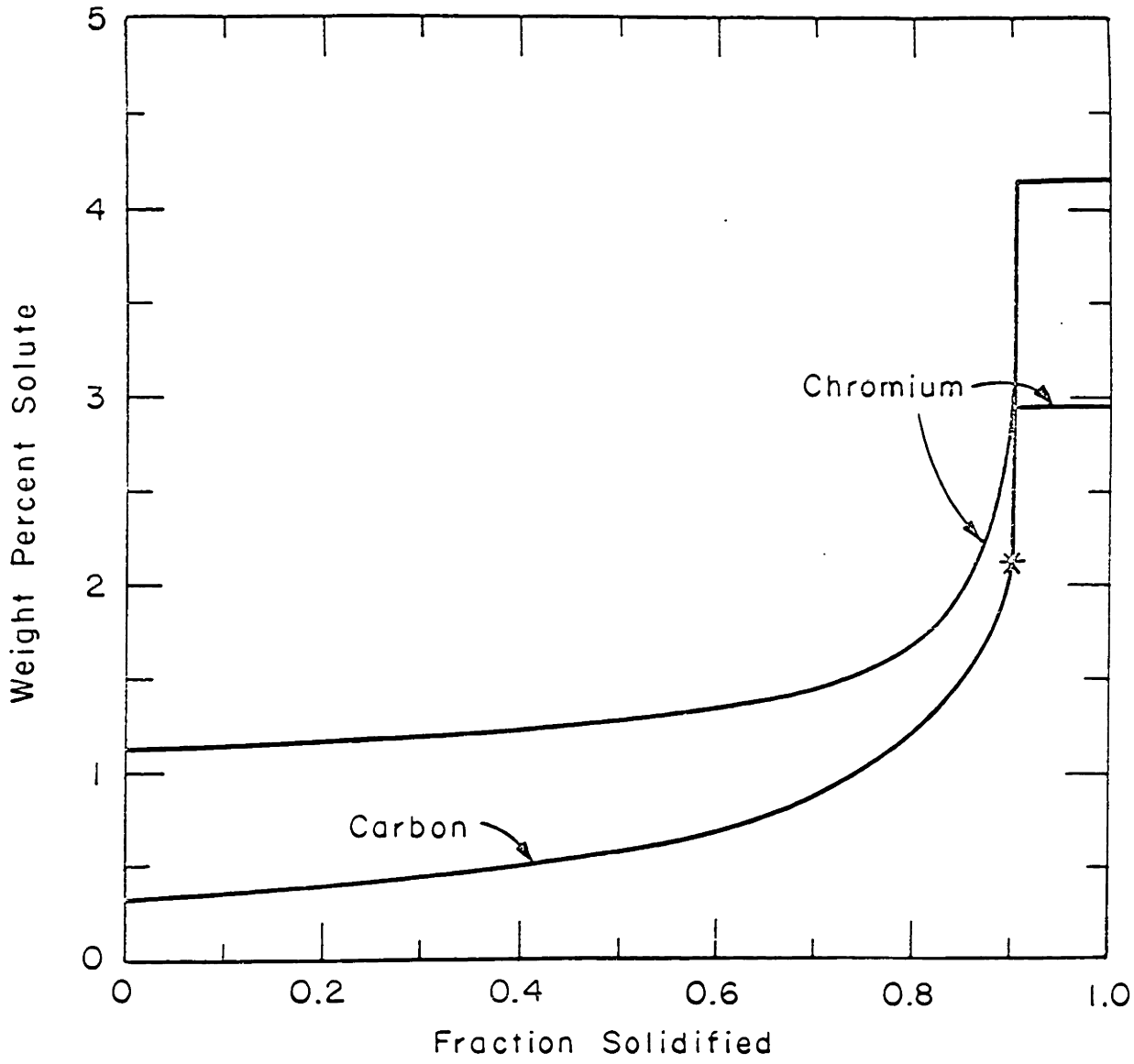

Figure 21: Composition of the solid for the non-equilibrium solidification of both solutes in Fe-1%C-1.5%Cr alloy, Case 2.

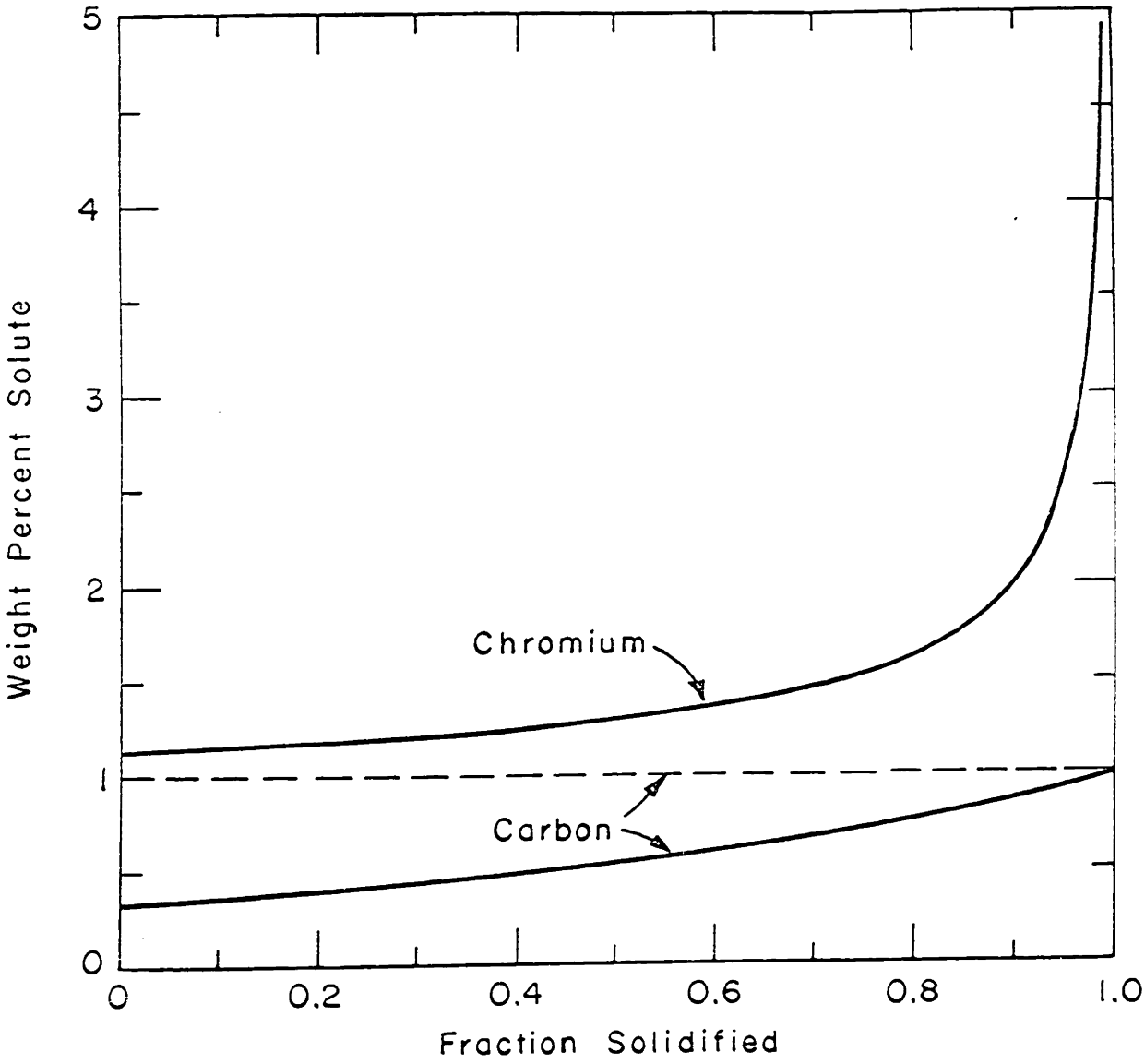

Figure 22: Composition of the solid for the solidification of Fe-1%C-1.5% Cr alloy assuming non-equilibrium solidification of chromium and equilibrium for carbon, Case 3.

The dotted line represents the final carbon distribution.

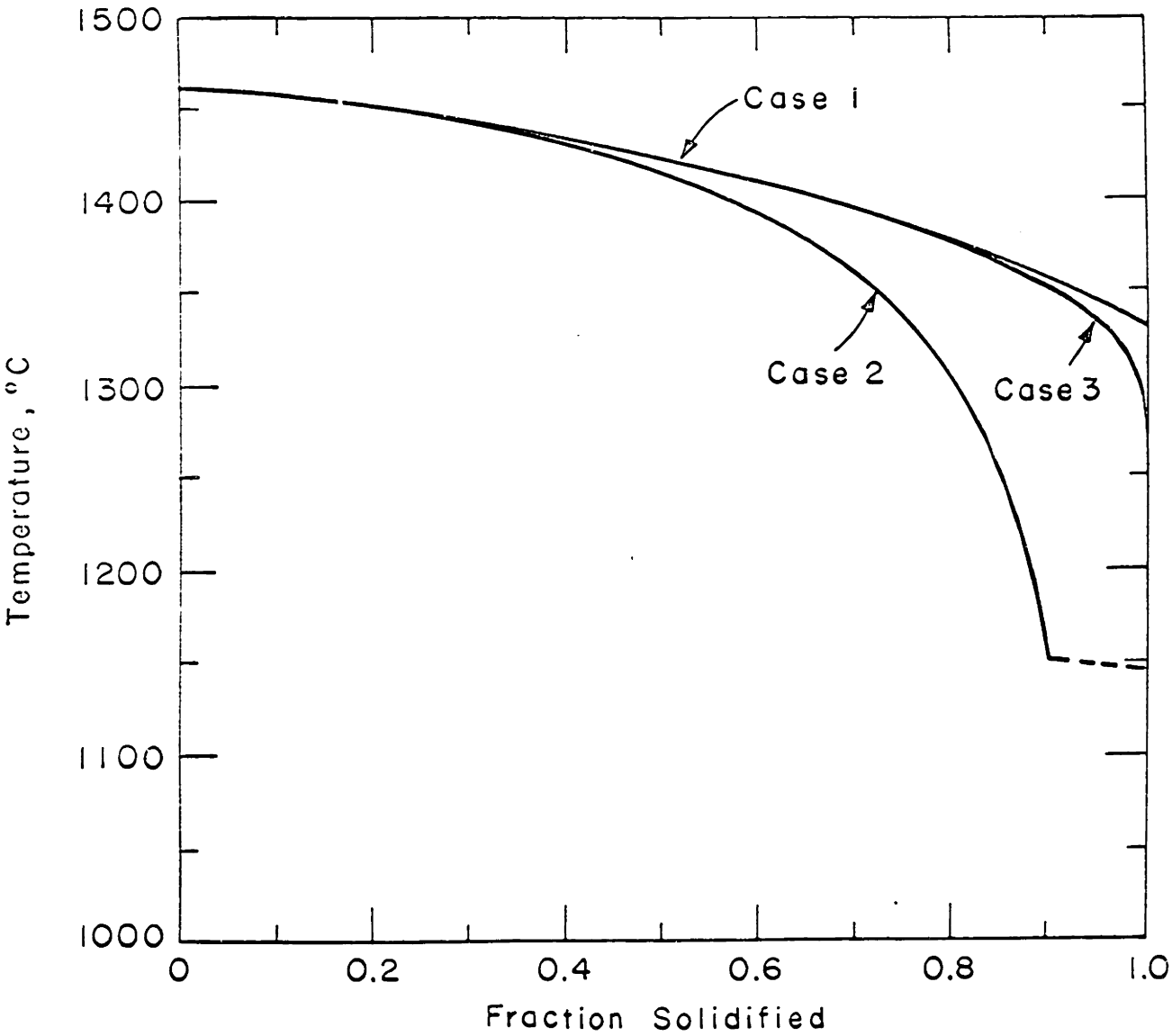

Figure 23: Fraction solidified versus temperature calculated for Fe-1%C-1.5%Cr alloy.

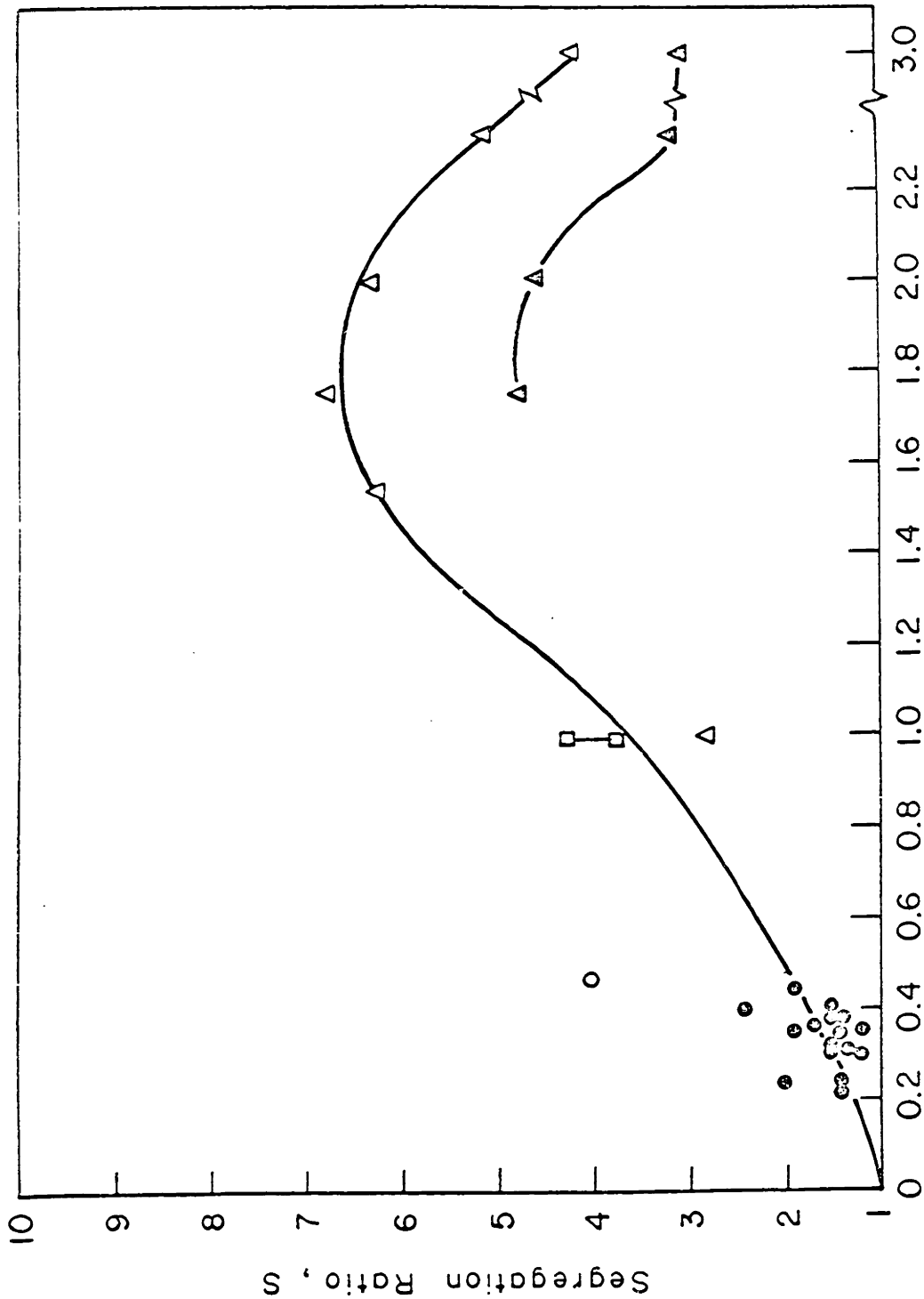

Figure 24: The segregation ratio of chromium in low alloy steels and iron-carbon-chromium alloys.

- ● low alloy steel, Table VII
- ○ 0.5 per cent chromium, Table VII
- □ 52100 unidirectional ingot
- △ iron-1.5 percent chromium based on maximum
- ▲ iron-1.5 per cent chromium based on eutectic

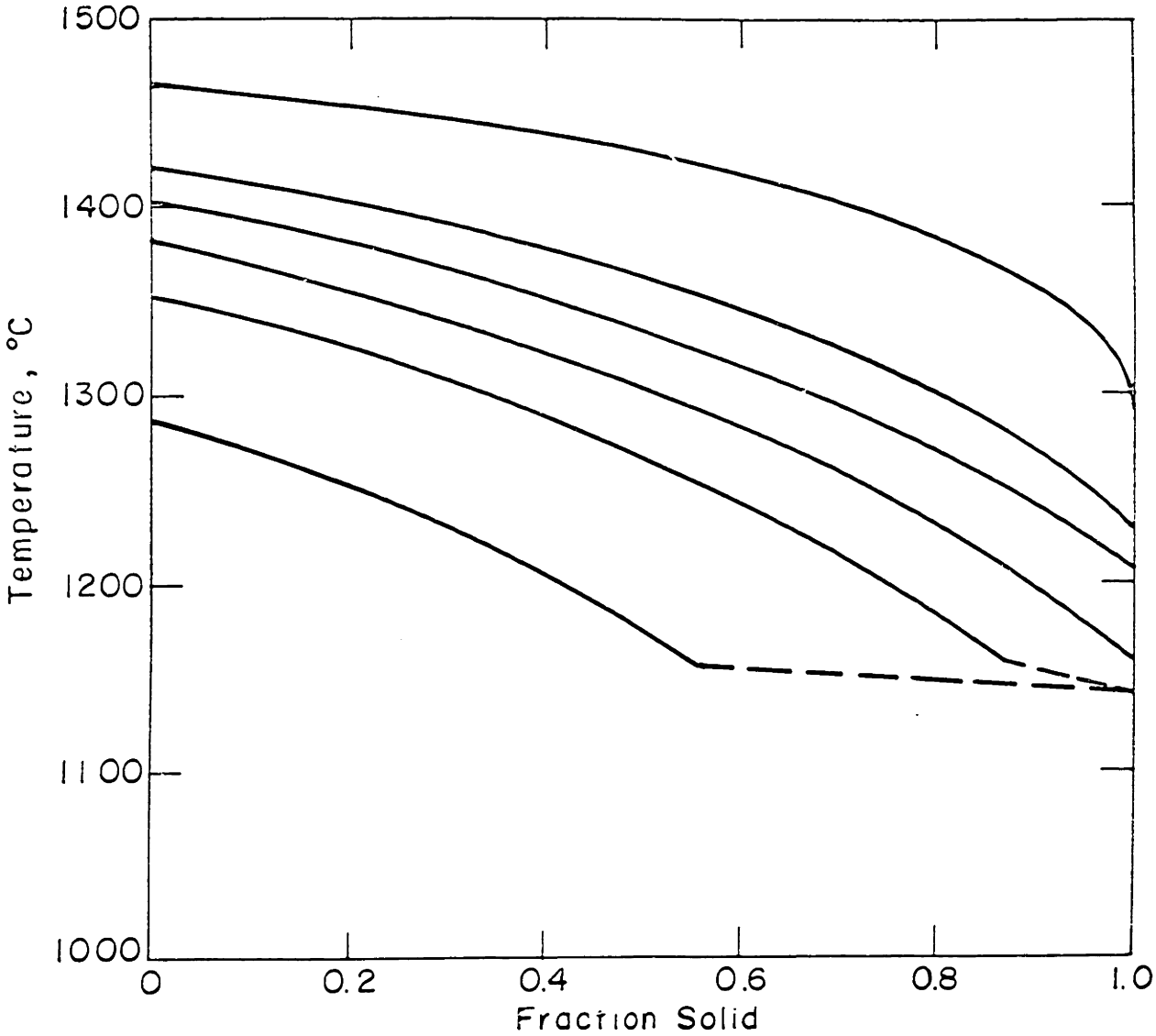

Figure 25: Fraction solid versus temperature for iron-carbon-chromium alloys calculated assuming no diffusion of chromium and complete diffusion of carbon in the solid.

All alloys have approximately 1.5 per cent chromium and carbon ranges from 0.96 to 3.00 per cent in the order of decreasing solidification temperatures. The alloy compositions are given in Table III.

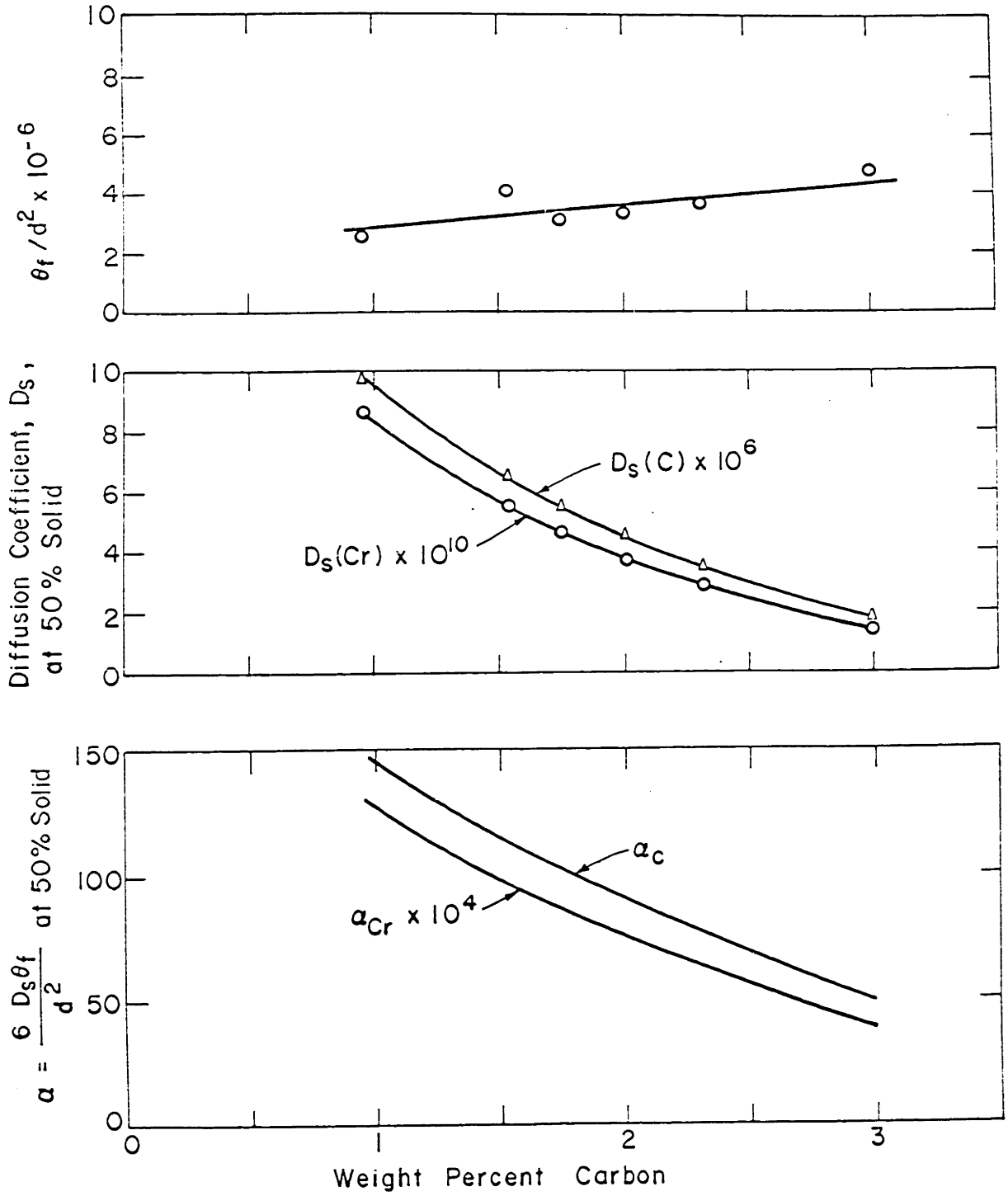

Figure 26: The extent of solid diffusion during solidification as estimated by the α factors.

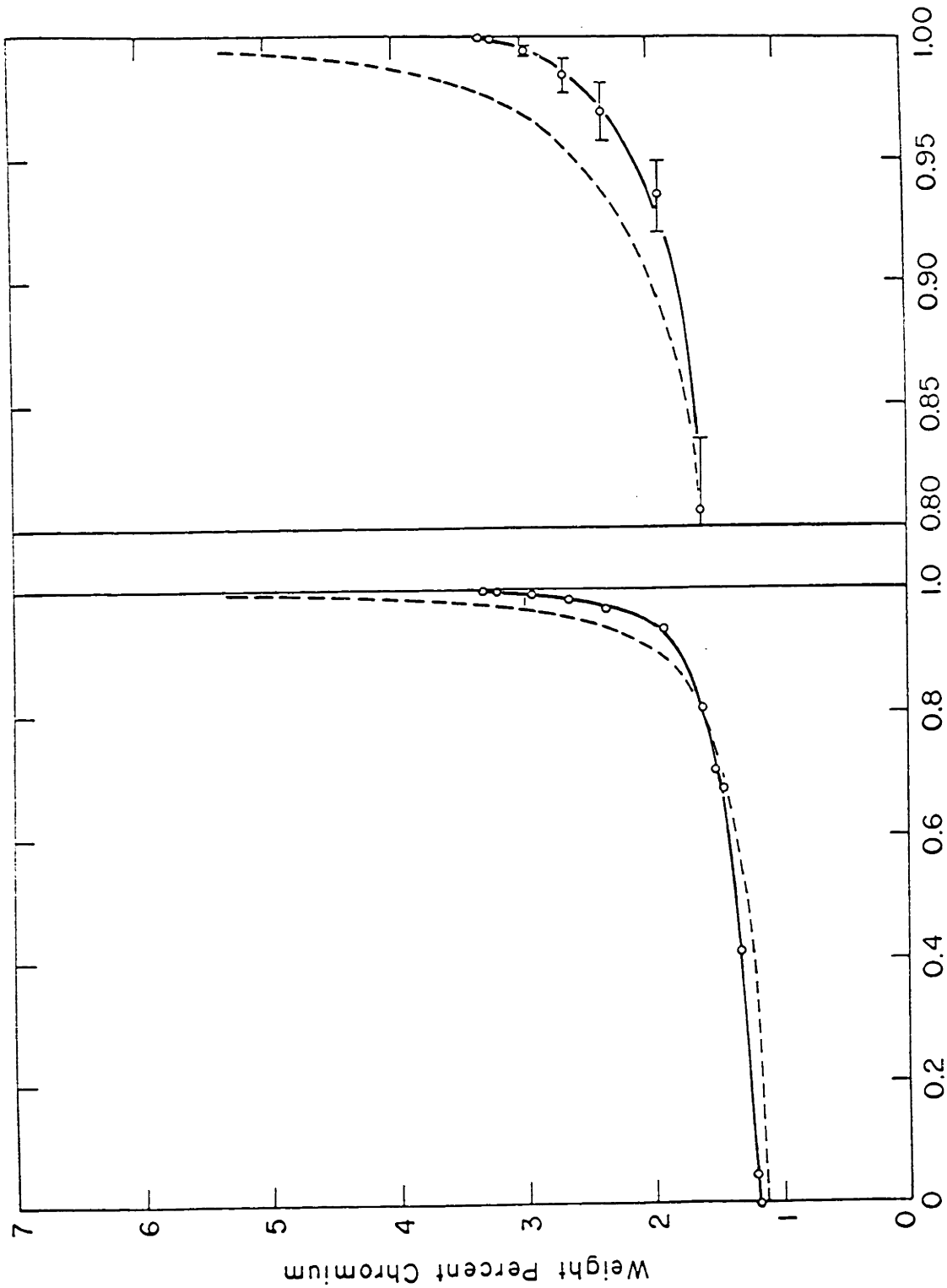

Figure 27: Concentration profile for iron-.96 per cent carbon-1.48 per cent chromium alloy. Solid curves are experimental and dashed curves are theoretical (Case 3). Statistical errors are indicated in the expanded portion for the last .20 volume fraction.

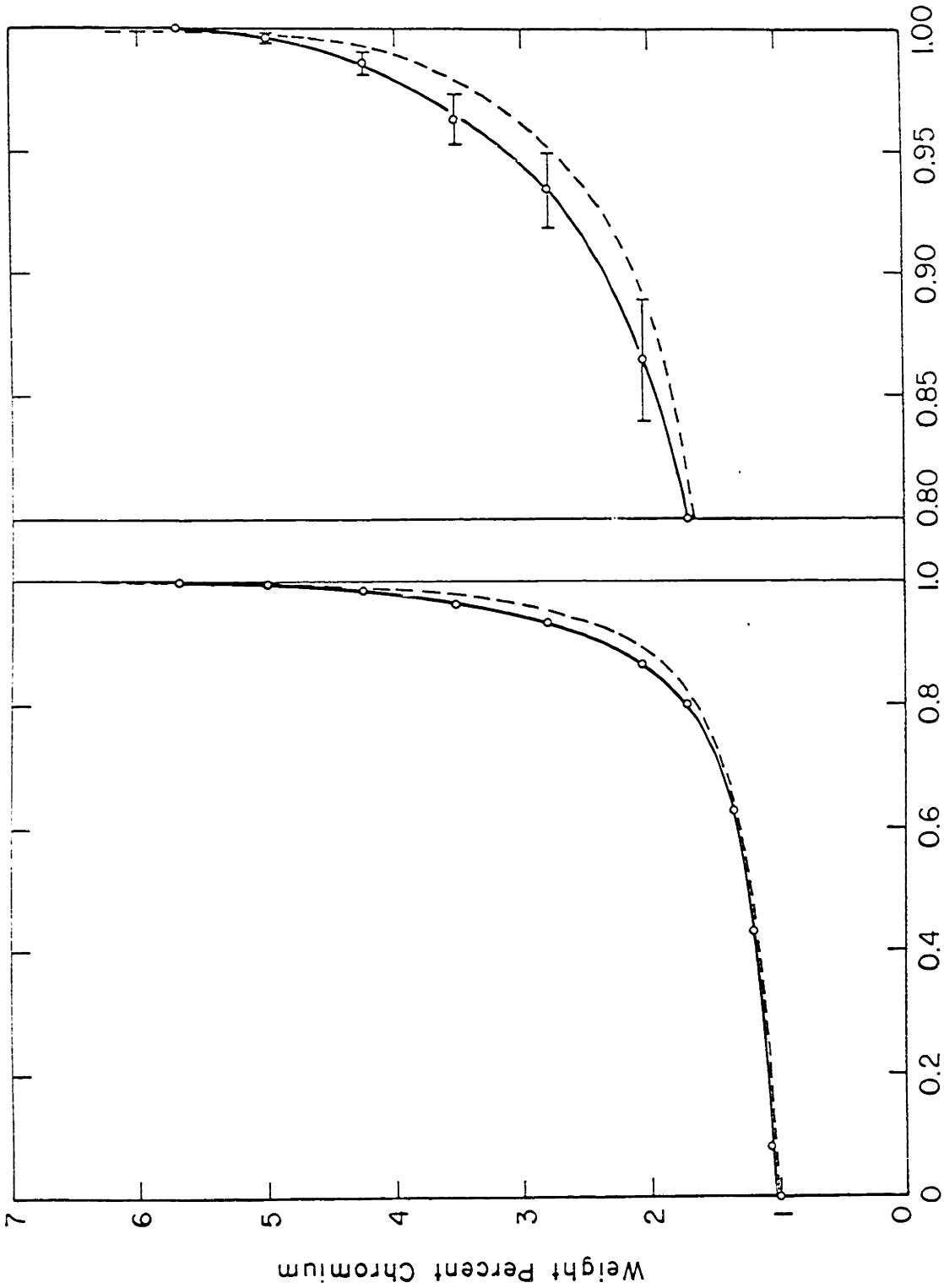

Figure 28: Concentration profile for iron-1.54 per cent carbon-1.45 per cent chromium alloy. For explanation of curves see Figure 27.

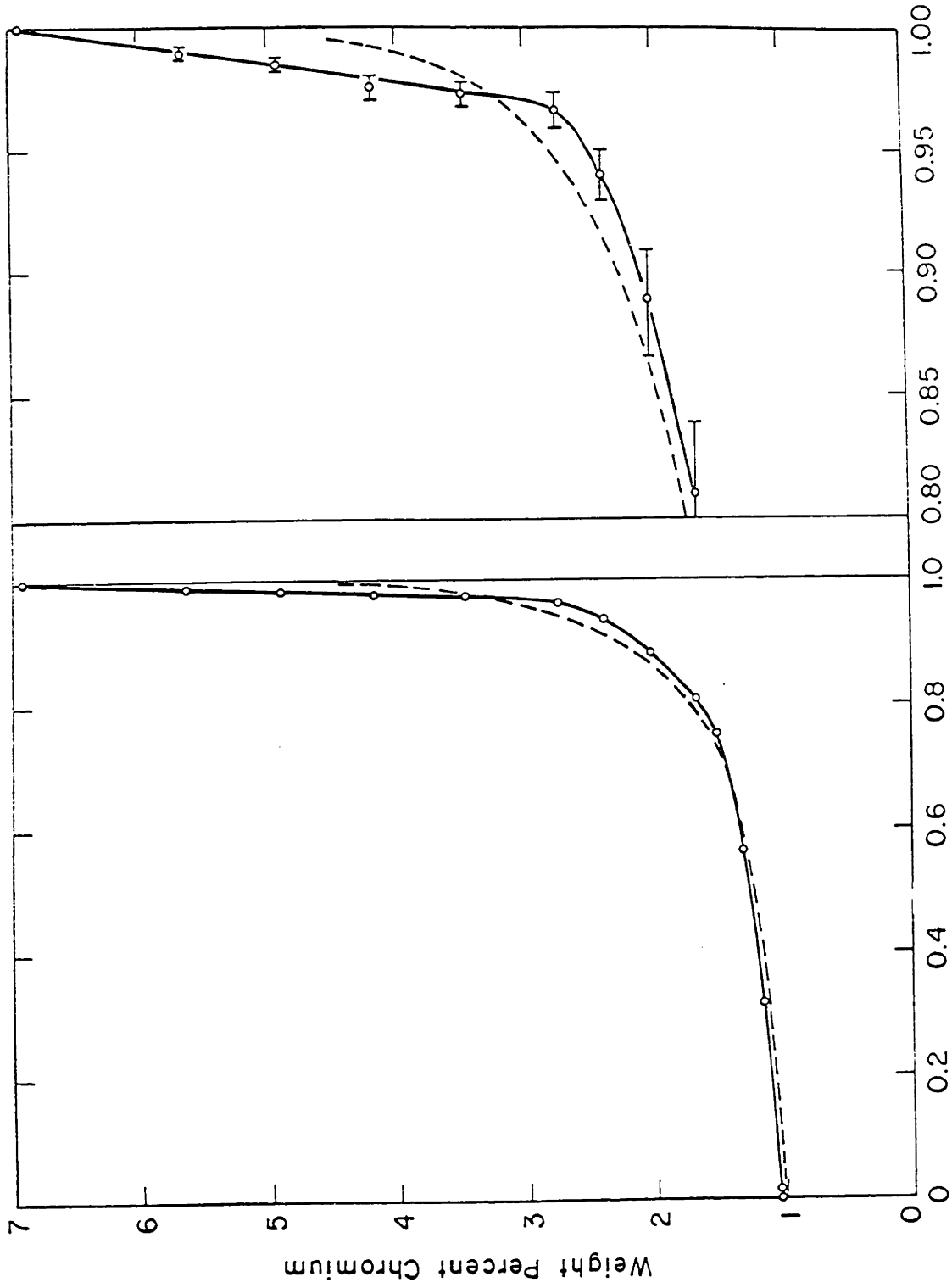

Figure 29: Concentration profile for iron-1.75 per cent carbon-1.48 per cent chromium alloy. For explanation of curves see Figure 27.

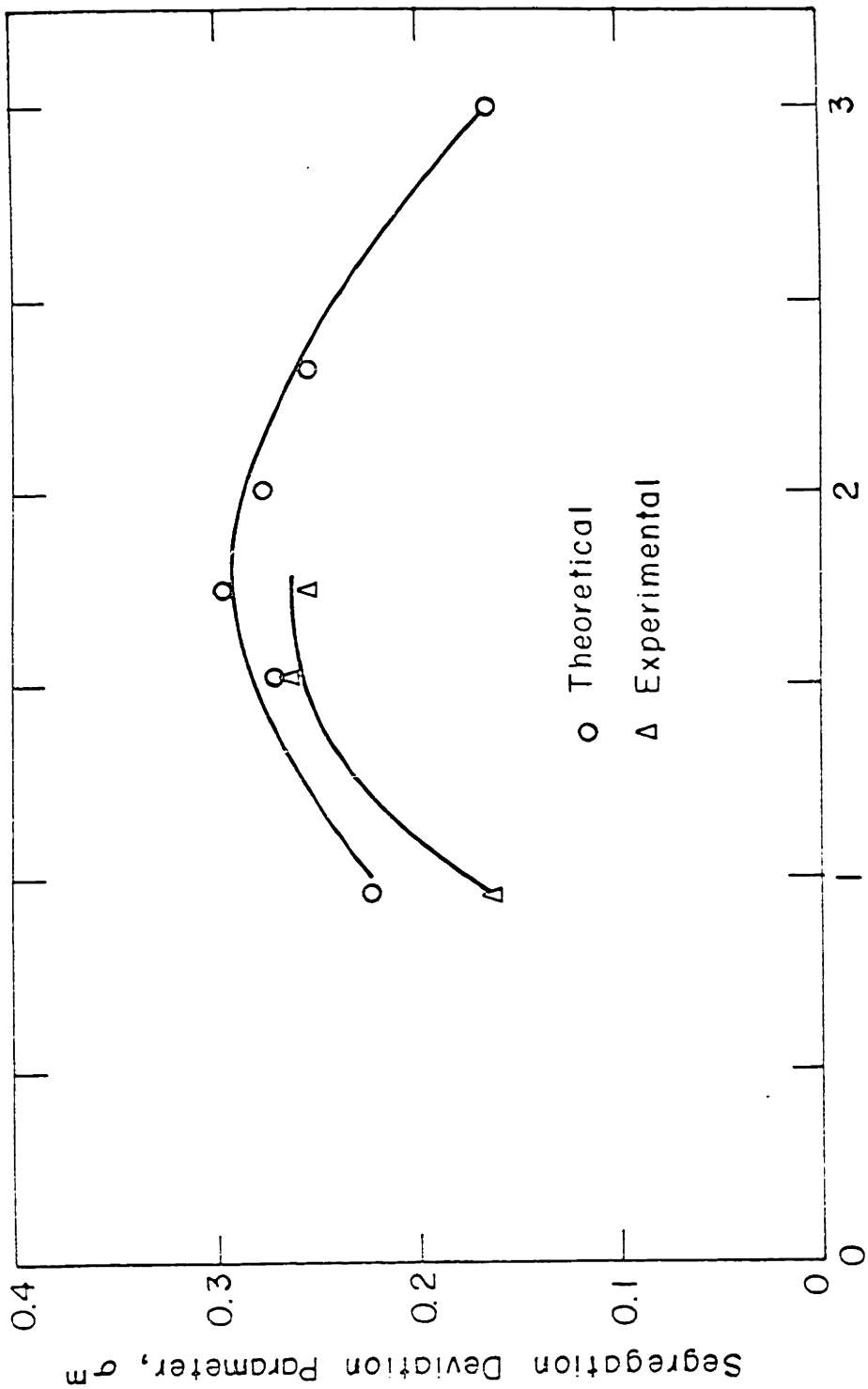

Figure 30: The segregation deviation parameter, σ^m, for iron-1.5 per cent chromium alloys versus carbon content.

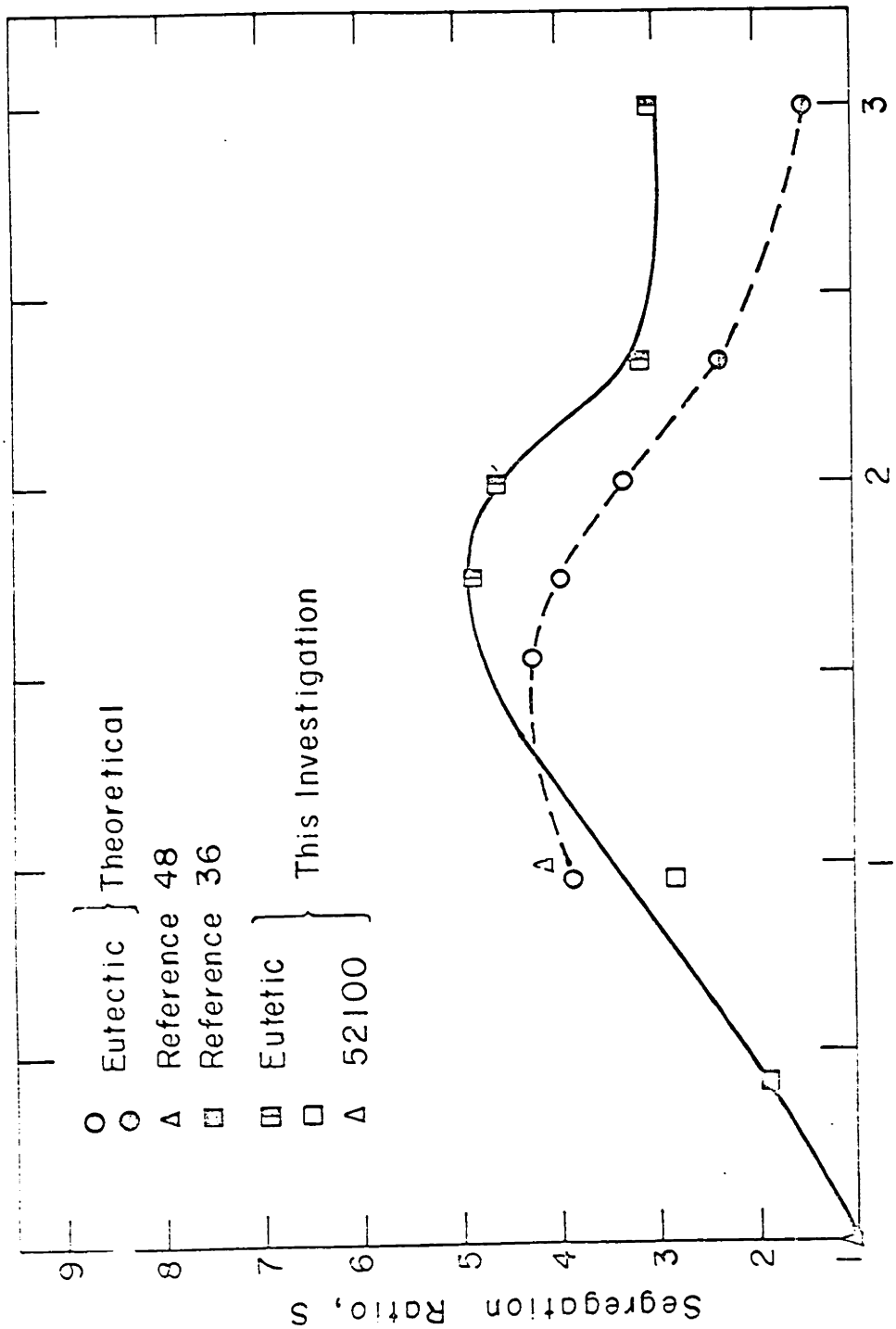

Figure 31: The segregation ratio for iron-1.5 per cent chromium alloys versus carbon content.

APPENDIX A

ACTIVITY OF CARBON IN AUSTENITIC AND LIQUID IRON-CARBON SOLUTIONS

A. Introduction

The activity of carbon in iron-carbon austenite as determined by Smith[49] (800, 1000 and 1200°C), Schenck and Kaiser[50] (800 and 1000°C), Scheil et al[51] (800, 900, 1000, 1100, and 1200°C), and Bungardt et al[52] (1000°C) is shown in Figure A1. The curves represented are merely drawn to separate the sets of data into the respective temperatures. The data, as presented, are inadequate to precisely determine the activity of carbon especially if it is necessary to know the activity at temperatures greater than 1200°C.

The activity of carbon in iron-carbon liquid solutions has been determined by Rist and Chipman[53] based on their data and the work of Richardson and Dennis[54]. It is the purpose of the following argument to accurately determine the activity of carbon in austenite as a function of temperature and carbon concentration and, then by the use of the most accurate austenite-liquid phase equilibria of Elliott and Benz[30], to reconcile this data with the activity in liquid iron-carbon alloys as determined by Rist and Chipman[53].

B. Thermodynamic Model for Austenite

Kirkaldy and Purdy[55] have presented a model based on nearest-neighbor interactions with regular behavior for ternary austenite.

Here, their analysis is carried through just for the binary (iron-carbon) austenite.

The carbon atoms occupy the octahedral interstices of the fcc austenite lattice. There are four such octahedral sites and four lattice sites per unit cell; thus, the number of available sites for carbon atoms is equal to the number of iron atoms. We will consider three different energy pairs: between nearest iron atoms, between iron atoms and their nearest carbon neighbors, and between nearest carbon atoms. The respective coordination numbers of these pairs are twelve, six and twelve.

In the following formulations, the subscript "1" denotes carbon and subscript "3" denotes iron. The Gibb's free energy of the solution, by the usual solid state approximation, is given by:

$$F = E - TS \tag{A1}$$

where: E = sum of energy pairs

S = configurational entropy

$$E = P_{11}E_{11} + P_{33}E_{33} + P_{13}E_{13} \tag{A2}$$

where: E_{ij} = energy of pair

P_{ij} = number of pairs

Now,

$$P_{13} = 6\,N_1 \tag{A3}$$

$$P_{33} = 6\,N_3 \tag{A4}$$

and the N_i represents the number of "i" atoms. The number of carbon pairs, P_{ii}, depends on the way the carbon atoms are distributed in the available octahedral sites. The usual assumption is made that they are randomly distributed; then:

$$P_{11} = 6 \frac{N_1^2}{N_3} \tag{A5}$$

By using (A3), (A4), and (A5) with (A3), the energy of the solution is given by:

$$E = 6 \frac{N_1}{N_3} N_1 E_{11} + 6 N_3 E_{33} + 6 N_1 E_{13} \tag{A6}$$

The configurational entropy for the random distribution of carbon atoms in the octahedral voids is:

$$S = k \ln \frac{N_3!}{N_1!(N_3 - N_1)!} \tag{A7}$$

and with Stirling's approximation

$$S = k[N_3 \ln \frac{N_3}{N_3 - N_1} - N_1 \ln \frac{N_1}{N_3 - N_1}] \tag{A8}$$

where: k = Boltzman's constant

With the energy and entropy formulated by (A6) and (A8), respectively, the free energy is:

$$F = 6 \frac{N_1}{N_3} N_1 E_{11} + 6 N_3 E_{33} + 6 N_1 E_{13} - kT [N_3 \ln \frac{N_3}{N_3 - N_1} - N_1 \ln \frac{N_1}{N_3 - N_1}] \tag{A9}$$

. . . . .

The partial molar free energy (chemical potential) is by definition

$$\bar{F}_1 = N_o \left(\frac{\partial F}{\partial N_i} \right)_{N_3,T} \qquad \text{(A10)}$$

Performing the indicated operation of (A10), the partial molar free energy of carbon is given as:

$$\bar{F}_1 = 12N_o \frac{N_1}{N_3} E_{11} + 6\, N_o E_{13} + kN_o T \ln \frac{N_1}{N_3 - N_1} \qquad \text{(A11)}$$

and since $\bar{F}_1 - F_1^\circ = RT \ln a_1$

$$\ln a_1 = \left(\frac{N_1}{N_3} \right)\left(\frac{12N_o E_{11}}{RT}\right) + \left(\frac{6N_o E_{13}}{RT}\right) + \ln \frac{N_1}{N_3 - N_1} - \frac{F_1^\circ}{RT} \qquad \text{(A12)}$$

where, F_1° = free energy of carbon in its standard state (pure graphite). In terms of mole fractions, X_1 and X_3, (A12) becomes

$$\ln a_1 = \left(\frac{X_1}{X_3} \right)\left(\frac{12N_o E_{11}}{RT}\right) + \frac{6N_o E_{13}}{RT} + \ln \frac{X_1}{X_3 - X_1} - \frac{F_1^\circ}{RT} \qquad \text{(A13)}$$

From Kirkaldy and Purdy[55], the activity of carbon in ternary austenite with an element that substitutes in the fcc lattice sites is:

$$\ln a_1 = \left(\frac{X_1}{X_3+X_2}\right)\left(\frac{12N_o E_{11}}{RT}\right) + \frac{6N_o E_{13}}{RT} + \ln \frac{X_1}{X_3+X_2-X_1} + \left(\frac{X_2}{X_3+X_2}\right)\left\{\frac{6N_o}{RT}(E_{12}-E_{13})\right\} - \frac{F_1^\circ}{RT}$$

. . . . . (A14)

This, of course, reduces to equation (A13) when the concentration of the substitutional element, X_2, is zero.

C. Application of the Model for Analyzing the Experimental Data

Equation (A13) can be written in a form convenient for plotting purposes.

$$RT\ln\left[\frac{a_1}{X_1}(1 - 2X_1)\right] = A_0 + A_1\left(\frac{X_1}{1 - X_1}\right) \qquad (A15)$$

where: $A_o = 6\,N_oE_{13} - F_1^\circ$

$A_1 = 12\,N_oE_{11}$

Because the energy pairs would be expected to vary with temperature, likewise the free energy of the standard state, the coefficients A_o and A_1 are functions of temperature. However, they will be assumed independent of composition.

The functional relationship between the activity of carbon and the concentration of carbon, as indicated by equation (A15), fits the data very well. An example of its validity is shown in Figure A2 where the data of Smith[49] at 1000°C has been plotted and the "least-squares" line drawn. All the data of the various investigators likewise follow the form of equation (A15) when plotted individually. However, when the "least-squares" lines are compared for all four investigators at 1000°C (Figure A3) obvious differences arise. Such differences between the various sets of data are not nearly so evident when Figure A1 is referred to. Thus it can be said that the thermodynamic model represents the dependence of carbon

concentration; furthermore the model provides a very sensitive critique of the experimental data.

The model as it stands does not indicate the temperature dependence of carbon's activity because, as previously mentioned, the coefficients are temperature dependent. Due to the fact that the various sets of data plotted in Figure A3 show wide variations in A_o and A_1 (the same is true at 800°C) and that the activity of carbon has not been measured enough at 900, 1100, and 1200°C, the temperature dependence of A_o and A_1 cannot be ascertained with any reliability solely from the data of Figure A1. However, recently the gamma solidus for the iron-carbon-system has been accurately determined by Elliott and Benz[30]. Their data (per cent carbon versus temperature for gamma solidus) in conjunction with the known activity of carbon in the liquid gives several carbon activities at temperatures ranging from 1153°C (gamma-graphite-liquid eutectic) to 1499°C (gamma-delta-liquid peritectic). This higher temperature data along with the data of Figure A1 can be combined to yield the temperature dependence of the activity if the functional dependence of the coefficients A_o and A_1 with temperature is described.

From chemical thermodynamics we can write:

$$\left[\frac{\partial \ln \gamma_1}{\partial(\frac{1}{T})}\right]_{X_1} = \frac{H_1^M}{R} \qquad \text{(A16)}$$

where: H_1^M = relative heat of mixing for carbon

γ_1 = activity coefficient of carbon ($\gamma_1 = \frac{a_1}{X_1}$)

The relative heat of mixing will be assumed independent of temperature but is a function of carbon concentration. For an alloy with zero carbon concentration, equation (A15) reduces to:

$$RT \ln \gamma_o = A_o \tag{A17}$$

where: $$\gamma_o = \lim_{X_1 \to 0} \left[\frac{a_1}{X_1} (1 - 2X_1) \right]$$

Combining (A16) and (A17), A_o is shown to be a linear function of temperature.

$$A_o = H + bT \tag{A18}$$

Substituting the linear function of A_o into equation (A15) and again applying (A16) for any concentration of carbon, the other coefficient, A_1, is likewise seen to be a linear function of temperature.

$$A_1 = G + cT \tag{A19}$$

Therefore, for an iron-carbon austenite, the functional dependence for the activity of carbon with respect to composition and temperature is given by:

$$RT \ln \left[\frac{a_1}{X_1} (1 - 2X_1) \right] = (H + bT) + (G + cT)\left(\frac{X_1}{1 - X_1} \right) \tag{A20}$$

The four constants (H, G, b and c) are evluated to best fit the data of Figure A1 along with the data taken from the gamma solidus in the following manner. Equation (A20) is rearranged to read:

$$R\ln\left[\frac{a_1}{X_1}(1 - 2X_1)\right] = \frac{1}{T}\left[H + G\left(\frac{X_1}{1 - X}\right)\right] + \left[b + c\left(\frac{X_1}{1 - X_1}\right)\right] \quad \ldots\ldots\ldots \text{(A21)}$$

Thus for a fixed carbon concentration, a plot of $R\ln\left[\frac{a_1}{X_1}(1 - 2X_1)\right]$ versus $\frac{1}{T}$ should yield a straight line in accoradance with equation (A16). Ten compositions along the entire temperature range of gamma solidus were selected. For each point, the left side of equation (A21) was evaluated along with the respective reciprocal temperatures and values of $X_1/(1 - X_1)$.

The activities for these compositions were calculated from Rist and Chipman's[53] equation applied to the compositions of the liquid in equilibrium with the respective austenite compositions. This equation will be presented below. From the thermodynamic model plots (such as Figure A2) which were derived from the data of Figure A1, the values of the left side of equation (A21) were taken at the carbon concentrations in question, i.e., $X_1/(1 - X_1)$. The plots were then made for each composition and the "least-squares" line drawn. Figure A4 shows two extremes of the compositions chosen. The agreement of the low temperature data with the points calculated from the phase diagram is very good. In fact the deviation of the phase diagram point shown for $(X_1/1 - X_1)$ equal to 0.1002 was the largest encountered for all ten plots. From these ten plots values of $R\ln\left[\frac{a_1}{X_1}(1 - 2X_1)\right]$ were taken and plotted versus $X_1/(1 - X_1)$ at constant reciprocal temperatures. These plots should also yield straight lines if equation (A20) is rearranged to read:

$$R\ln\left[\frac{a_1}{X_1}(1 - 2X_1)\right] = \left(\frac{H}{T} + b\right) + \left(\frac{G}{T} + c\right)\left(\frac{X_1}{1 - X_1}\right) \qquad (A22)$$

This is shown in Figure A5 where, by the use of the "least-squares" method, the slopes and intercepts were determined. The four constants, H, b, G and c were finally evaluated by determining the variation of the slopes and intercepts with the reciprocal temperature as shown in Figure A6. The results are:

$$\begin{aligned} H &= 10{,}550 \text{ cal/mole} \\ G &= -5{,}125 \text{ cal/mole} \\ b &= -4.106 \text{ cal/mole-deg} \\ c &= 15.967 \text{ cal/mole-deg} \end{aligned} \qquad (A23)$$

Using these values the restuls are replotted in Figure A6 where it is seen that the results agree very closely with the individual "least-squares" lines applied to each temperature.

D. Comparison with the Phase Diagram

Using equation (A25) the activity of carbon is calculated for various points along the liquidus, and then equation (A24) is used to calculate the composition of the corresponding points along the solidus. By applying the Gibbs-Duhem relation to equation (A25), the activity of iron in the liquid is expressed as:

$$\log \gamma_3 = \alpha X_1^2 \qquad (A26)$$

$$\text{where: } \alpha = [-4350/T][1 + .0004(T - 1770)] \qquad (A27)$$

The activity of carbon in iron-carbon solution of austenite is:

$$RT\ln\left[\frac{a_1}{X_1}(1 - 2X_1)\right] = (10{,}550 - 4.106T) + (-5{,}125 + 15.967T)\left(\frac{X_1}{1 - X_1}\right) \quad \ldots\ldots\ldots (A24)$$

The activity of carbon in liquid iron-carbon alloys[53] is:

$$\log\left[\frac{a_1}{X_1}(.0462 + 8.785 \times 10^{-5}T)\right] = \frac{4350}{T}\left[(.9538 - 8.785 \times 10^{-5}T)^2 - (1-X_1)^2\right] \quad \ldots\ldots\ldots (A25)$$

The Gibbs-Duhem relation applied to equation (A15) yields:

$$RT\ln\gamma_3 = RT\ln\left[\frac{(1 - 2X_1)}{(1 - X_1)^2}\right] - \left[\frac{X_1}{1 - X_1}\right]^2 \frac{A_1}{2} \qquad (A28)$$

With equations (A26) and (A28), the activity of iron in the liquid, a_3^{ℓ} (standard state, pure liquid iron), and in austenite a_3^{γ} (standard state, pure austenite) are calculated.

The results of these calculations are presented in Table AI. The calculated points along the solidus agree within 4 per cent error of the phase diagram points. A plot of a_3^{γ}/a_3^{ℓ} versus reciprocal temperature is given in Figure A7. Such a plot yields the change in standard state from pure liquid iron to pure austenite iron, and is compared to a plot derived from Elliott et al[56], where

$$\ln\frac{a_3^{\gamma}}{a_3^{\ell}} = \frac{\Delta H^{\circ}}{R}\left[\frac{1}{T} - \frac{1}{T_e}\right] \qquad (A29)$$

and ΔH° = heat of fusion between liquid and austenite iron

T_e = freezing point between liquid and austenite iron, 1801°K

Equation (A29) becomes:

$$\log \frac{a_3^\gamma}{a_3^\ell} = \frac{878.9}{T} - .4880 \qquad \text{(A30)}$$

The data calculated from the phase diagram agree very closely with (A30) at higher temperatures but yield lower ratios as the temperature decreases. This discrepancy is probably due to the relationship developed by Rist and Chipman[53] for the liquid activities which were based on data mainly at the higher temperatures. Also any inaccuracies within the development for the activities in austenite would also be reflected as well as the possibility that the heat of fusion in equation (A29) might not be a constant.

In order that the thermodynamics involved be consistent with the phase diagram, a change in the standard state for iron will be based on the expressions for the activity of carbon, i.e.,

$$T > 1640°K, \log \frac{a_3^\gamma}{a_3^\ell} = \frac{837.7}{T} - .4644$$

$$T < 1640°K, \log \frac{a_3^\gamma}{a_3^\ell} = \frac{620.3}{T} - .3318 \qquad \text{(A31)}$$

TABLE AI

Comparison of Phase Diagram Solidus with Calculated Solidus and the Activity of Iron

Temperature °C	Solidus Atom Fraction of Carbon, X_1		Activity of Iron		
	Calculated	Phase Diagram	Liquid, $a_3^{\prime}$	Solid, a_3^{γ} (based on calculated X_1)	Solid, a_3^{γ} (based on phase diagram)
1475	.0131	.0138	.9529	.9861	.9855
1450	.0200	.0201	.9299	.9780	.9781
1400	.0342	.0326	.8835	.9606	.9627
1300	.0584	.0569	.8024	.9265	.9288
1200	.0786	.0806	.7273	.8939	.8906
1153	.0876	.0911	.6933	.8789	.8726

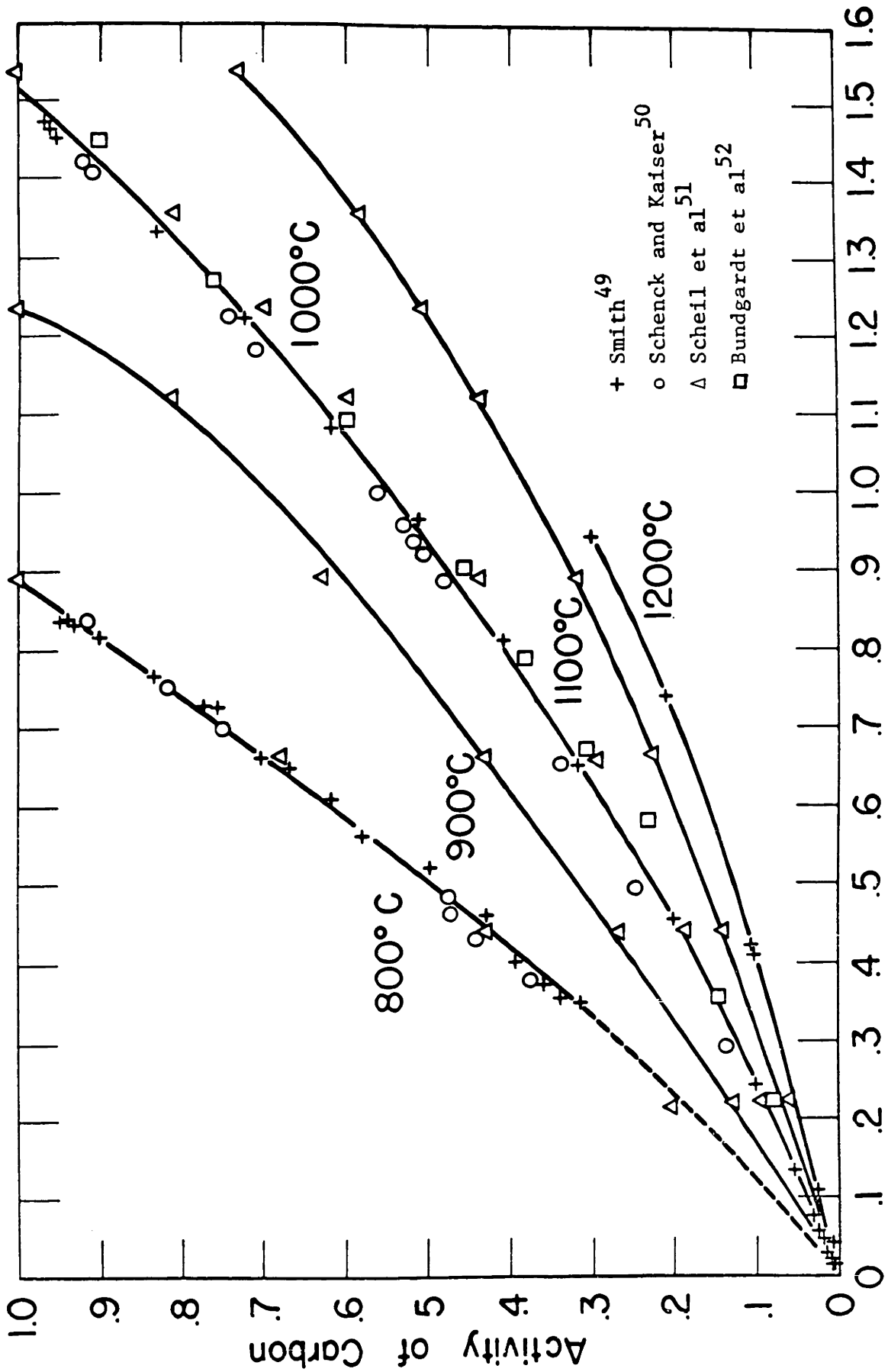

Figure A1: The activity of carbon in austenite as determined by various investigators.

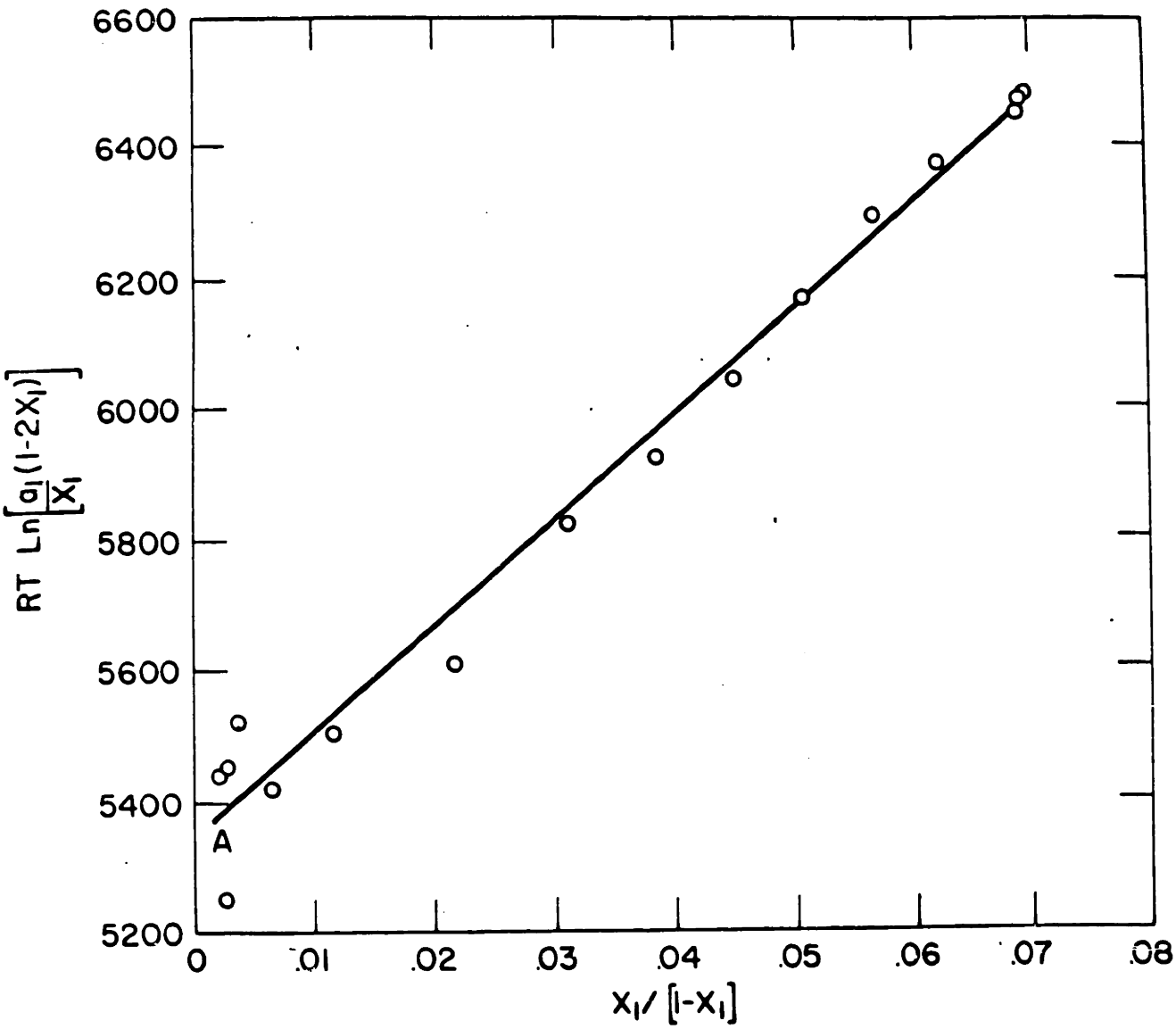

Figure A2: Application of the thermodynamic model. Data from Smith[49] at 1000°C.

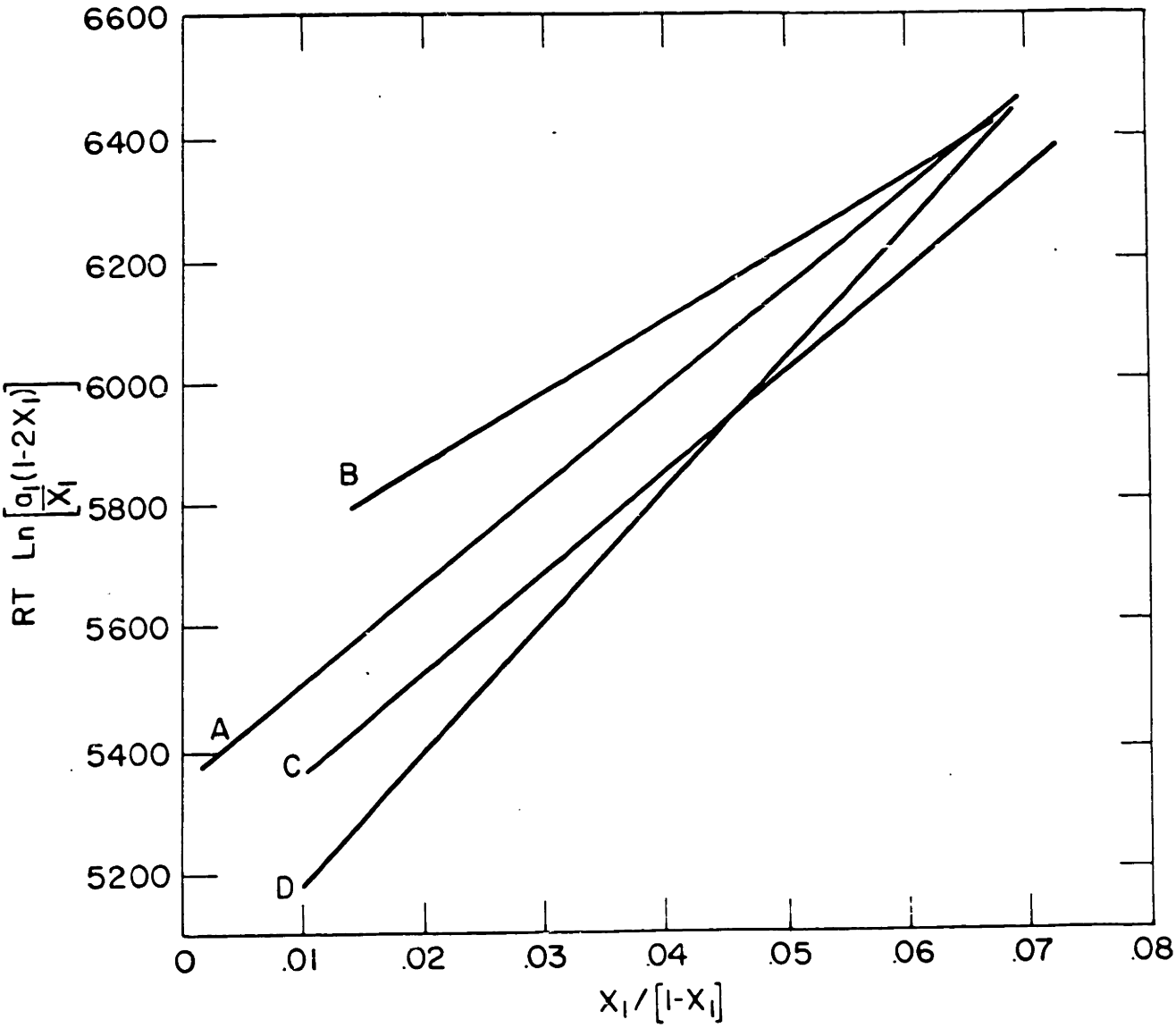

Figure A3: The activity of carbon as depicted by the thermodynamic model applied at 1000°C.

A. Smith[49]

B. Schenk and Kaiser[50]

C. Scheil, Schmidt, and Wünnig[51]

D. Bundgardt, Preisendanz, and Lehnert[52]

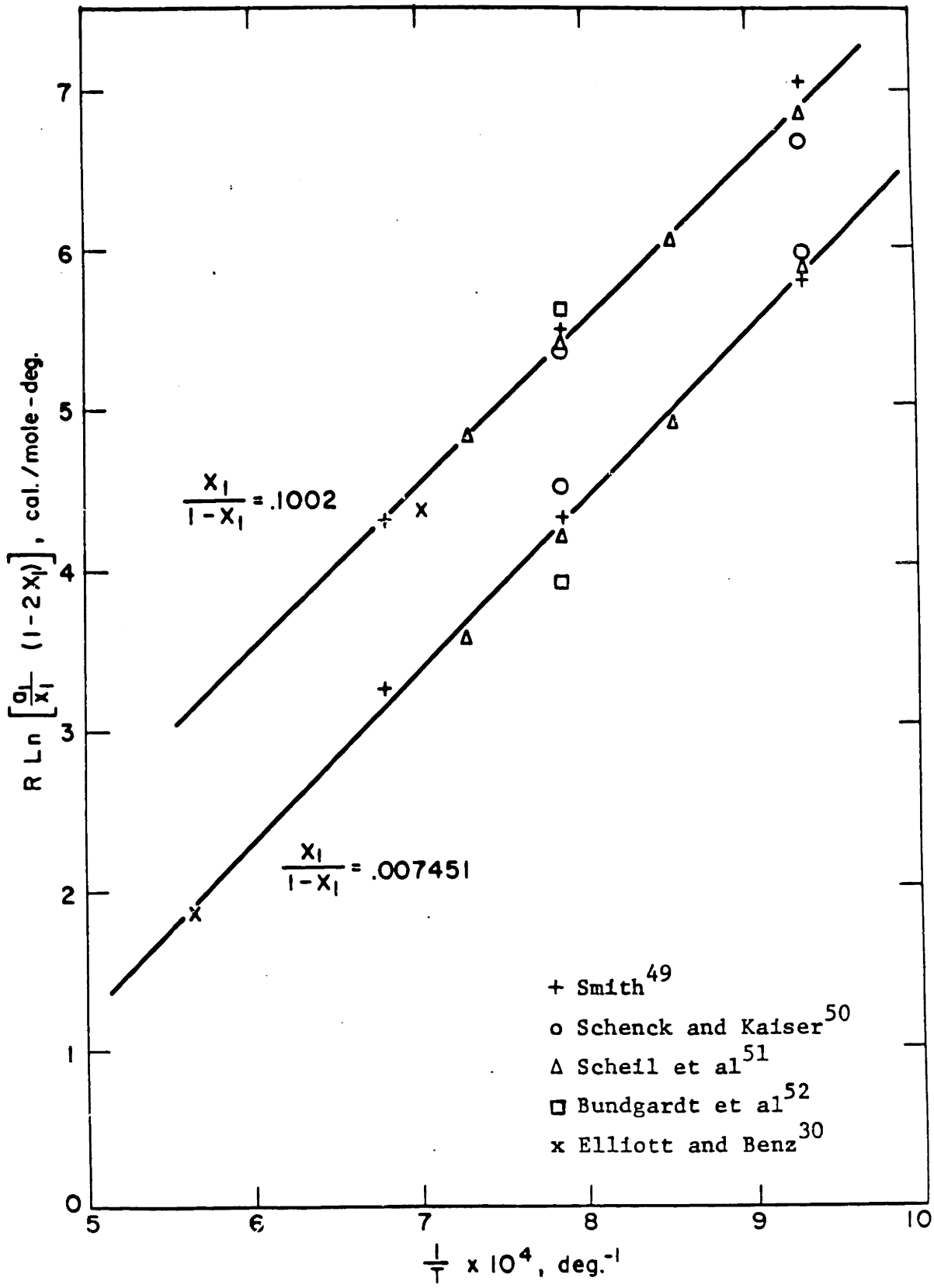

Figure A4: Temperature dependence of the activity of carbon for two concentrations.

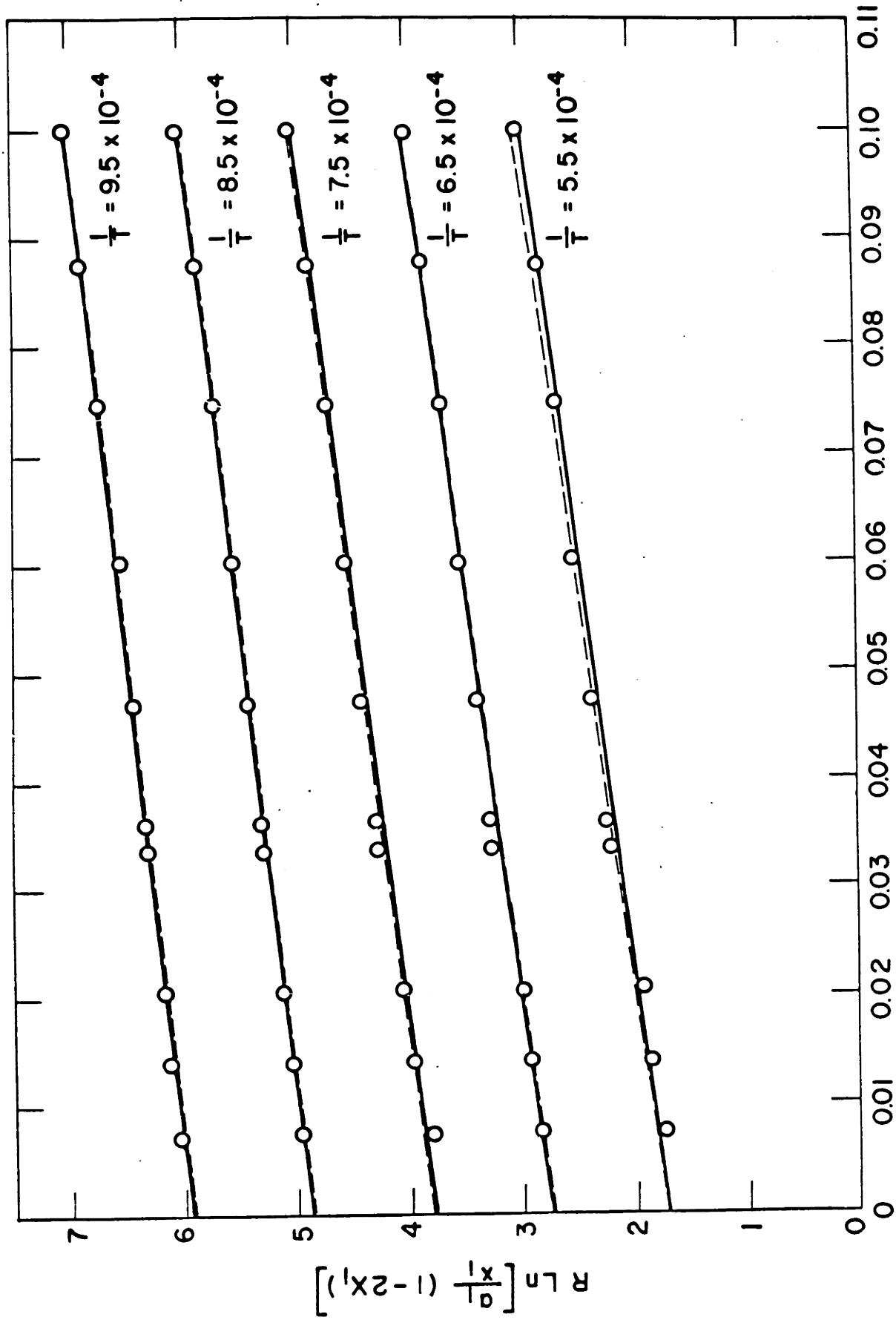

Figure A5: Plots derived from data of which Figure A4 is typical.

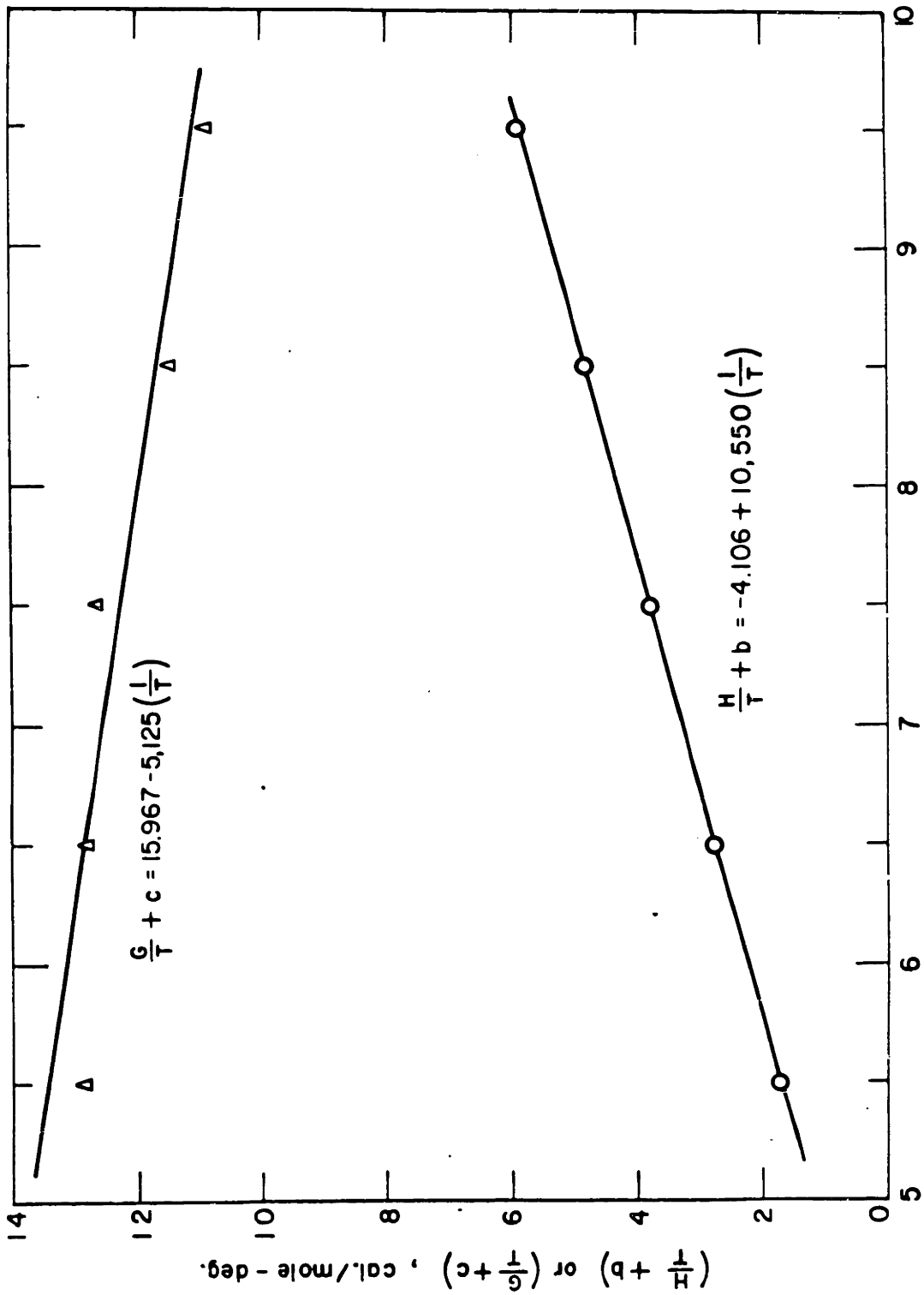

Figure A6: Determination of the four constants H, G, b and c.

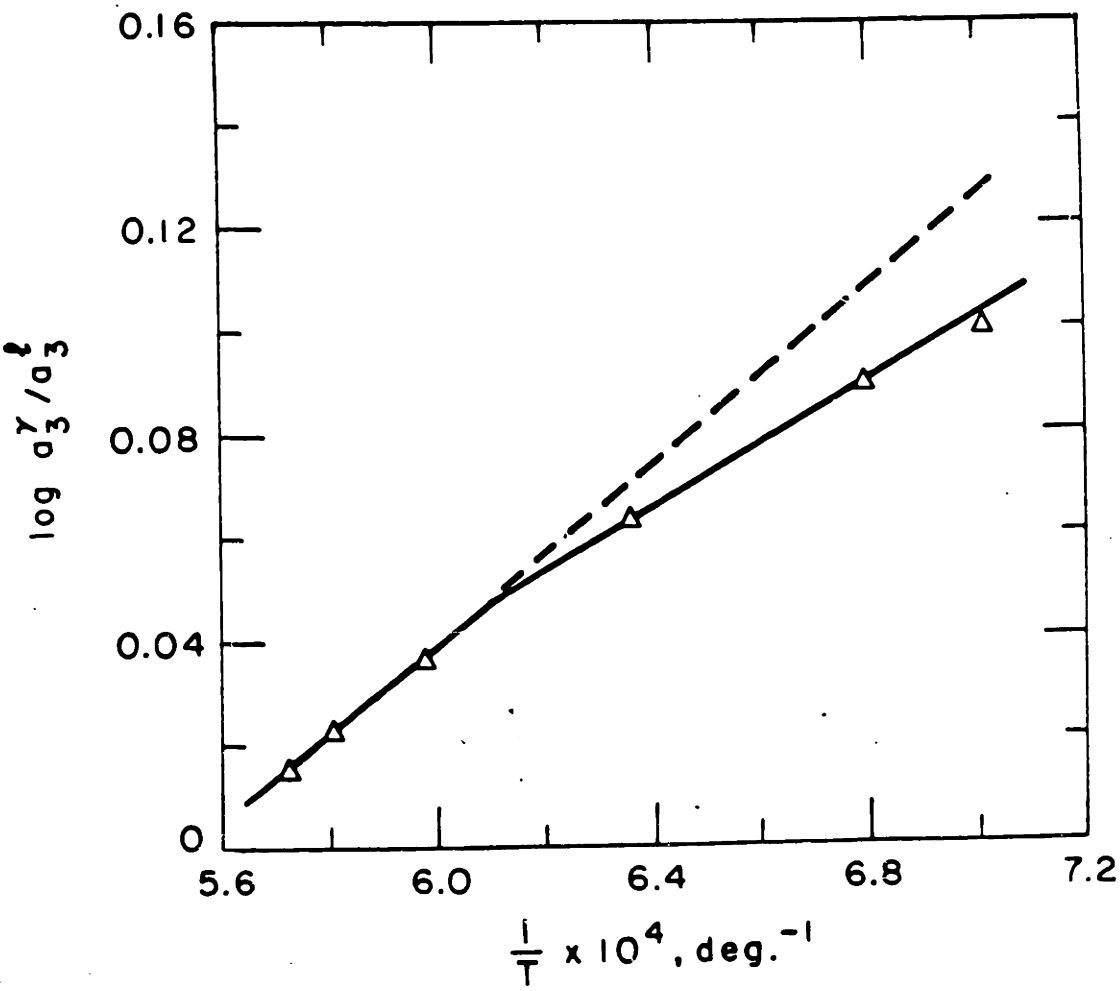

Figure A7: Change of standard state for iron between liquid and austenite. Solid line is calculated using the phase diagram and the activities of iron coexisting in the two phases, and the dotted is based on free energy differences between austenite and liquid iron.

APPENDIX B

ACTIVITY OF CARBON IN LIQUID IRON-CARBON-CHROMIUM SOLUTIONS

A. Introduction

The activity of carbon in iron-carbon-chromium liquid solutions has been measured by Richardson and Dennis[60] (1560°C, 1660°C, 1760°C), Fuwa and Chipman[59] (1560°C), Goto et al[3] (1560°C). Fuwa and Chipman[59] have presented their data along with data of Richardson and Dennis[60] and utilized an interaction parameter. However, the interaction parameter is only valid for dilute solutions of carbon because, as they indicated, the same interaction parameter does not apply to more concentrated solutions of carbon (i.e., the effect of chromium on the saturation of graphite in liquid iron). Ohtani[58] has attempted to account for the effect of carbon concentration on the interaction parameter; however even his analysis does not apply to the saturation data. Also, the effect of temperature on interaction parameters must be taken into account[62]. Therefore, in any process where the concentration of carbon changes appreciably and/or the temperature changes (such as solidification), the use of an interaction parameter is not adequate to know the activity of carbon.

B. Empirical Relation for the Activity of Carbon

The purpose of the following argument is to make use of the existing data on the effect of chromium on the activity of carbon in liquid iron solutions in such a way that the activity can be

described as a function of both composition and temperature. The method is an extension of Rist and Chipman's[53] analysis for the binary iron-carbon solutions. As in Rist and Chipman's analysis, the activity coefficient is assumed to obey the relation:

$$\log \gamma_1 = \alpha(1 - X_1)^2 + I \qquad \text{(B1)}$$

where γ_1 = activity coefficient of carbon (a_1/X_1)

X_1 = atom fraction of carbon

α = factor dependent on temperature and chromium concentration

I = factor depending on choice of standard state

As in the previous section that dealt with the activity of carbon in austenite, the standard state referred to is graphite. Thus

$$I = -\alpha(1 - X_{1S})^2 - \log X_{1S} \qquad \text{(B2)}$$

where: X_{1S} = saturation atom fraction of carbon which depends on temperature and chromium concentration.

C. Saturation of Graphite in Iron-Carbon-Chromium Melts

The saturation of carbon in iron melts containing chromium was determined from the data of Ban-Ya and Matoba[63] (1400°C to 1600°C) and Griffing et al[27] (1600°C to 1800°C). The data of Sanbongi et al[64] and Neumann et al[65] are not used. The data of Ban-Ya and Matoba[63] are

the most consistent with that of Griffing et al[27] and the saturation in iron-carbon binary melts. These data are presented in Figure B1 and by least-square analysis are found to obey the relation:

$$X_{1S} = X_1^o + 0.2552\ X_2 \qquad (B3)$$

where: X_1^o = saturation of graphite in iron-carbon binary melts

X_2 = mole fraction of chromium.

In the review by Neumann et al[65], the coefficient for X_2 was found to be 0.275. From Elliott and Benz's[30] recent review of the iron-carbon phase diagram:

$$X_1^o = 0.0462 + 8.785 \times 10^{-5}\ T \qquad (B4)$$

D. Application of the Empirical Relation for the Experimental Data

The data of Richardson and Dennis[60] (chromium contents up to 25 per cent) are used exclusively to determine the factor α in equation (B1). Fuwa and Chipman's[59] data are not used because they are limited to only one activity and have wide scatter while the data of Gota et al[61] yield somewhat lower activities than Richardson and Dennis[60]. Also, the measurements of Richardson and Dennis[60] were made at three temperatures while those of the other workers are only at one temperature. Another factor for using Richardson and Dennis's data is the agreement of Chipman and Rists' equation for binary melts with the activity of carbon in austenite as discussed

in the previous section. Much of the data used in the development of Rist and Chipman's equation comes from measurements by Richardson and Dennis[54] on binary melts. Figure B2 shows the data of Richardson and Dennis[60] at 1660°C where equation (B1) is assumed to hold for a constant ratio of X_2/X_3 and the equilibrium constant for the CO/CO_2 reaction of Rist and Chipman[53] is used. Along with the data, saturation points are shown derived from equation (B3); equation (B1) for binary melts is also represented. Similar plots were made at 1560°C and 1760°C and all slopes, α, were determined by least-square analysis. The effect of chromium on the activity of carbon is then shown in Figure B3, where

$$T\ (\alpha - \alpha_b) = -4880\ \left(\frac{X_2}{X_3}\right) \tag{B5}$$

and

$$\alpha_b = \frac{-4350}{T}\ [1 + .0004\ (T - 1700)] \tag{B6}$$

Equation (B6) is that used in the relation for the activity of carbon in binary iron-carbon melts.

E. Summary

The activity of carbon in iron-carbon-chromium melts is:

$$\log \gamma_1 = \alpha(1 - X_1)^2 + I \tag{B1}$$

$$\alpha = -\frac{4880}{T}\left(\frac{X_2}{X_3}\right) - \frac{4350}{T}\ [1 + .0004(T - 1770)] \tag{B7}$$

$$I = -\alpha(1 - X_{1S})^2 - \log X_{1S} \tag{B2}$$

$$X_{1S} = 0.0462 + 8.785 \times 10^{-5}\ T + 0.2552\ X_2 \tag{B3}$$

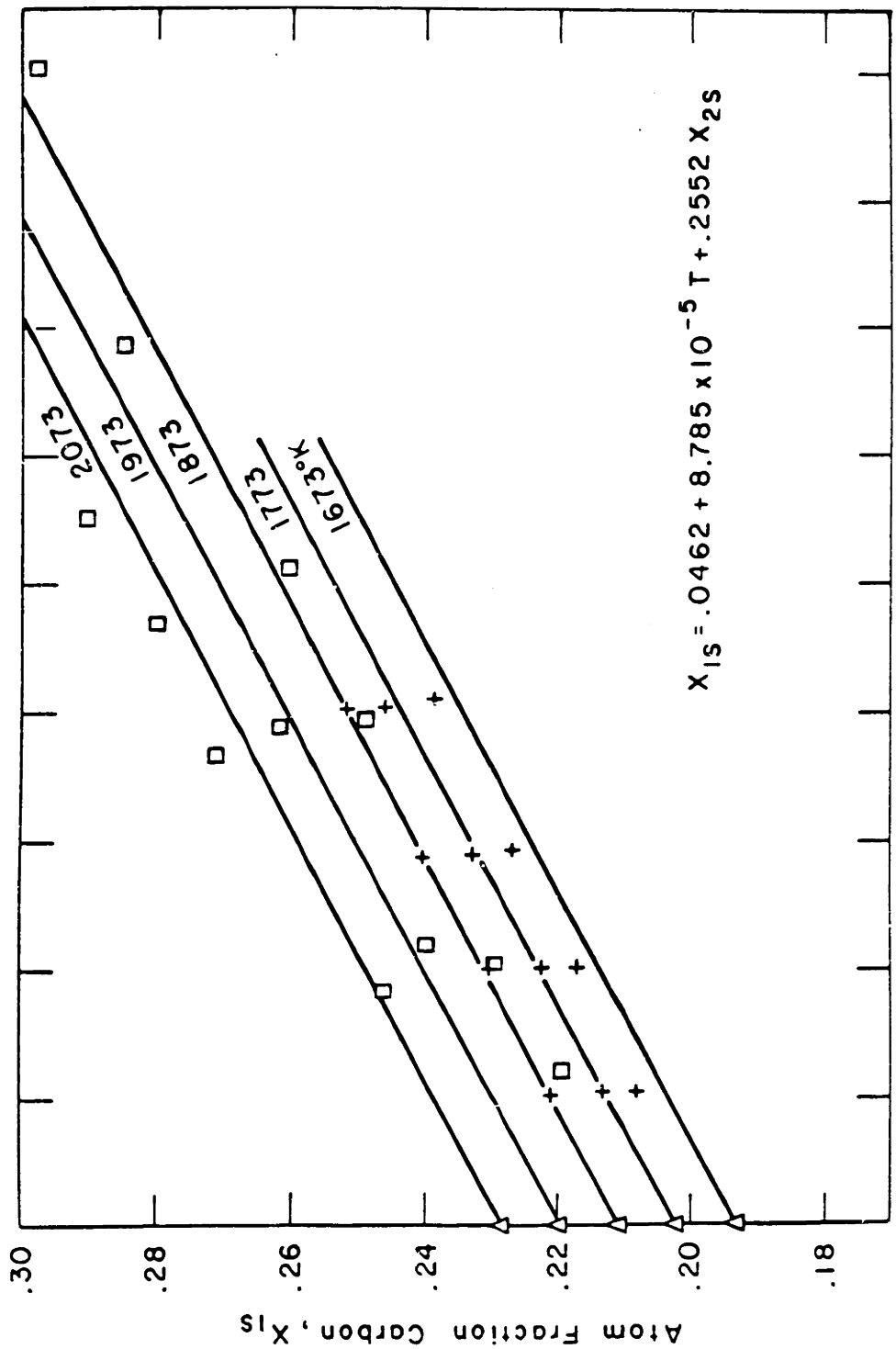

Figure B1: Effect of chromium on the saturation of graphite in liquid iron.
+ Ban-ya and Matoba[63] □ Griffing et al[27] Δ Benz and Elliott[30]

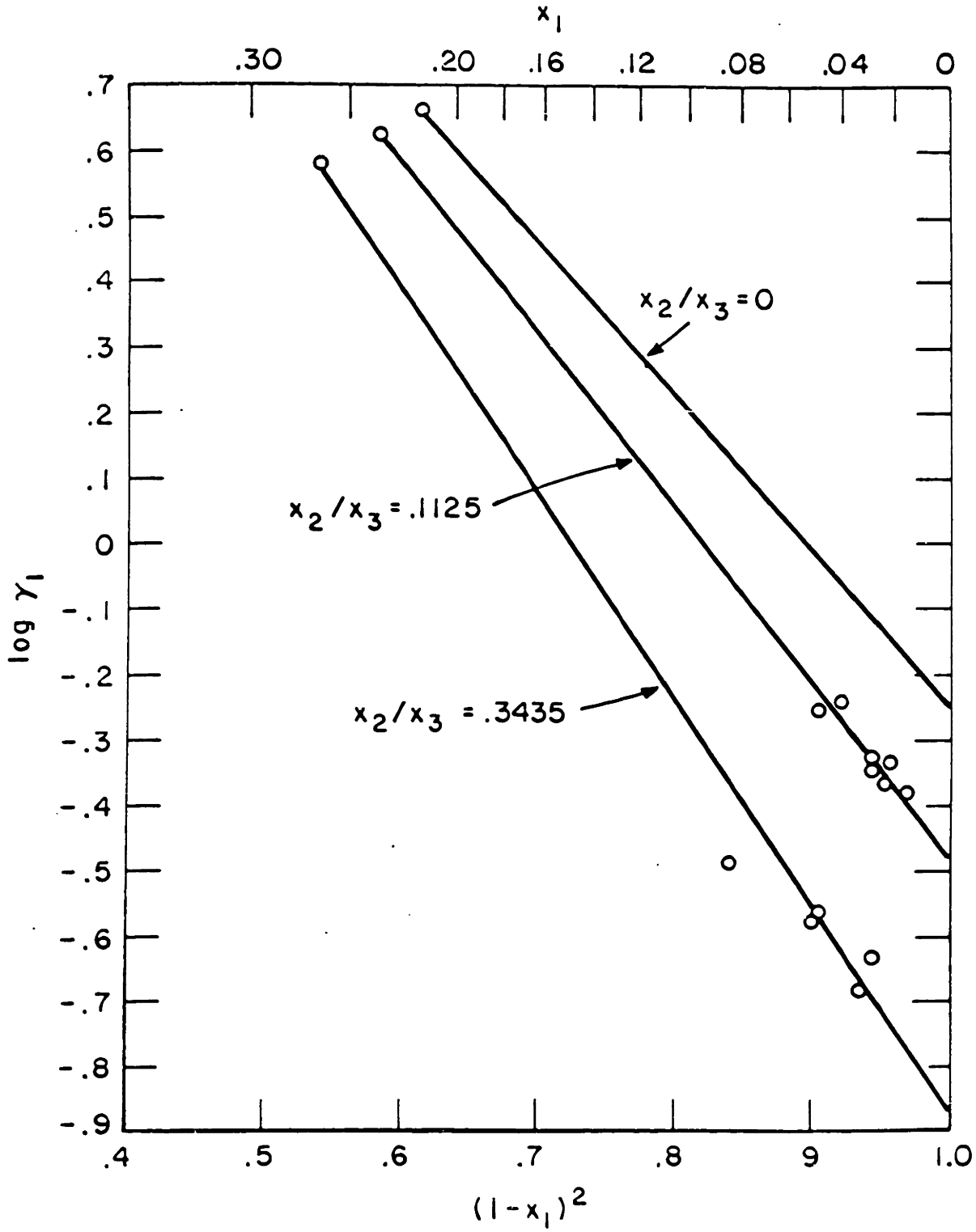

Figure B2: Activity coefficient of carbon in liquid iron at 1660°C for different chromium concentrations.

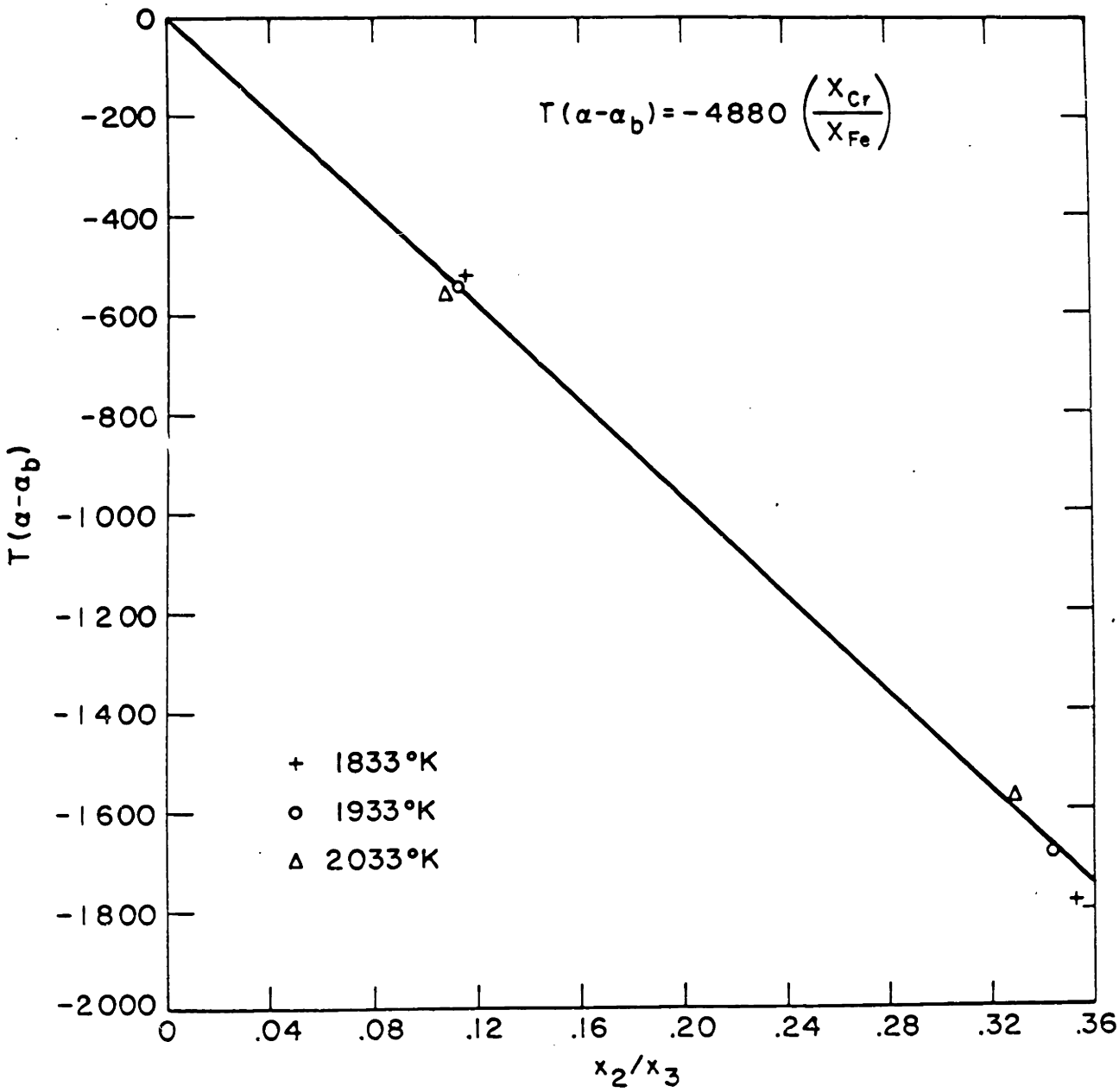

Figure B3: Effect of chromium on the parameter, α, in liquid iron-carbon-chromium alloys.

APPENDIX C

ACTIVITY OF CARBON, CHROMIUM, AND IRON IN AUSTENITIC AND LIQUID SOLUTIONS

A. Introduction

The activity of carbon in iron-carbon-chromium austenite has been measured by Kirkaldy and Brigham[66] (1000°C), Schenck and Kaiser[50] (950, 1000, and 1050°C), and Bundgardt et al[52] (1000°C). All these investigators measured the activity by the use of $CO-CO_2$ or CH_4-H_2 gas mixtures. In addition Kirkaldy and Brown[67] have made measurements at 1050°C by a "transient equilibrium" method. The quasi-chemical model as described and used for the activity of carbon in binary iron-carbon austenite is also utilized herein. Extending this analysis for a ternary austenite [see equation (A14)] yields:

$$RT\ln\left[\frac{a_1}{X_1}(1 - 2X_1)\right] = A_o + A_1\left(\frac{X_1}{1 - X_1}\right) + A_2\left(\frac{X_2}{1 - X_1}\right) \quad (C1)$$

where:
$$A_2 = \frac{6N_o}{RT}(E_{12} - E_{13}) \quad (C2)$$

Just as A_o and A_1 were shown to be linear functions of temperature in Appendix A, A_2 is also a linear function of temperature and is likewise assumed to be independent of composition.

Therefore, one purpose of this section is to determine A_2, and then the effect of chromium on the activity of carbon in austenite

can be described. The available data in the literature are limited to a small temperature range, 950° to 1050°C. To supplement this the data of the literature, the experimentally measured chromium distributions between liquid alloys and austenite (Table V) are used to evaluate A_2 at higher temperatures.

B. Evaluation of Data from Literature for the Activity of Carbon in Fe-C-Cr Austenite

For the determinations involving the use of gas mixtures all the data were reduced in order to evaluate the parameters in equation (C1). The data for each investigator were reduced in a manner that the activity of carbon was determined at constant values of $X_2/(1 - X_1)$. For each investigator the term $A_2(X_2/1 - X_1)$ was calculated using equation (C1) in the following form:

$$A_2\left(\frac{X_2}{1 - X_1}\right) = RT\ln\left[\frac{a_1}{X_1}(1 - 2X_1)\right] - A_o - A_1\left(\frac{X_1}{1 - X_1}\right) \qquad \text{(C1a)}$$

The values of A_o and A_1 chosen are those determined from the binary system for the particular investigator, i.e., Bundgardt et al's[52] data are referred to as their own particular carbon activities in binary austenite; the same is true for Schenck et al[50]. Kirkaldy and Brigham's data[66] refer to Smith's[49] activity of carbon in binary austenite because they reported using the same experimental method. The different binary reference levels for the various investigators is used in order to isolate the effect of chromium, alone, that they measured.

At a given temperature and $X_2/(1 - X_1)$ value, the average value of $A_2(X_2/1 - X_1)$ was determined. Finally, the parameter attributed to a particular investigator was evaluated by:

$$A_2 = \frac{\sum_i [(\frac{X_2}{1 - X_1})^2 (A_2)n]_i}{\sum_i [(\frac{x_2}{1 - X_1})^2 n]_i} \qquad (C3)$$

where: n = number of determinations at a particular $(X_2/[1 - X_1])$ value.

Before the method for reducing the "transient equilibrium" data of Kirkaldy and Brown[67] is described, a brief description of the technique should be described. A thin wafer of binary iron-carbon alloy is bonded between two thin wafers of ternary iron-carbon-chromium alloy. The diffusion distance for carbon is several times greater than the wafers' thicknesses, whereas chromium hardly diffuses. Thus the carbon redistributes itself very quickly to a constant activity across the three wafers while the chromium maintains its original concentrations.

By measuring the concentrations of carbon and chromium in the respective wafers, the effect of chromium on the activity of carbon can be determined. Applying equation (C1) to the binary and ternary wafers in contact yields:

$$RT\ln\left[\frac{1 - 2X_1^t}{1 - 2X_1^b} \cdot \frac{X_1^b}{x_1^t}\right] = A_1\left[\frac{X_1^t}{1 - X_1^t} - \frac{X_1^b}{1 - X_1^b}\right] + A_2\left(\frac{X_2^t}{1 - X_1^t}\right)$$

The superscripts "b" and "t" represent the binary and ternary alloys, respectively.

C. Evaluation of the Experimental Chromium Distributions Between Liquid Alloys and Austenite

The experiments used to determine the chromium distribution between the liquid alloys and austenite yielded the temperature, composition of both carbon and chromium in the liquid, but only the composition of chromium in the solid. Thus, the activity of carbon in the liquid is known, but when equation (C1) is applied to the solid to satisfy the requirement that the activity of carbon in both phases must be equal, two unknowns (X_1 and A_2) arise. Therefore, the activity of iron and/or chromium in both phases must also be considered. This is accomplished by the Gibbs-Duhem requirement as applied to ternary solutions.

1. Activities in Ternary Systems

Following a discussion of Wagner[68], the Gibbs-Duhem relation applied to a ternary solution of components, i, j, k yields

$$F_i^E = F^E + (1 - X_i)\left(\frac{\partial F^E}{\partial X_i}\right)_{X_j/X_k} \qquad (C5)$$

where: X = mole fractions

F^E = integral excess molar free energy

F_i^E = partial excess molar free energy

By dividing equation (C5) through with $(1 - X_2)^2$ and rearranging, it follows that

$$\left\{ \frac{\partial [F^E/(1 - X_i)]}{\partial X_i} \right\}_{X_j/X_k} = \frac{F_i^E}{(1 - X_i)^2} \qquad (C6)$$

Equation (C6) may be integrated in several ways; the choice depends upon what activity data is known. In the case at hand, the activity of carbon is functionally described for both the liquid and solid phases. Hence, the following integration is chosen as the most suitable.

$$F^E = (1 - X_1)\left[F^E(X_1 = 0) + \int_o^{X_1} \frac{F_1^E}{(1 - X_1)^2} \, dX_1\right]_{X_2/X_3,T} \qquad (C7)$$

Remembering that,

$$F_1^E = RT \ln \frac{a_1}{X_1} = RT \ln \gamma_1 \qquad (C8)$$

and supposing the integral excess molar free energy is known for the binary iron-chromium solutions, equation (C7) enables the calculation of F^E for the ternary solutions. From F^E, and referring to equation (C5), the activity of iron and chromium can then be determined as:

$$RT \ln \gamma_2 = F_2^E = F^E + (1 - X_2)\left(\frac{\partial F^E}{\partial X_2}\right)_{X_1/X_3} \qquad (C9)$$

and

$$RT \ln \gamma_3 = F_3^E = F^E + (1 - X_3)\left(\frac{\partial F^E}{\partial X_3}\right)_{X_1/X_2} \qquad (C10)$$

2. Application of Gibbs-Duhem Relation to the Liquid.

Referring to the Summary for the activity of carbon in liquid iron-carbon-chromium solutions, (equations B1-3, B7) we can write:

$$F^E = (1 - X_1)[F^E(X_1 = 0) + 4.576T \int_0^{X_1} \frac{\alpha(1 - X_1)^2 + I}{(1 - X_1)^2} dX_1]_{X_2/X_3,T}$$

. . . . . .(C11)

At a constant X_2/X_3,T both α and I are constants. Also, the integral excess molar free energy (F^E) for liquid iron-chromium solutions is zero because iron and chromium form ideal solutions[57,58]. Performing the integration, equation (C11) becomes:

$$F^E = 4.576\ T\ [\alpha X_1(1 - X_1) + IX_1] \qquad (C12)$$

Referring to equation (C9) F_2^E can be found if $(\partial F^E/\partial X_2)_{X_1/X_3}$ is established. When X_1/X_3 is held constant, the differentiation of equation (C12) is tedious because α and I vary. For this reason only the results of this operation are presented.

$$F_2^E = RT \ln \gamma_2 = F^E + (1 - X_2)\left(\frac{\partial F^E}{\partial X_2}\right)_{X_1/X_3} \qquad (C9)$$

where,

$$\left(\frac{\partial F^E}{\partial X_2}\right)_{X_1/X_3} = 4.576T\{-[A]\frac{X_1}{X_1+X_3} + [B]\left(\frac{\partial \alpha}{\partial X_2}\right)_{X_1/X_3} + [C]\left(\frac{\partial X_{1S}}{\partial X_2}\right)_{X_1/X_3}\}$$

. . . . . .(C13)

$$[A] = \alpha[(1 - 2X_1) - (1 - X_{1S})^2] + \log \frac{1}{X_{1S}} \quad (C14)$$

$$[B] = X_1[(1 - X_1) - (1 - X_{1S})^2] \quad (C15)$$

$$[C] = X_1[2\alpha(1 - X_{1S}) - \frac{1}{2.303X_{1S}}] \quad (C16)$$

$$\left(\frac{\partial \alpha}{\partial X_2}\right)_{X_1/X_3} = \frac{-4880}{T} \left(\frac{1}{X_3}\right) \left[\frac{1}{X_3 + X_1}\right] \quad (C17)$$

$$\left(\frac{\partial X_{1S}}{\partial X_2}\right)_{X_1/X_3} = .2552\left(\frac{1 - X_1^o}{1.2552X_2 + X_3}\right)\left[1 - \left(\frac{X_2}{1.2552X_2 + X_3}\right)\left(\frac{.2552X_3 + 1.2552X_1}{X_3 + X_1}\right)\right]$$

. . . . . .(C18)

To evaluate the partial excess molar free energy for iron, the following expression is used:

$$F^E = X_1F_1^E + X_2F_2^E + X_3F_3^E \quad (C19)$$

3. Application of Gibbs-Duhem Relation to the Solid.

Referring to equation (C1), the partial excess molar free energy for carbon in austenite can be written as

$$F_1^E = A_o + A_1\left(\frac{X_1}{1 - X_1}\right) + A_2\left(\frac{X_2}{1 - X_1}\right) - RT \ln (1 - 2X_1) \quad (C20)$$

The binary system for austenitic iron-chromium alloy is assumed to be regular so that

$$F^E(X_1 = 0) = \Omega X_2^b X_3^b \quad (C21)$$

where: X_2^b, X_3^b represent binary concentrations.

The activities in iron-chromium austenitic alloys have been measured by Jeannin et al[69] at 1200°C and Kubaschewski and Heymer[70] at 1341 to 1370°C. At these temperatures the standard states for the reported activities are pure gamma iron and pure delta chromium. Since the present argument concerns only austenite, the activity of iron was treated in order to determine Ω for equation (C21). For a regular solution of iron and chromium

$$RT \ln \gamma_3 = \Omega X_2^2 \qquad (C22)$$

Jeannin's[69] data could be fitted to equation (C22) within experimental error if

$$\Omega_1 = 2165 \text{ cal/mole}$$

Kubaschewski and Heymer's[70] data yield

$$\Omega_2 = 2969 \text{ cal/mole}$$

Weighing Ω_1 and Ω_2 according to the number of determinations of the respective investigators, a mean value was established.

$$\Omega = 2490 \text{ cal/mole}$$

This value of Ω is good for $0 \leq X_2 \leq 0.092$.

Performing the operations indicated by equations (C7), (C9), and (C10) and noting that

$$X_2^b X_3^b = \frac{X_2 X_3}{(1 - X_1)^2} \qquad (C23)$$

the excess free energies are developed.

$$F^E = (1 - X_1)\{\Omega\frac{X_2\,X_3}{(1-X_1)^2} + A_o(\frac{X_1}{1-X_1}) + A_1[\frac{X_1^2}{2(1-X_1)^2}] + A_2\frac{X_1\,X_2}{(1-X_1)^2}$$

$$-RT[\frac{\ln(1-2X_1)}{(1 - X_1)} + 2\ln(\frac{1-X_1}{1-2X_1})]\} \qquad \text{(C24)}$$

$$F_2^E = \frac{\Omega X_3^2}{(1-X_1)^2} - [\frac{X_1^2}{2(1-X_1)^2}]\,A_1 + \frac{X_1\,X_3}{(1-X_1)^2}\,A_2 + RT\ \ln\,[\frac{(1-2X_1)}{(1-X_1)^2}] \qquad \text{(C25)}$$

$$F_3^E = \frac{\Omega X_2^2}{(1-X_1)^2} - [\frac{X_1^2}{2(1-X_1)^2}]A_1 - \frac{X_1X_2}{(1-X_1)^2}\,A_2 + RT\ \ln\,[\frac{(1-2X_1)}{(1-X_1)^2}] \qquad \text{(C26)}$$

As a check, equations (C20), (C24), (C25), and (C26) satisfy

$$F^E = X_1F_1^E + X_2F_2^E + X_3F_3^E$$

4. Calculation of the Effect of Chromium from the Solid-Liquid Equilibria.

The activities of carbon, iron and chromium are calculated for the liquid alloys using equations (B1), (C12), (C9), and (C19). The activity of carbon in the solid is then known since the standard state (pure graphite) is the same for both phases. By changing the standard state from pure liquid iron to pure gamma iron for the activity of iron in the liquid, the activity of iron in the solid is calculated. The relationship (equation A31) used for this change of standard state was previously discussed. Equation (C1) is rearranged

to read

$$A_2X_2 = RT(1 - X_1)\ln\left[\frac{a_1}{X_1}(1 - 2X_1)\right] - A_o(1 - X_1) - A_1X_1 \qquad (C1b)$$

Since the per cent chromium was measured in the solid, the mole fraction of carbon is fixed for a given per cent carbon. Thus successive trials were made by varying the per cent carbon and a set of corresponding values of X_1, X_2 and A_2 were generated.

These values are then substituted into equation (C26) to determine the activity of iron apart from its calculated activity in the liquid phase. Thus a plot of the activity of iron versus per cent carbon can be made. An example of such a plot is shown in Figure C1. The curve displays a minimum and because only one solution is physically possible, the minimum is the solution. These minimums never exactly correspond with the activity of iron as calculated for the liquid but all were within ± 1 per cent error, which are quite acceptable.

A comparison of the iron activities calculated from the liquid and as above is given in Table I. The value of A_2 that corresponds to the minimums was also calculated. However, as Figure C1 shows, the suitable A_2 is extremely sensitive to the concentration of carbon. For this reason the plot of A_2 versus temperature, Figure C2, includes limites that correspond to $\pm$ 2.5 per cent error in the carbon concentration found at the minimums. When least square

analysis is applied to this high temperature, as well as the low temperature data, an expression for A_2 is finally developed.

$$A_2 = 82.64\ T - 135,000 \qquad (C27)$$

Figure C2 does show appreciable scatter; this is true not only at high temperatures derived herein but also for the low temperature data of the other investigators.

The accuracy of the high temperature data is limited to the uncertainties that enter into formulating the activities in the liquid phase. Rist and Chipman's equation[53] for the activity of carbon in the liquid is not universally accepted, and the measurements of the effect of chromium on the activity of carbon are limited to only the three temperatures investigated by Richardson and Dennis[60].

The low temperature data reflect scatter primarily due to the measurements of the activity of carbon in ternary austenite. The data for the binary austenite seem good in view of the agreement with Benz and Elliott's gamma solidus line[30] as shown in a previous section. In order to measure the effect of chromium on the activity of carbon in austenite, it might have been better if the activity of chromium itself had been measured in iron-carbon-chromium alloys. The parameter, A_2, could then be evaluated from equation (C25). This could conceivably be a better method because then the effect of chromium on the carbon's activity would be isolated and not a

contributing part to all the factors that affect the activity of carbon. Also, more measurements by the "transient equilibrium" method of Kirkaldy and Brown seem in order. This method is very direct because it only involves the determination of alloy compositions.

TABLE CI

COMPARISON OF IRON ACTIVITIES CALCULATED FOR THE LIQUID AND FOR THE SOLID

Equilibrium Temperature, °C	Activity of Iron* Calculated for Solid	Activity of Iron* Calculated for Liquid
1444	.9688	.9678
1265	.8850	.8944
1318	.9164	.9237
1336	.9271	.9339
1370	.9422	.9492
2159	.9017	.9012
1295	.9051	.9163
1410	.9560	.9599

* Standard state is pure gamma iron.

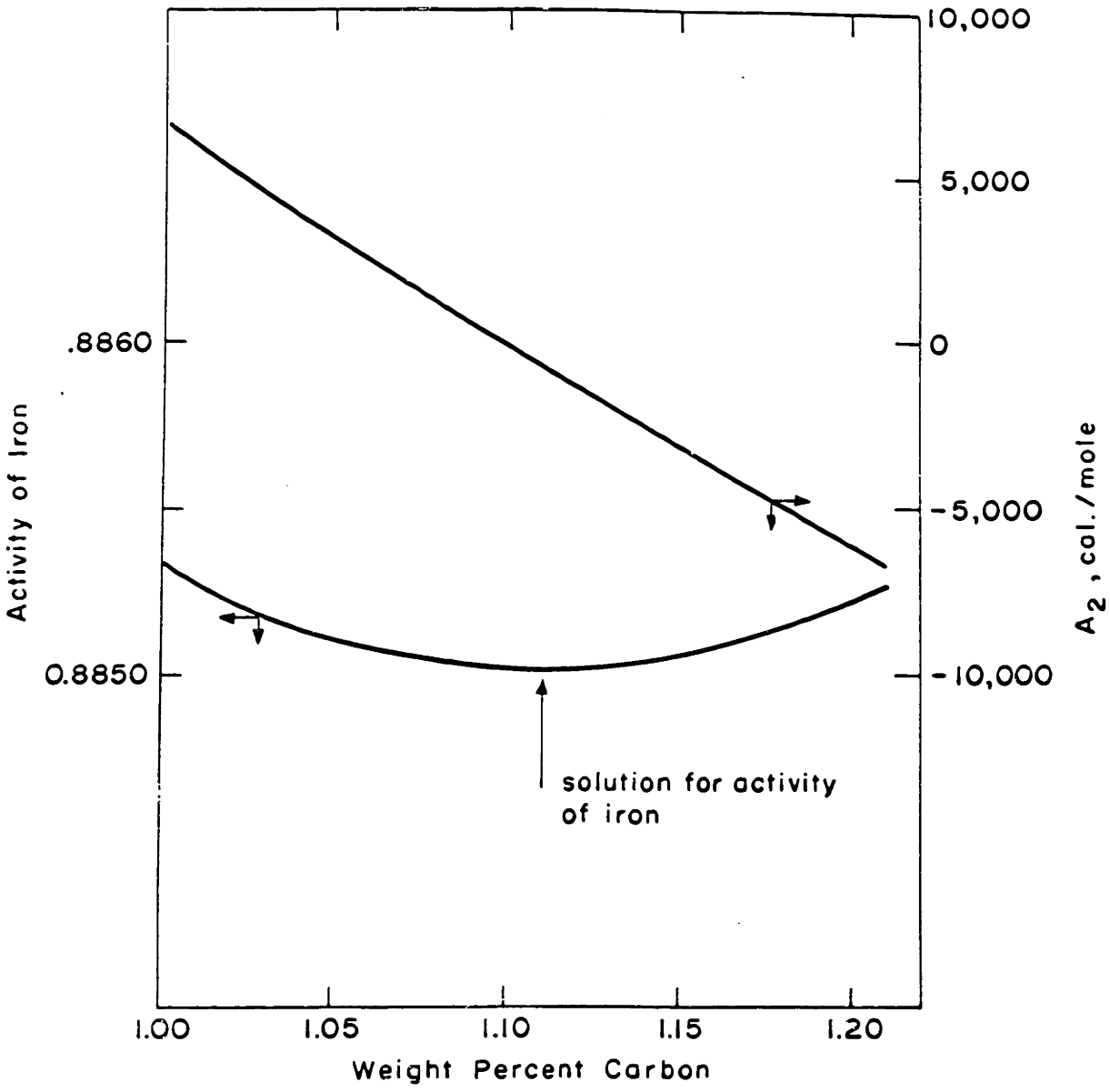

Figure C1: A calculation for the activity of iron in austenite and the corresponding A_2 value. Heat 18, Table V is chosen as the example.

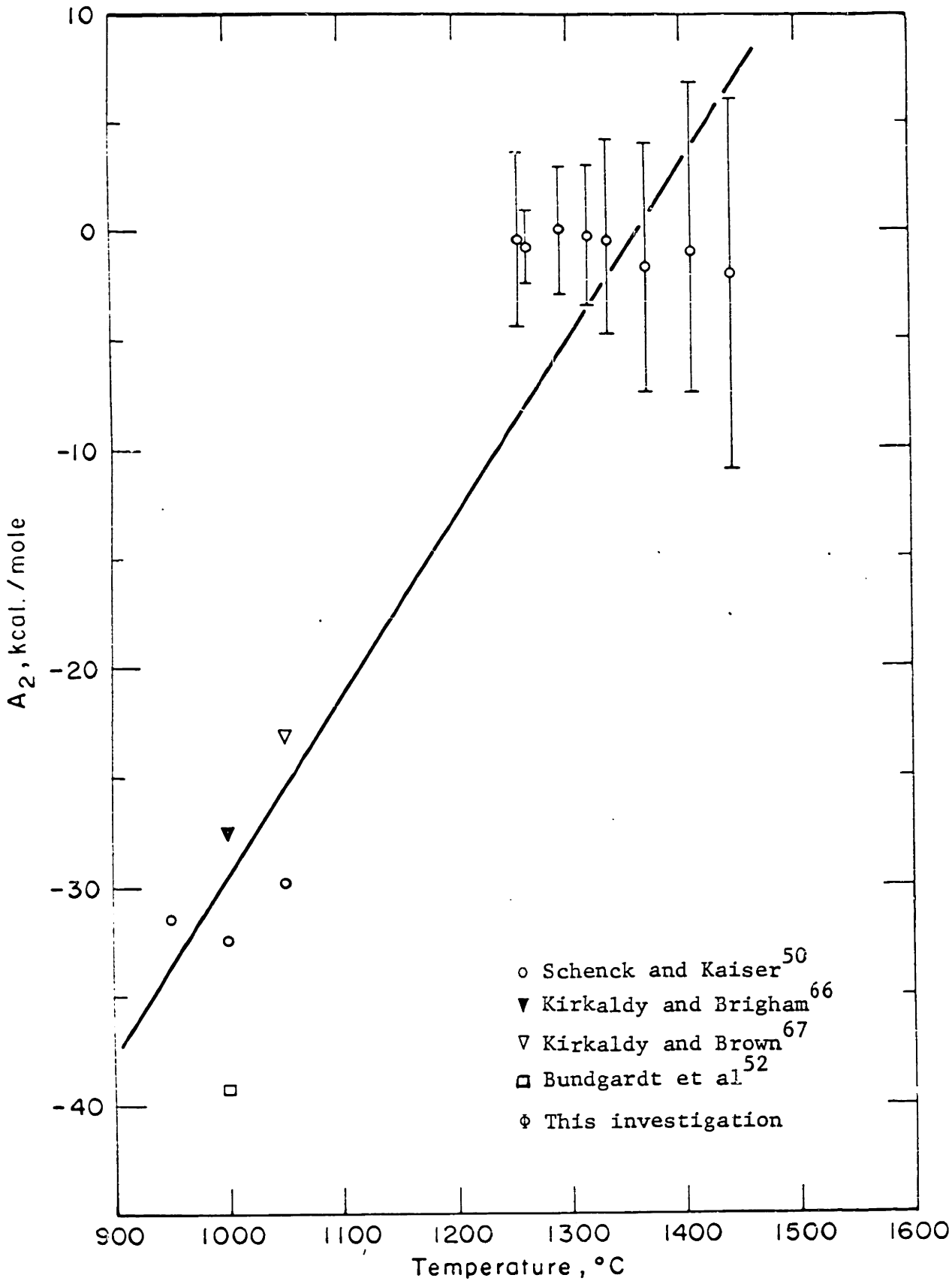

Figure C2: The parameter, A_2, versus temperature.

APPENDIX D

CALCULATION OF THE LIQUID-AUSTENITE EQUILIBRIA

In principle if the activities of all three components can be described for two phases, then the equilibrium between the two phases can be completely described. In the case at hand, this means that the entire gamma liquidus and gamma solidus can be constructed with tie lines. However, since the liquidus is known, it is only necessary to consider the activity of two components. Carbon is an obvious choice for one of the components; iron has an advantage over the selection of chromium because the standard state for iron can be changed from pure liquid iron to pure gamma iron whereas the standard state transition for chromium is not available because pure gamma chromium does not exist. If iron is chosen as the second component difficulties arise so that a means is developed to use chromium as the standard state.

Referring to Figure C1 and Table CI, the activity of iron is seen to be hardly sensitive to the concentration of carbon; because the activity of iron is only known to within .01, the weight per cent of chromium could only be known to about $\pm$ 1 per cent (absolute, not a relative value).

To avoid the difficulty of working with the activity of iron, a relation was developed to express the change of state from chromium from the liquid to the hypothetical standard state of pure austenitic chromium. Using the eight experimental chromium equilibria

determinations and accepting the activities for carbon and chromium calculated in the liquid by equations (B1) and (C9), equations (C20) and (C25) are solved simultaneously for the concentration of carbon, X_1, and the activity of chromium in austenite, a_2. The carbon concentrations derived in this manner were within the limits specified for the determination of A_2 in Figure C2. The ratio of chromium activities for the austenite relative to the liquid is plotted in Figure D1 which yields the following relation for the change of standard state for chromium:

$$\log \frac{a_2^{\gamma}}{a_2^{\ell}} = \frac{2411}{T} - 1.076 \qquad (D1)$$

With this equation the solidus surface can now be constructed by requiring that the activity of carbon and chromium in both phases be equal when based on the same standard state. Equation (D1) is compared with the analogous equation for the change of standard state between δ-chromium and liquid-chromium in Figure D1. The curve involving γ-chromium is higher than δ-chromium as it should be because δ-chromium is the stable phase.

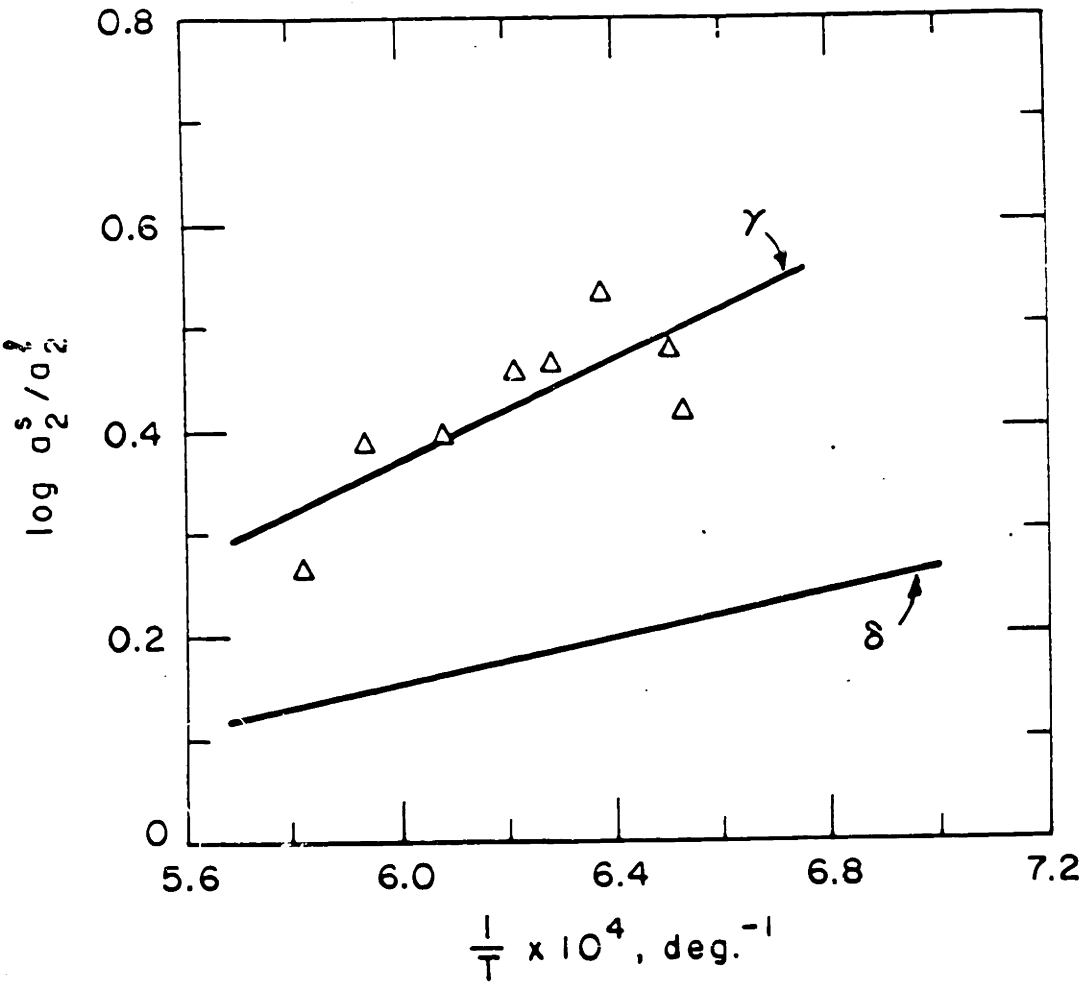

Figure D1: Change of standard state for chromium between pure liquid chromium and the hypothetical pure γ-chromium and comparison with the change of standard state involving δ-chromium.